

PDF hosted at the Radboud Repository of the Radboud University Nijmegen

The following full text is a publisher's version.

For additional information about this publication click this link.

<http://hdl.handle.net/2066/19037>

Please be advised that this information was generated on 2017-12-05 and may be subject to change.

The nature of the band gap in switchable mirror metal hydrides

een wetenschappelijke proeve op het gebied van de
Natuurwetenschappen, Wiskunde en Informatica

Proefschrift

ter verkrijging van de graad van doctor
aan de Katholieke Universiteit Nijmegen,
volgens besluit van het College van Decanen
in het openbaar te verdedigen
op vrijdag 9 november 2001,
des namiddags om 3.30 uur precies
door

Peter van Gelderen

geboren op 14 maart 1971 te Nijmegen

Promotores: Prof. dr. P.J. Kelly (Universiteit Twente)
Prof. dr. R.A. de Groot (Rijksuniversiteit Groningen)

Co-promotor: Dr. P.A. Bobbert (Technische Universiteit Eindhoven)

Manuscriptcommissie:

Prof. dr. R.P. Griessen (Vrije Universiteit Amsterdam)
Prof. dr. L.F. Feiner (Universiteit Utrecht, Philips Research)
Dr. G. Brocks (Universiteit Twente)

The work described in this thesis is part of the research program of the Stichting voor Fundamenteel Onderzoek der Materie (FOM), which is financially supported by the Nederlandse Organisatie voor Wetenschappelijk Onderzoek der Materie (NWO). This work is supported by Philips Research.

Contents

1	Switchable mirrors	1
1.1	The discovery of switchable mirrors	1
1.2	Simplified picture of the electronic structure	5
1.3	Conventional LDA calculations	8
1.3.1	The reflecting and metallic dihydride	9
1.3.2	The transparent and insulating trihydride	10
1.3.3	Failure of the LDA	11
1.4	LDA calculations for LaH_3	12
1.5	Proposed mechanisms for the large gap	13
1.5.1	Strong electron correlation	14
1.5.2	Weak correlation and strong electron phonon-coupling	16
1.6	Aim of this thesis	20
2	Quasi-particles in YH_3	27
3	<i>GW</i> calculations for YH_3	39
3.1	Introduction	40
3.2	Theory	45
3.2.1	<i>GW</i> calculations	45
3.2.2	Implementation	47
3.2.3	Self-consistency	50
3.3	Results	52
3.3.1	The lattice structures	52
3.3.2	Computational details	53
3.3.3	The LaF_3 structure	54
3.3.4	The HoD_3 structure; dielectric function	57
3.3.5	The broken symmetry structure	58
3.4	Discussion	61

4	Phonon spectrum of YH_3	71
5	Structure and dynamics of YH_3	81
5.1	Introduction	82
5.2	Calculation of lattice vibrations	86
5.2.1	Motion of single atoms	88
5.2.2	Ellipsoids of vibration	89
5.2.3	Debye-Waller factors	89
5.3	Results for YH_3	90
5.3.1	The proposed lattice structures for YH_3	90
5.3.2	Computational details	92
5.3.3	Supercell and Brillouin zone sampling	95
5.3.4	Phonon band structures	96
5.3.5	Raman and infrared spectra	99
5.3.6	Densities of states and NVS experiments	100
5.4	Results for YD_3	106
5.5	Discussion	108
6	<i>GW</i> calculations for LaH_3	119
6.1	Introduction	120
6.2	Quasi-particle calculations for LaH_3	121
7	Quasi-particles in CaB_6	131
	Samenvatting	141
	Curriculum vitae	145

Chapter 1

Switchable mirrors

1.1 The discovery of switchable mirrors

At the end of 1994 a Ph.D. student, Hans Huiberts, made an exciting accidental discovery in the solid state physics laboratory at the Free University of Amsterdam while studying the possibility of superconductivity occurring in so-called “dirty” metallic hydrogen. Wigner had predicted theoretically [1] that the H_2 -molecules in hydrogen gas should come close enough at sufficiently high pressures for the molecular bonds to break allowing an atomic metal to be formed. Subsequent calculations by, among others, Ashcroft [2] predicted that metallic atomic hydrogen might be superconducting up to relatively high temperatures. However, in practice the crystallization and metallization of atomic hydrogen requires huge pressures to break the molecular bonds in H_2 -molecules and studying the insulator-to-metal transition in this way is far from trivial. Assuming that the transition is caused by closing the energy gap between the valence and conduction levels, an alternative scheme was proposed to obtain atomic metallic hydrogen. It is known that the introduction of impurities into a solid may induce donor or acceptor states in the gap. If the number of such impurities is sufficiently large the impurity state wave functions may overlap and induce metallic behavior in the impurity band. On the basis of this analogy, it was suggested that introducing impurities into atomic hydrogen might reduce the pressures required to metallize this system, and thus make it easier to look for the predicted superconducting state [3]. This is the concept of “dirty” metallic hydrogen.

It is well known that many metals can absorb large amounts of hydrogen. Such metal-hydrogen systems may equally well be considered as solid hy-

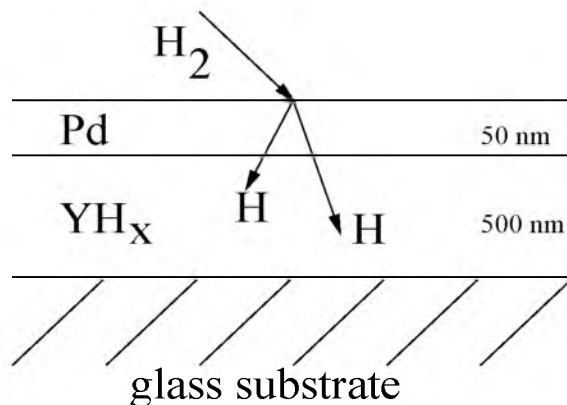


Figure 1.1: Schematic outline of the switchable mirror experiment.

drogen in which metal atoms are absorbed. Possibly, these systems behave as “dirty” metallic hydrogen. Pursuing this idea, Huiberts was exposing yttrium and lanthanum to hydrogen gas. These metals can accommodate up to three hydrogen atoms per metal atom. Unfortunately, when the trihydride is formed, the material usually falls apart into a powder. This severely complicates the investigation of its electrical and optical properties. Huiberts *et al.* [4] tackled this problem by using a layered geometry. A thin film (typically 500 nm) of yttrium (or lanthanum) was deposited on a glass substrate and covered with an optically thin layer (typically 20-50 nm) of palladium. The palladium caplayer protects the very reactive yttrium against oxidation. If such a sample (which is schematically shown in Fig. 1.1) is exposed to moderate hydrogen pressures, H_2 -molecules are dissociated and the resulting hydrogen atoms move into the yttrium film. Surprisingly, the thin yttrium film changes from a shiny mirror into a transparent window, shortly after it has been exposed to hydrogen gas. A spectacular transition had occurred which could be witnessed with the naked eye. By decreasing the hydrogen pressure the film could be “switched” back to a reflecting mirror. These results suggest that a metal-insulator transition occurs as a function of the hydrogen “loading” of the yttrium film. Such a film which can be switched between a reflecting and a transparent state by varying its hydrogen content is called a switchable mirror [4].

In the layered configuration the yttrium film remains intact when it absorbs hydrogen and the electrical resistivity of the YH_x system (where x is the number of hydrogen atoms per yttrium atom in the film) as well as the optical transmission could be determined accurately for x in the

range between 0 and 3 [4]. These data were first taken as a function of time but they could subsequently be related to the amount of hydrogen in the sample using a quartz crystal microbalance [5]. It was found that the thin film becomes transparent at a hydrogen content x of about 2.8. The results of the x -dependent transmission and resistivity measurements are interpreted in the following way. Yttrium is a metal with a low resistivity. A layer of yttrium reflects most of the incoming light in the visible regime and therefore behaves as a good mirror. When hydrogen starts to move into the yttrium film first the resistivity slightly increases due to impurity scattering but then it decreases considerably until the β -YH₂ phase is reached. In this phase the resistivity is minimal which shows that YH₂ is an even better conductor than pure yttrium. The transmission of light remains practically constant when going from the α -Y phase to the β -YH₂ phase. When the dihydride phase is reached there is a small increase in the transmission which is sometimes referred to as the “Huiberts window”. This window causes the dihydride to appear reddish in transmission [6]. If more hydrogen is absorbed by the switchable mirror film the γ -YH₃ phase starts to nucleate. This is accompanied by an increase in both the transmission of light through the film and in the resistivity of it by at least two orders of magnitude. At this stage the switchable mirror becomes almost fully transparent for light in the visible regime. This observation together with the large increase in resistivity suggest that YH₃ is a semiconductor with a large band gap. However, in the switchable mirror experiments the stoichiometric limit YH₃ is not accessible since it requires prohibitively large hydrogen pressures to reach this limit. Therefore, the transparent phase in switchable mirrors actually corresponds to YH_{3- δ} with δ usually ~ 0.1 . When the hydrogen pressure is decreased hydrogen moves out of the thin film until the dihydride phase is recovered. It is not possible to recover the pure yttrium phase without additional treatment of the sample. The optical switching in yttrium and lanthanum switchable mirror devices is therefore between the dihydride and the trihydride phase.

The described changes in the optical properties are spectacularly large. Since the switching process is reversible (the films can be switched many times without very serious degradation), and because this process can be established at room temperature and at moderate hydrogen pressures, this discovery might form the basis for a number of commercially interesting applications. For several years now researchers at the Philips Research Laboratories in Eindhoven, The Netherlands, have been exploring these possibilities, and they have been trying to match the stringent industrial

requirements for applications. Meanwhile they have found that the thin films can be switched electrochemically [7], and that besides yttrium and lanthanum films also most rare earth metals and some compounds can be used as switchable mirror materials. So far, GdMg compounds seem to exhibit most of the required properties, such as a large contrast between reflection in the transparent state and in the reflecting state [8]. Moreover, this alloy is color-neutral in the transparent state, in contrast to the yttrium films which appear yellowish in this state. Using multilayer configurations faster optical switching has been achieved [9]. Very recently Philips researchers have succeeded to tackle a very serious problem connected to the hydrogen needed for the optical switching. Applications using large amounts of externally stored hydrogen gas are very unattractive. The construction of an all-solid-state device is therefore of large practical importance. In such a device hydrogen is moved using electrodes from a buffer layer into a switchable mirror layer and vice versa. Recently also other researchers have reported the construction of such all-solid-state devices [10].

The research into superconductivity by closing the gap in “dirty” metallic hydrogen that had led to the accidental discovery of switchable mirrors was simmered due to this spectacular discovery. Some activity has been reported though by Wijngaarden *et al.* [11] who have found that the gap in YH_3 films decreases if external pressure is imposed upon these samples in a diamond anvil cell. The gap is estimated to close at a pressure of 55 GPa. Besides this work, the experimentalists were now facing both numerous technological issues which needed to be solved in view of possible applications of the switchable mirrors, and more fundamental questions related to the mechanism underlying the metal-insulator transition. Theorists were mainly concerned with the nature of the band gap in YH_3 . A fundamental problem had been raised by the prediction of state-of-the-art band structure calculations that YH_3 should be a metal [12-14]. The transparent and semiconducting trihydride phase in the switchable mirror experiments clearly confronted theorists with an intriguing problem. From the position of the absorption edge in $\text{YH}_{3-\delta}$ an optical gap was deduced of about 2.7 eV. This value was very recently confirmed both by van Gogh *et al.* [15] and by Lee and Shin [16]. It should be stressed, however, that the optical gap of a material is not always identical to the fundamental gap. For example, the latter gap may be indirect or matrix elements for direct optical transitions at lower energies may vanish. For many semiconductors the size of the fundamental gap can be deduced from temperature-dependent mea-

measurements of the resistivity. Such experiments for switchable mirrors [17] are difficult to interpret because the system is nonstoichiometric to begin with, and because hydrogen moves out of the sample if the temperature is increased, which consequently also changes the resistivity. Moreover, the presence of a metallic palladium caplayer imposes a limit upon the accuracy of the deduced resistivity. However, because of the large increase in the resistivity, its inverse proportionality to δ in substoichiometric $\text{YH}_{3-\delta}$, and its negative temperature dependence it was concluded that YH_3 is a true semiconductor [4]. It remains to be demonstrated experimentally that the optical gap can be identified with the fundamental band gap.

1.2 Simplified picture of the electronic structure

For a proper understanding of the electrical and optical properties of a solid the quantum mechanics of the electrons in the material must be studied. If those electrons are tightly bound to the atoms which constitute the solid, the ability of this material to sustain an electrical current will be weak. On the other hand, if the electrons are not so strongly localized at particular atomic sites, but free to move through the solid, the electrical conductivity will be good. If there is an energy gap between the occupied and the unoccupied quantum mechanical states of the electrons, light with energies smaller than this energy difference cannot be absorbed in strong interband transition processes and will be transmitted through the solid. The material then appears transparent. Detailed knowledge of the energy spectrum of the electrons is therefore required for an accurate prediction of the electrical and optical properties of a material. The coherent picture of the properties of the electrons in a particular solid is usually referred to as the electronic structure of that solid. It can be found by solving the Schrödinger equation for the electrons. If the results of such electronic structure calculations depend on no adjustable parameters these calculations are called *ab-initio*, from first principles, or parameter-free. Parameter-free electronic structure calculations are the main topic of this thesis.

In a rather simplified atomic picture the electronic structure of the YH_x system can easily be understood. Although the results of more advanced calculations complicate this simple picture to a large extent, it does provide a good starting point for the interpretation and discussion of those more advanced results. An yttrium atom is trivalent which means that in a chemical environment where it can transfer its electrons to other atomic species it is likely to more or less donate its outer three electrons to other

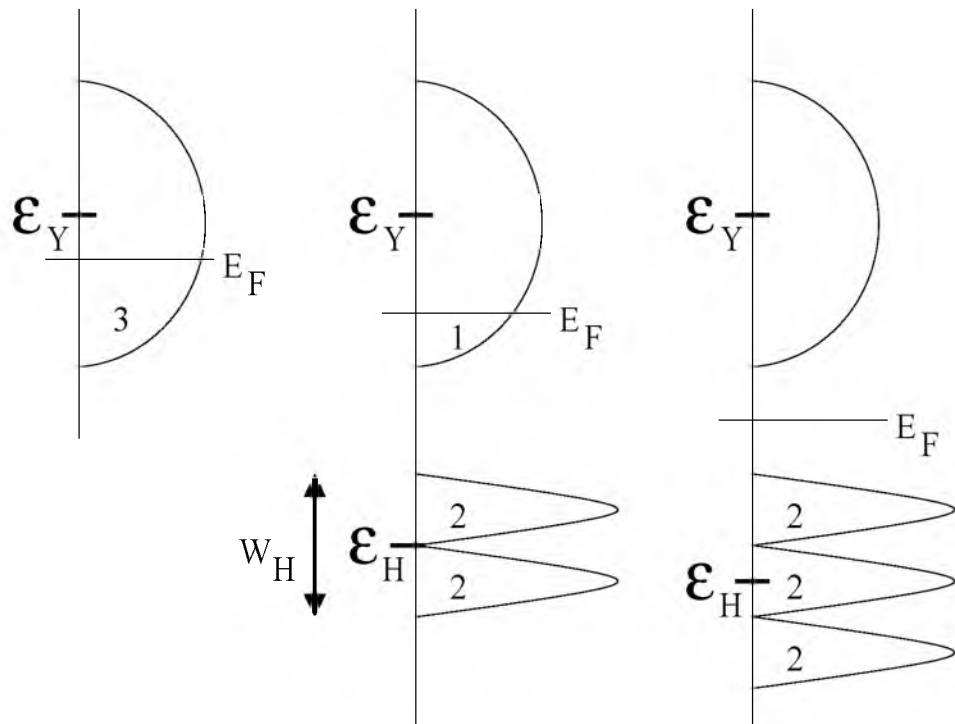


Figure 1.2: Simplified pictures of the electronic structure (schematic density of states) for the YH_x system; from left to right Y, YH_2 and YH_3 respectively (see text for the details).

atoms and become an Y^{3+} ion. The other 36 electrons of an yttrium atom are so-called core electrons which are tightly bound to the strongly negatively charged nucleus. These electrons hardly notice any change in the chemical environment. In solid yttrium where there are no atoms of other atomic species to donate electrons to, the valence electrons form delocalized metallic bonds. In this way the yttrium atoms “share” their outer electrons. The valence electronic wave functions now also have large amplitudes in between the yttrium atoms, which supports the cohesion of the atoms.

In atomic yttrium the outer three electrons occupy the $5s$ and $4d$ atomic levels. Actually there are two of these $5s$ levels available (one for each spin direction) and ten $4d$ levels. Due to overlap of the atomic wave functions in a solid these levels broaden in energy and due to the periodicity of a solid the energies of these states may be represented in a band structure

picture. The number of quantum mechanical states per energy range per unit cell, which are available for the electrons in a particular material, is called the density of states (DOS). In the left picture of Fig. 1.2 the DOS (plotted horizontally) for solid yttrium is schematically given as a function of energy (plotted vertically), in the range where the levels which are derived from the atomic $5s$ and $4d$ levels are to be found. The center of energy (the band center) of this structure in the DOS is denoted by ϵ_Y . In the ground state the three states lowest in energy are occupied by the three yttrium valence electrons. The Fermi energy (denoted by E_F) is the energy which separates the three occupied states from the 9 unoccupied states in this figure. Because this part of the DOS is only partially filled with the three outer yttrium electrons, the energy gap between the occupied and the unoccupied levels vanishes. This is a property which is typical for metals.

When hydrogen is inserted in yttrium it induces additional bands which lie below the complex of yttrium-derived bands. Since a hydrogen atom has only one electron each hydrogen-derived band in YH_x can accommodate another electron from the yttrium atom. Inserting hydrogen therefore leads to a depopulation of the bands derived from the atomic yttrium $5s$ and $4d$ levels. This simplified picture of the electronic structure is known as the anionic model; yttrium is the anion which donates electrons and becomes positively charged. In YH_2 two electrons are transferred from the yttrium-derived bands to the hydrogen-related bands (cf. Fig. 1.2; middle picture). The center of energy of these hydrogen-related bands is denoted by ϵ_H and the total band width of these bands is indicated by W_H in this figure. One electron remains occupying the yttrium-derived DOS, leaving the Fermi level in this structure, and therefore YH_2 is still a metal. In YH_3 (cf. Fig. 1.2; right picture) also the third electron from yttrium is transferred to the hydrogen-derived bands. If the DOS due to these three hydrogen-related bands is well separated from the DOS of the yttrium-related bands (as they are in the figure) there is a finite energy gap between the occupied and the unoccupied states in YH_3 . If this energy gap is large enough, the material is unable to absorb or to reflect light in the visible regime and the system is transparent for this light. The conduction of an electrical current in such a system will be much poorer than in a metal. Such a material is called a semiconductor or insulator depending on the size of this energy gap which is called the band gap.

1.3 Conventional LDA calculations

Many years before the discovery of switchable mirrors metal-hydrogen systems, including those which are now used in switchable mirror devices, have been the subject of research. Besides much experimental work devoted to these systems some theoretical studies have been reported in literature. The electronic structure of metal-hydrides has obviously been investigated as well. Band structure calculations for these materials go back to the 1970s which is shortly after the development of Density Functional Theory (DFT) [18,19] and the Local Density Approximation (LDA) [19]. Switendick pioneered the use of LDA calculations for studying the electronic structure of metal-hydrides [20]. These non-selfconsistent calculations predicted that YH_2 is a good metal. Since YH_3 has a complicated lattice structure and a large unit cell and because of limited computational resources in those days, Switendick studied YH_3 in a simplified lattice structure, which is known as the BiF_3 structure. This is a face-centered cubic structure with the metal atom in the origin and the hydrogen atoms occupying the ideal octahedral and tetrahedral interstices of the metal lattice. Switendick calculated a large band gap for YH_3 in this simplified lattice structure [20]. These calculations essentially confirmed the anionic model. Moreover, they are not in contradiction with the switchable mirror experiments.

The issue of self-consistency had been completely neglected in those calculations. On the one hand, because of limited computer facilities at that time, and on the other hand because of a more fundamental questioning of the necessity to perform electronic structure calculations self-consistently. Nowadays the importance of self-consistency in electronic structure calculations is no longer questioned and LDA band structures are almost exclusively calculated self-consistently. However, this self-consistency dramatically changes Switendick's results for YH_3 . The system is no longer predicted to have a large gap in the LDA spectrum. Dekker *et al.* [12] showed that the LDA band structure for YH_3 in the BiF_3 structure has a large band overlap at the Fermi level. This is also found when exchange and correlation are included in an improved fashion using so-called generalized gradient corrections [21]. For YH_3 in the experimentally determined (so-called HoD_3) lattice structure both Dekker *et al.* [12] and Wang and Chou [13,14] have calculated band overlap of the hydrogen-derived and yttrium-derived bands of more than 1 eV at the Fermi level. These results are in strong disagreement with the switchable mirror experiments.

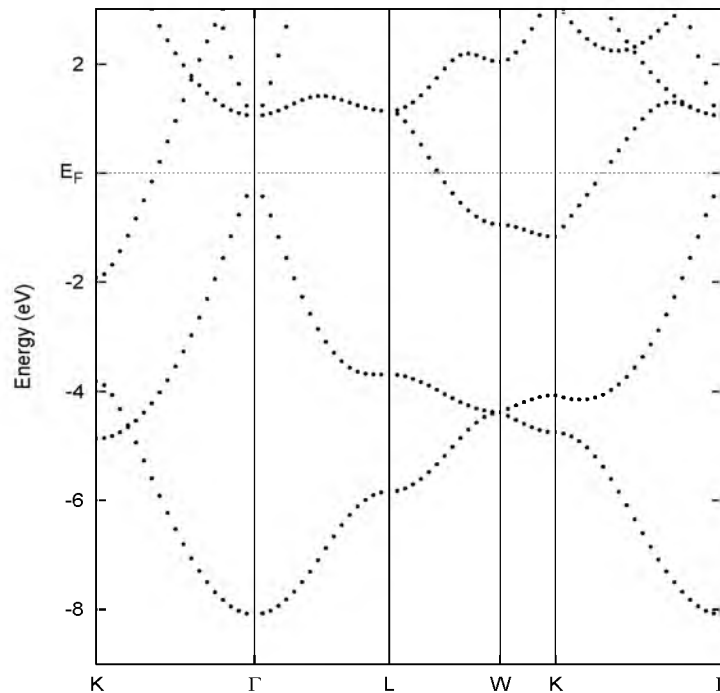


Figure 1.3: LDA band structure for YH₂.

1.3.1 The reflecting and metallic dihydride

YH₂ has a simple face-centered cubic structure with hydrogen atoms occupying the ideal tetrahedral interstices at $(\frac{1}{4}\frac{1}{4}\frac{1}{4})$ and $(\frac{3}{4}\frac{3}{4}\frac{3}{4})$ of the yttrium sublattice (fixed in the origin). The results of self-consistent LDA calculations using the Korringa-Kohn-Rostoker method for YH₂ have been reported by Peterman *et al.* [22]. On the basis of these calculations optical experiments and photoelectron spectroscopy data could be successfully interpreted by Weaver *et al.* [23,24]. We have repeated the LDA calculation for YH₂ with a Car-Parrinello pseudopotential plane wave code [25] and using a lattice constant of 9.83445 a.u. The results which are essentially identical to the results of Peterman *et al.* are shown in Fig. 1.3. The simplified picture of the electronic structure of YH₂ is more or less confirmed. There are two hydrogen-related bands mostly below the yttrium-derived bands. However, there is indirect overlap of the third (yttrium-related) band near K and the second (hydrogen-related) band at Γ . The hydrogen-related bands accommodate four out of five valence electrons in YH₂. The

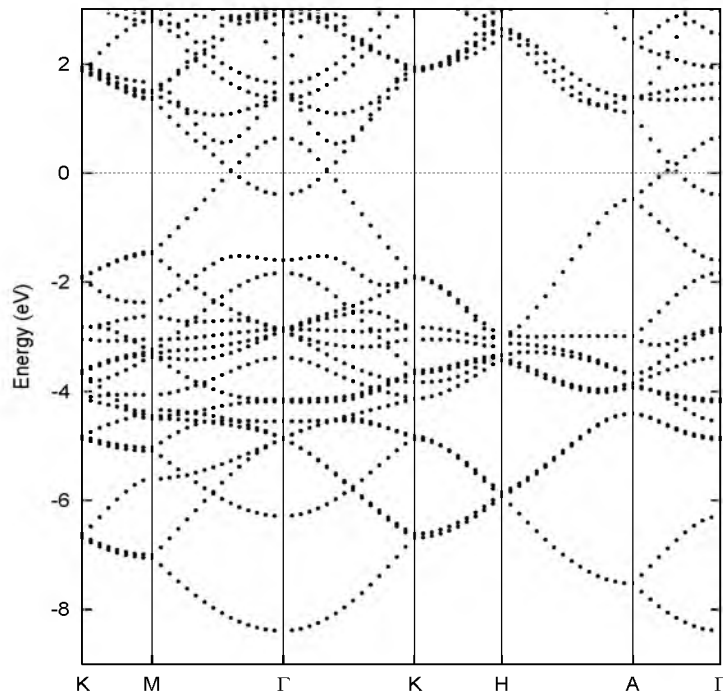


Figure 1.4: LDA band structure for YH₃ in the HoD₃ structure.

remaining electron is partially occupying the yttrium-derived bands. This band structure corresponds to a metal, in agreement with the switchable mirror experiments. The total band width of the two lowest hydrogen-derived bands is rather large, almost 8 eV. This indicates that the electronic wave functions are not very localized at the hydrogen sites.

1.3.2 The transparent and insulating trihydride

The experimentally observed lattice structure of YH₃ is the structure which was first found for HoD₃ by Mansmann *et al.* [26]. For YD₃ it was reported from an early study by Miron *et al.* [27] and recently confirmed by Udovic *et al.* [28] using neutron powder diffraction (NPD) experiments. Therefore, this lattice structure is usually referred to as the HoD₃-structure, or as the high-symmetry structure, in order to distinguish it from a closely related structure with a lower symmetry, which is the so-called broken symmetry structure. This latter structure was predicted later from total energy calculations. From the results of NPD experiments Remhof *et al.* [29,30] have

concluded that YD_3 also has the HoD_3 lattice structure in thin epitaxially grown switchable mirror layers. The HoD_3 structure is a rather complicated lattice structure with 24 atoms in the unit cell. LDA calculations predict YH_3 to be a metal in this lattice structure with large band overlap of more than 1 eV at the Fermi level. Such calculations have been reported by Dekker *et al.* [12] and by Wang and Chou [13,14] Using the same code and parameters as in Ref. [31] we have reproduced this LDA band structure in Fig. 1.4. Since YH_3 in the HoD_3 structure has stoichiometry Y_6H_{18} there are 18 hydrogen-related valence bands in this band structure. Near Γ these bands partially overlap the yttrium-derived conduction bands. Therefore this band structure corresponds to a metal. Since there are partially filled electron and hole bands such a band structure is characteristic for a semimetal. Clearly, this band structure is not in agreement with the switchable mirror experiments which suggest that YH_3 is a semiconductor with a considerable band gap.

1.3.3 Failure of the LDA

If the LDA results were to be summarized in a simplified picture similar to the picture in Fig. 1.2 the picture shown in Fig. 1.5 would be obtained. The schematic picture for pure yttrium is essentially confirmed by the LDA results (the LDA band structure for Y is not shown in this thesis). For YH_2 there are minor differences between the simplified picture and the present LDA results. For example, the yttrium-derived and hydrogen-derived bands have a small indirect overlap. On the other hand, there is always a direct gap separating these bands in the LDA calculation. Somewhat more prominent is the fact that the calculated hydrogen band width in the LDA band structure for YH_2 is rather large. Large dispersions indicate that the electronic wave functions are delocalized. For YH_3 the LDA results more seriously deviate from the proposed simple anionic picture. Most importantly, the calculated yttrium-derived and hydrogen-derived bands overlap and there is no band gap. This is clearly at variance with the switchable mirror experiments. Again, the hydrogen-related bands correspond to a rather large total valence band width of about 9 eV.

Starting from the LDA results for YH_3 there are basically two ways to reconcile the calculated band structure with the interpretation of the switchable mirror experiments in the simplified model. The first way is to reduce the band width W_H of the hydrogen bands (or the band width of the yttrium bands), and the second way is to increase the separation between the centers of the bands, ϵ_Y and ϵ_H .

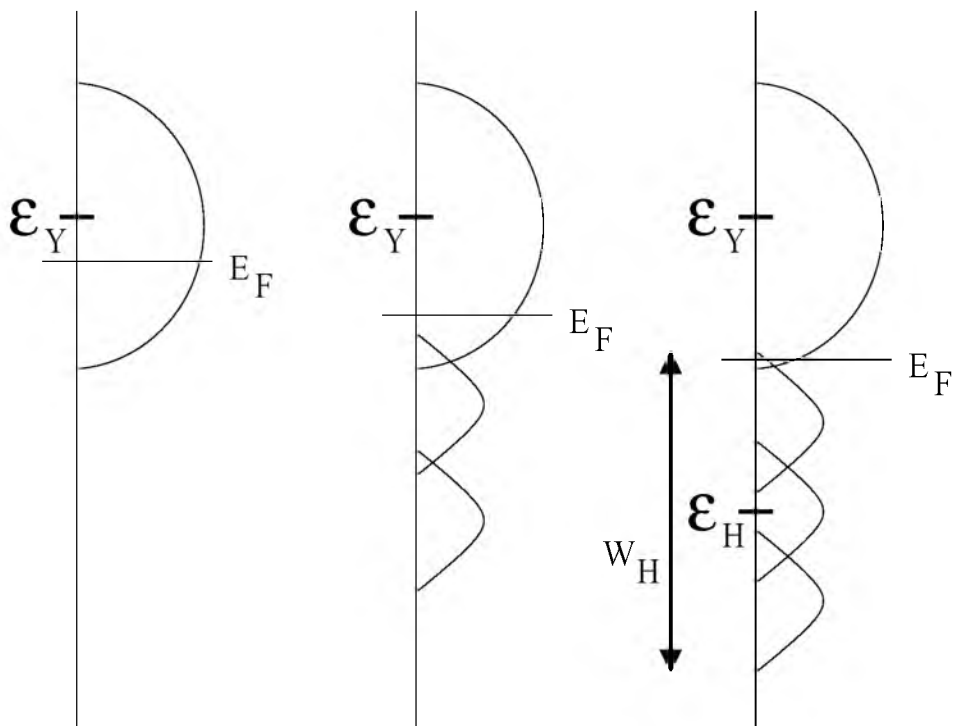


Figure 1.5: LDA results for YH_x in a simplified picture.

1.4 LDA calculations for LaH_3

In their original work on switchable mirrors Huiberts *et al.* [4] have already shown that switchable mirrors can also be made using lanthanum films. Essentially the results for both materials are the same. However, an important difference between these systems is the lattice structure. The LaH_x films remain cubic for x in the full range between 0 to 3. This is contrary to the YH_x system where there are structural phase changes from hexagonal to cubic and vice versa. The fact that the switchable mirrors operate essentially in the same way when using lanthanum instead of yttrium strongly suggest that the structural phase change in the YH_x system when going from the dihydride phase to the trihydride phase is not related to the opening of a band gap.

For LaH_2 and LaH_3 several band structure calculations have been reported in literature. Photoelectron and optical data taken for LaH_2 and LaH_3 by Peterman *et al.* [32] were found to be in reasonable agreement with

non-self-consistent band structure calculations by Gupta and Burger [33] (which predict a band gap of 0.53 eV for LaH_3) and with self-consistent calculations by Misemer and Harmon [34] (who find a gap of only 3 meV for LaH_3). Kulikov [35] finds small band overlap for LaH_3 and speculates on the existence of an excitonic insulator phase. In such a phase electrons and holes form bound states and the material appears as if it had a band gap. Recent self-consistent calculations by Dekker *et al.* predict band overlap of about 0.2 eV for LaH_3 [12]. We have also studied the LDA electronic structure of LaH_3 and have found essentially the same results as Dekker *et al.*, i.e. band overlap. We conclude that, although the discrepancy is not as severe as in YH_3 , also for LaH_3 the LDA results are at variance with the switchable mirror experiments.

1.5 Proposed mechanisms for the large gap

As the LDA calculations failed to predict a gap for LaH_3 and YH_3 in any of the proposed lattice structures at the time of the discovery of the switchable mirrors, explanations were sought for this failure. Basically two different mechanisms were proposed.

The first mechanism is essentially a “weak correlation” approach. DFT-LDA calculations are essentially ground state calculations and usually produce very accurate total energies and electronic charge densities. Excitation spectra are often less accurately predicted in these type of calculations. For example, it is well known that band gaps in semiconductors and insulators are usually underestimated. Much better band gaps can be obtained for a wide range of materials using the so-called *GW* method. For LaH_3 the discrepancy between the LDA results and the experimental data is not exceptionally large and it may be expected that a *GW* calculation for this material will predict a gap in close agreement with experiment. However, for YH_3 the discrepancy between LDA theory and the experimentally obtained band gap is so large that a “usual” *GW* correction to the LDA spectrum is not enough to explain the large band gap found experimentally for this material. Therefore, in the first mechanism an alternative lattice structure was proposed, in addition to the anticipated *GW* correction to the band gap. DFT-LDA total energy calculations predict a lower total energy for YH_3 in a lattice structure which slightly differs from the so-called HoD_3 -structure which was deduced from diffraction experiments. Small displacements of the hydrogen atoms from their assumed positions break the high symmetry, lower the total energy, and open up a gap of

about 0.8 eV in the electronic spectrum at the LDA level. On the basis of the results of GW calculations for many other materials, one may expect that applying this method to YH_3 will produce a band gap in close agreement with experiment. Since the calculated displacements are small but drastically change the LDA electronic structure from a metal into an insulator, this mechanism is sometimes referred to as strong electron-phonon coupling.

The second mechanism proposes that strong local electron correlation effects are responsible for the large band gap in YH_3 and LaH_3 . Since the discrepancy between the calculated band gap for YH_3 in LDA theory and the experimental gap deduced from the switchable mirror experiments is as large as in transition metal oxides, in which strong local interactions between localized d -orbitals are important but poorly described in LDA calculations, it has been suggested that YH_3 and LaH_3 are strongly correlated materials as well. Model Hamiltonians have been postulated invoking such strong local correlation effects. The diagonalization of these parameterized model Hamiltonians shows that such models are indeed capable of opening a gap in the single-particle excitation spectrum. Unfortunately, these results depend on free parameters.

1.5.1 Strong electron correlation

The strong correlation model for LaH_3 proposed by Ng *et al.* [36,37] adopts a local picture of the electronic structure. It is assumed that the transfer of the lanthanum valence electrons to the hydrogen sites is complete. The metal trihydrides are essentially viewed as lattices of H^- ions which are only slightly disturbed by the presence of the metal ions. From the point of view that the H^- ion is the key entity in the metal hydrides, the electrons in H^- should be described well to begin with. Very accurate results for this ion can be obtained using explicitly correlated wave functions. Such expressions for the two-electron wave function $\Psi(\mathbf{r}_1, \mathbf{r}_2)$ can not be factorized into the product $\phi(\mathbf{r}_1)\phi(\mathbf{r}_2)$ of two (effectively) independent single-particle wave functions. These explicitly correlated wave functions seem to work fine for the H^- -ion if appropriate numbers are chosen for the unknown parameters in such a parameterized wave function.

The form of the many-body (electron removal) H^- bands is determined by the hopping integrals between a hydrogen atom and a H^- ion. In the extreme atomic picture this matrix element is given by the energy splitting of the lowest levels in the H_2^- ion. Therefore, this ion is studied in detail as a function of the ion-ion distance. The crystal field perturbation due to the

La³⁺ ions is assumed to be small. It is estimated to effectively only slightly reduce this hopping matrix element. For the solid Ng *et al.* [36,37] propose a large U-limit Anderson lattice model. The large U represents the Coulomb interaction between two holes on a hydrogen site. It prevents any hydrogen site to have two holes on it. A Slater-Koster fit to the LDA band structure is made to extract those hopping parameters which are believed to be well described in an LDA calculation. The double hole state is projected out of the tight-binding solution. Using the Gutzwiller method the correlated many-body problem is mapped onto an effective one-electron model again. The effect of strong local electron correlations in this model for a lattice of H⁻ ions is a large reduction of the hydrogen hopping parameters in the tight-binding representation of the model. Furthermore, the on-site energies at the hydrogen sites (ϵ_H) are somewhat lowered by the binding energy of the outer electron in the H⁻ ion, for which the free-space value of 0.7 eV is used. With much lower hopping parameters for the hydrogen bands, the band width W_H is largely reduced as compared to the LDA band width. The lower on-site energy for the hydrogen sites moves the hydrogen band center down in energy. This results in a band structure with a large band gap. The estimated effect of the crystal field is small but even increases the gap. The final value for the band gap obtained for LaH₃ by Ng *et al.* is 2.1 eV.

A same type of model was proposed by Eder *et al.* [38] for YH₃. A free H⁻ ion is large in its spatial extent while neutral H⁰ is much smaller. This is also reflected in the fact that the electron in neutral H⁰ is bound by a large energy of exactly 1 Rydberg (13.6 eV) whereas the second electron in H⁻ is bound by only 0.7 eV. Eder *et al.* argue that the occupation dependence of the sizes of the hydrogen orbitals is not well accounted for in an LDA calculation. The fact the electronic wave function at the hydrogen sites is so much larger for H⁻ than for H⁰ is referred to as “breathing”. In order to deal with this breathing property of hydrogen Eder *et al.* propose a model that includes hopping parameters which depend explicitly upon the occupation of the hydrogen sites. For a small cluster this model could be diagonalized exactly. The ground state corresponds to local singlet states bound by the hydrogen nuclei with one electron on a hydrogen site and one electron on the neighboring metal atoms. Remarkably, the results of the exact diagonalization could be reproduced by a mean-field approximation to the model in which the introduction of occupation dependent hopping parameters effectively results in a large reduction of the on-site hydrogen energies ϵ_H . From a nearest-neighbor tight-binding fit to the LDA band

structure for YH_3 in a simplified so-called LaF_3 structure (to be discussed later) the hopping parameters and the on-site energies could be obtained. Using these parameters in the mean-field model the stability of the local singlets is calculated. Having only two parameters left, the Coulomb repulsion U at the hydrogen sites and λ , the ratio between the hopping parameters to respectively an occupied and an unoccupied hydrogen site, it is shown that for reasonable values of these parameters a band gap of about 2 eV is obtained.

The results of both model calculations can be summarized in the following way. In the model of Ng *et al.* the most prominent feature is a large reduction of W_H , the band width of the H^- bands, as compared to the LDA band width. This reduction leads to a band gap of about 2 eV. On the other hand, in the model by Eder *et al.* the effect of breathing at the hydrogen sites results in a large reduction of the on-site hydrogen energies ϵ_H . This also opens up a considerable gap in the spectrum.

1.5.2 Weak correlation and strong electron phonon-coupling

Kelly *et al.* [31] have proposed a “weak correlation” mechanism, in which they suggested that the band gap problem in LaH_3 could be solved by an improved treatment of the electronic excitations based on standard electron gas theory (e.g. in the GW -method). For YH_3 where the discrepancy between LDA theory and the experimentally obtained band gap is much larger, they suggested that in addition to the improved treatment of the electronic excitations in GW theory, a symmetry-breaking could explain the large band gap in this material. This strong electron-phonon coupling mechanism was proposed on the basis of first-principles total energy calculations. These calculations predict that small symmetry-breaking hydrogen displacements lower the total energy and open up a gap in the LDA spectrum.

We shall now first describe the experimentally obtained HoD_3 structure and then later discuss the symmetry lowering that leads to the broken symmetry structure. The lattice structure of YH_3 is most easily explained starting from a hexagonal yttrium lattice. In this lattice both tetrahedral and octahedral interstitial sites exist. Two out of every three hydrogen atoms in YH_3 occupy positions close to the tetrahedral sites. We denote these atoms by H(T) . Every third hydrogen atom does not reside at an octahedral site but instead moves into or close to the metal plane. Therefore they are often called metal-plane hydrogen atoms, and they are denoted by H(M) . At the left side of Fig. 4.2 the metal planes in this lattice structure

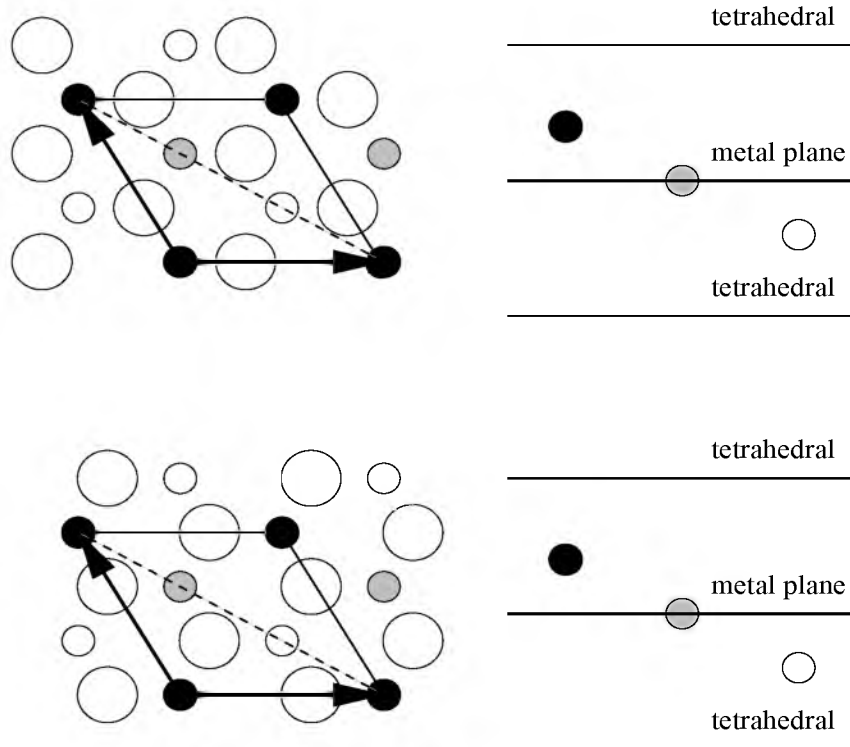


Figure 1.6: YH_3 in the HoD_3 structure (see text for details).

are shown. These two planes lie in the ab -plane of the hexagonal structure where they are alternated and stacked in the c -direction. Large circles represent the yttrium atoms, smaller circles correspond to the H(M) atoms. The lattice vectors in the ab -plane are also indicated, as well as the size of the unit cell. The H(M) atoms are either exactly in the metal planes (those indicated with gray circles), above the plane (black circles) or below the plane (white circles). The H(T) atoms are in between the metal planes.

If an intersection is made of this structure, perpendicular to the metal planes, and through the dashed lines indicated in the metal planes in the left part of Fig. 4.2, the picture at the right side of Fig. 4.2 is obtained. This picture shows both where planes containing the H(T) atoms are to be found along the c -direction and where the H(M) atoms are located with respect to the metal planes. If all H(M) atoms are exactly in the metal planes, the structure is known as the LaF_3 structure. In this geometry the stoichiometry is Y_2H_6 . Starting from this structure and modulating

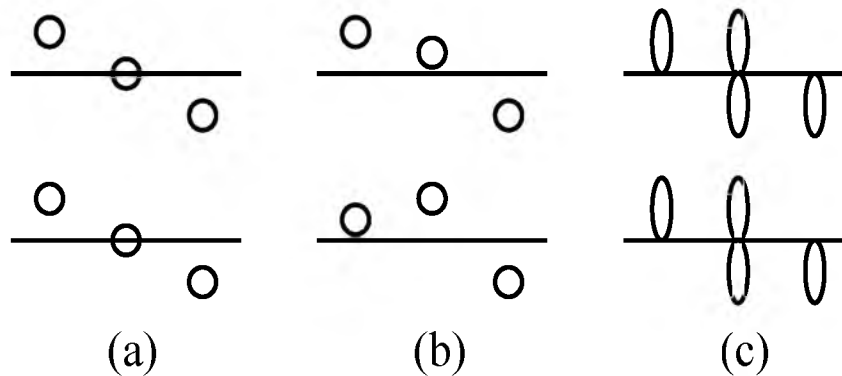


Figure 1.7: Caricatural pictures of (a) the HoD_3 structures, (b) the broken symmetry structure, and (c) the superposition of 4 broken symmetry structures.

the H(M) atoms in the wave-like fashion indicated in Fig. 4.2 the unit cell becomes three times larger in the ab -plane and the HoD_3 structure is recovered. Along with the described displacements of the H(M) atoms the H(T) atoms are also slightly displaced from their positions in the LaF_3 structure. This is described in detail in references [14] and [31].

The positions of the H(M) atoms with respect to the metal planes provide a simplified but very compact way to represent the different lattice structures proposed for YH_3 in a unique way. We indicate the proposed lattice structures of YH_3 very schematically by plots which are derived from the right picture of Fig. 4.2, but from which the tetrahedral planes are excluded. In this way we obtain for the HoD_3 structure the picture given in Fig. 1.7 (a). In a similar caricatural plot of the lattice structure the broken symmetry structure is represented in Fig. 1.7 (b). In this broken symmetry structure *all* the H(M) are moved out the metal-plane. Two out of every three H(M) atoms are about twice as far displaced out of the metal planes as the third H(M) atom. Also the H(T) atoms have slightly different positions as compared to the HoD_3 structure (details can be found in Ref. [31]). These additional hydrogen displacements lower the symmetry of the structure. The glide plane and inversion symmetry operations of the HoD_3 structure do no longer apply. There is a screw axis present now, through the H(M) atoms which are displaced downwards with respect to both yttrium planes in Fig. 1.7 (b). As a result of the symmetry lowering the bands which cross near the Fermi level in the HoD_3 structure have an interaction now and repel each other. This leads to the opening of a considerable band gap,

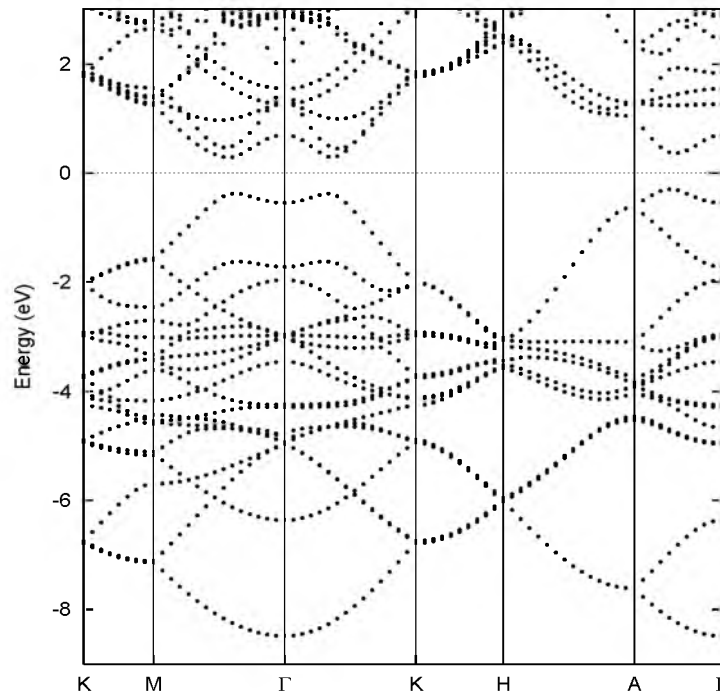


Figure 1.8: *LDA bands for YH_3 in the broken symmetry structure.*

as can be seen from the band structure for YH_3 in the broken symmetry structure in Fig. 1.8. The fundamental band gap is about 0.8 eV along ΓM . At Γ the (direct) gap is about 1.2 eV. Apart from the bands which are responsible for the opening of the gap the band structure is practically identical to that of YH_3 in the HoD_3 structure (cf. Fig. 1.4).

Starting from the HoD_3 structure the symmetry lowering can be established in four different but equivalent ways. By applying those symmetry elements of the HoD_3 structure which no longer exist in the broken symmetry structure (glide and inversion) different representations of this broken symmetry structure can be transformed into each other. If the “average” is taken of these four lattice structures the schematic picture of Fig. 1.7 (c) would be obtained. This average structure has the high symmetry of the HoD_3 structure again. Since the total energy difference between the HoD_3 structure and the broken symmetry structures is small and comparable to the zero point energy, the system should be in a superposition of broken symmetry structures, and appear to have the HoD_3 structure in diffraction.

1.6 Aim of this thesis

This thesis deals with the nature of the large band gap in YH_3 and LaH_3 . We discuss to what extent the LDA calculations fail to describe the switchable mirror experiments, and investigate both proposed explanations for the large band gap in these materials. We shall study from first principles the effects of correlations, beyond those included in LDA calculations, on the quasi-particle band structures of YH_3 and LaH_3 . In the discussed model calculations only a very limited number of rather complicated local electron-electron correlations is included, and the final results in these calculations rely on the choice of free parameters. Strong local electron correlations may indeed be important in these systems. But before subscribing this conclusion, we first study the more obvious problems an LDA description of YH_3 might suffer from. There is a well-known problem with the LDA lowest Kohn-Sham level in a single-electron hydrogen atom [39]. This ionization level is only about half the exact binding energy of 1 Ry (13.6 eV), although the total energy of H^0 is very good. Therefore, the bands in YH_3 derived from this atomic state may be positioned too high in energy in such an LDA calculation. Since DFT-LDA calculations are ground state calculations this method should not be blamed for producing a single-particle gap in the Kohn-Sham spectrum which is much too low for LaH_3 and YH_3 . In fact, it is well known that DFT-LDA calculations underestimate band gaps for many semiconductors and insulators [40-42]. It is possible to obtain the single-particle excitation energies much more accurately directly from the single-particle's Green's Function. This Green's Functions can be obtained from Dyson's equation, and expressions for the self-energy operator in this equation can be systematically derived from many-body perturbation theory. Usually such calculations are performed in the so-called *GW* approximation [43-45] to the self-energy operator. They produce excellent results for a wide range of materials [46-49].

Concerning the strong electron-phonon coupling mechanism, we reconsider the prediction of the LDA total energy calculations that YH_3 has a lattice structure which slightly differs from the HoD_3 structure. From the NPD experiments by Udovic *et al.* [28] which were refined using the HoD_3 structure, unusually large anisotropic temperature factors have been found for the deuterium atoms, in particular for the metal-plane deuterium atoms (denoted by D(M)). Udovic *et al.* have proposed a measure of disorder on this D(M) sublattice. They have incorporated this in their refinement by defining additional, fractionally occupied sites for these atoms. The atoms involved in this order-disorder equilibrium are exactly those atoms

which are displaced from their high symmetry positions in the proposed symmetry-breaking. Therefore, it has been suggested that the symmetry-lowering displacements might have been overlooked in the interpretation of the experimental data [50]. However, also in low temperature NPD experiments [51] small additional Bragg peaks in the powder diffraction pattern due to the proposed symmetry lowering are not found and thermal broadening could be excluded as an explanation for this failure. It is conceivable though that large hydrogen zero point motion could reconcile the measured powder diffraction pattern with the broken symmetry structure [50].

We present the results of *ab-initio* calculations of the phonon dispersion curves of YD_3 and YH_3 . The root mean square displacements of the atoms, the Debye-Waller factors, as well as the ellipsoids of thermal and zero point motion are obtained from the calculated eigenvalues and eigenvectors of the dynamical matrix. The Debye-Waller factors can be compared directly to the values derived from the NPD experiments for YD_3 . They may also reveal whether the additional peaks expected for a broken symmetry structure have escaped detection as a result of large zero point motion. In addition we interpret neutron vibrational spectroscopy (NVS) data for YH_3 obtained by Udovic *et al.* [52,53]. From the calculated eigenvectors we can identify the modes of vibration which predominate in particular energy ranges.

Complicating the issue of the lattice structure of YH_3 even further, Udovic *et al.* [54] have very recently found that the results of NPD experiments for thin epitaxial films of YD_3 are also consistent with $\text{P6}_3\text{cm}$ symmetry. Kierey *et al.* [55] have concluded from the results of Raman spectroscopy measurements that YH_3 films have either $\text{P6}_3\text{cm}$ symmetry or P6_3 symmetry (broken symmetry structure), but not the high $\text{P}\bar{3}\text{c1}$ symmetry of the HoD_3 structure. In our calculations for the lattice dynamics we also study the phonon spectrum of YH_3 in this $\text{P6}_3\text{cm}$ symmetry structure. The LDA spectrum for YH_3 in this structure is very similar to the results obtained for YH_3 in the HoD_3 structure. It is plotted in Fig. 1.9

The final chapter of this thesis deals with another class of materials, known as hexaborides. Very recently it was discovered that La-doped alkaline-earth hexaboride compounds exhibit ferromagnetism at high temperatures and low dopant concentrations. The results of *GW* calculations for CaB_6 question explanations which have been given in literature for the ferromagnetic behaviour of these systems.

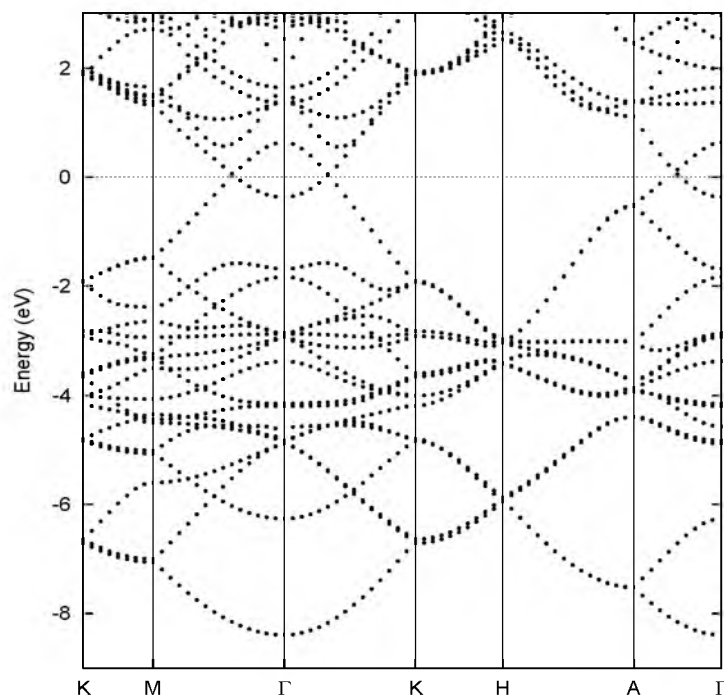


Figure 1.9: LDA bands for YH_3 in the structure with $P6_3cm$ symmetry.

References

- [1] E. Wigner, and H.B. Huntington, *J. Chem. Phys.* **3**, 764 (1935).
- [2] N.W. Ashcroft, *Phys. Rev. Lett.* **21**, 1748 (1968).
- [3] A.E. Carlsson, and N.W. Ashcroft, *Phys. Rev. Lett.* **50**, 1305 (1983).
- [4] J.N. Huiberts, R. Griessen, J.H. Rector, R.J. Wijngaarden, J.P. Dekker, D.G. de Groot, and N.J. Koeman *Nature (London)* **380**, 231 (1996).
- [5] J.N. Huiberts, J.H. Rector, R.J. Wijngaarden, S. Jetten, D. de Groot, B. Dam, N.J. Koeman, R. Griessen, B. Hjörvarsson, S. Olafsson, and Y.S Cho, *J. Alloys and Compounds* **239**, 158 (1996).
- [6] M. Kremers, N.J. Koeman, R. Griessen, P.H.L. Notten, R. Tolboom, P.J. Kelly, and P.A. Duine, *Phys. Rev. B* **57**, 4943 (1998).
- [7] P.H.L. Notten, M. Kremers, and R. Griessen, *J. Electrochem. Soc.* **143**, 3348 (1996).

-
- [8] P. van der Sluis, M. Ouwerkerk, and P.A. Duine, *Appl. Phys. Lett.* **70**, 3356 (1997).
- [9] P. van der Sluis, *Appl. Phys. Lett.* **73**, 1826 (1998).
- [10] R. Armitage, M. Rubin, T. Richardson, N. O'Brien, Y. Chen, *Appl. Phys. Lett.* **70**, 3356 (1997)
- [11] R. Wijngaarden, J.N. Huiberts, D. Nagengast, J.H. Rector, R. Griessen, M. Hanfland, and F. Zontone, *J. Alloys and Compounds* **308**, 44 (2000).
- [12] J.P. Dekker, J. van Ek, A. Lodder, and J.N. Huiberts, *J. Phys. Condens. Matter* **5**, 4805 (1999).
- [13] Y. Wang and M.Y. Chou, *Phys. Rev. Lett.* **71**, 1226 (1993).
- [14] Y. Wang and M.Y. Chou, *Phys. Rev. B* **51**, 7500 (1995).
- [15] A.T.M. van Gogh E.S. Kooij and R. Griessen, *Phys. Rev. Lett.* **83**, 4614 (1999).
- [16] M.W. Lee and W.P. Shin, *J. Appl. Phys.* **86**, 6798 (1999).
- [17] J.N. Huiberts, R. Griessen, R.J. Wijngaarden, M.Kremers, and C. van Haesendonck *Phys. Rev. Lett.* **79**, 3724 (1997).
- [18] P. Hohenberg, and W. Kohn, *Phys. Rev.* **136**, 864 (1964).
- [19] W. Kohn, and L.J. Sham, *Phys. Rev.* **140**, 1133 (1965)
- [20] A.C. Switendick, *Sol. State Comm.* **8**, 1463 (1970).
- [21] G.A. de Wijs, private communication.
- [22] D.J. Peterman, B.N. Harmon, J. Marchiando, and J.H. Weaver, *Phys. Rev. B* **19**, 4867 (1979).
- [23] J.H. Weaver, D.T. Peterson, and R.L. Renbow, *Phys. Rev. B* **19**, 4855 (1979).
- [24] J.H. Weaver, D.T. Peterson, and R.L. Renbow, *Phys. Rev. B* **20**, 5301 (1979).
- [25] R. Stumpf and M. Scheffler, *Computer Physics Communications* **79**, 447 (1994).
- [26] M. Mannsmann and W.E Wallace, *J. Phys. (Paris)* **25**, 454 (1964).
- [27] N.F. Miron, V.I. Shcherbak, V.N. Bykov, and V.A. Levдик, *Sov. Phys. Crystallog.* **17**, 342 (1972).
- [28] T.J. Udovic, Q. Huang, and J.J. Rush, *J. Phys. Chem. Solids* **57**, 423 (1996).

- [29] A. Remhof, G. Song, K. Theis-Bröhl, and H. Zabel, *Phys. Rev. B* **56**, R2897 (1997).
- [30] A. Remhof, G. Song, Ch. Sutter, R. Siebrecht, H. Zabel, F. Güthoff and J. Windgasse, *Phys. Rev. B* **59**, 6689 (1999).
- [31] P.J. Kelly, J.P. Dekker, and R. Stumpf, *Phys. Rev. Lett.* **78**, 1315 (1997).
- [32] D.J. Peterman, J.H. Weaver, and D.T. Peterson, *Phys. Rev. B* **23**, 3903 (1981).
- [33] M. Gupta and J.P. Burger, *Phys. Rev. B* **26**, 5634 (1982).
- [34] D.K. Misemer and B.N. Harmon, *Phys. Rev. B* **26**, 5634 (1982).
- [35] N.I. Kulikov, *J. Less Common Metals* **88**, 307 (1982).
- [36] K.K. Ng, F.C. Zhang, V.I. Anisimov, and T.M. Rice, *Phys. Rev. Lett.* **78**, 1311 (1997).
- [37] K.K. Ng, F.C. Zhang, V.I. Anisimov, and T.M. Rice, *Phys. Rev. B* **59**, 5398 (1999).
- [38] R. Eder, H.F. Pen, and G.A. Sawatzky, *Phys. Rev. B* **56**, 10115 (1997).
- [39] O. Gunnarsson, B.I. Lundqvist, and J.W. Wilkins, *Phys. Rev. B* **10**, 1319 (1974).
- [40] L.J. Sham, M. Schlüter, *Phys. Rev. Lett.* **51**, 1888 (1983).
- [41] L.J. Sham, M. Schlüter, *Phys. Rev. B* **32**, 3883 (1983).
- [42] J.P. Perdew, M. Levy, *Phys. Rev. Lett.* **51**, 1884 (1974).
- [43] L. Hedin, *Phys. Rev.* **139** A796 (1963).
- [44] F. Aryasetiawan and O. Gunnarsson, *Rep. Prog. Phys.* **61**, 237 (1998).
- [45] L. Hedin, *J. Phys. Condens. Matter* **11**, R489 (1999).
- [46] M.S. Hybertsen, and S.G. Louie, *Phys. Rev. Lett.* **55**, 1418 (1985).
- [47] M.S. Hybertsen, and S.G. Louie, *Phys. Rev. B* **34**, 5390 (1988).
- [48] R.W. Godby, M. Schlüter, and L.J. Sham, *Phys. Rev. Lett.* **56**, 2415 (1986).
- [49] R.W. Godby, M. Schlüter, and L.J. Sham, *Phys. Rev. B* **37**, 10159 (1988).
- [50] P.J. Kelly, J.P. Dekker, and R. Stumpf, *Phys. Rev. Lett.* **79**, 2920 (1997).

-
- [51] T.J. Udovic, J.J. Rush, Q. Huang, and I.S. Anderson, Phys. Rev. Lett. **79**, 2920 (1997).
- [52] T.J. Udovic, and J.J. Rush, Q. Huang, and I.S. Anderson, J. Alloys and Compounds **253-254**, 241 (1997).
- [53] T.J. Udovic, Q. Huang, and J.J. Rush, Mat. Res. Soc. Symp. Proc. **513**, 197 (1998)
- [54] T.J. Udovic, Q. Huang, R.W. Erwin, B. Hjörvarsson, and R.C.C. Ward, Phys. Rev. B **61**, 12701 (2000).
- [55] H. Kierey, M. Rode, A. Jacob, A. Borgschulte, and J. Schoenes, Phys. Rev. B **63**, 134109 (2001).

Chapter 2

Quasi-particles in YH_3

ABSTRACT

Electronic structure calculations for YH_3 within the local density approximation result in a metallic ground state with the bands at the Fermi energy overlapping by more than 1 eV, whereas a band gap of 2.8 eV is deduced from optical experiments. Here, we report the results of parameter-free GW calculations which predict a fundamental gap of 1 eV. When we take into account electric dipole matrix elements a large optical gap of almost 3 eV is obtained. A combination of photoemission and inverse photoemission spectroscopy could test the prediction of a small fundamental band gap.

This chapter is based on: *Parameter-free quasi-particle calculations for YH_3* , P. van Gelderen, P.A. Bobbert, P.J. Kelly, and G.Brocks, Phys. Rev. Lett. **85**, 2989 (2000).

Recently, Huiberts *et al.* [1] discovered a spectacular metal-insulator (MI) transition in thin films of YH_x and LaH_x as x approaches 3. In the metallic dihydride phase these layers appear mirror-like, whereas the insulating trihydride phase is transparent for visible light. The transition is reversible, and occurs at room temperature and at moderate hydrogen pressures, making it easy to observe experimentally. Because the hydrogen-to-yttrium ratio can be easily varied these layers can be used as “switchable mirrors”, which opens up the possibility of a range of interesting technological applications. Since the basic mechanism underlying the MI transition is still poorly understood, progress in trying to improve the performance of switchable mirror devices is made largely empirically.

The absorption edge of YH_3 is found at 2.8 eV in optical reflection and transmission experiments [2]. Since these experiments probe only symmetry-allowed direct transitions, the fundamental band gap may be quite different. The strongest evidence for the existence of a fundamental band gap comes from the increase of the electrical resistivity by at least two orders of magnitude as the trihydride phase is formed [1]. The negative temperature coefficient of the resistivity and its inverse proportionality to δ in substoichiometric $\text{YH}_{3-\delta}$ support the conclusion that YH_3 is a semiconductor. Unfortunately, it has not been possible to obtain an estimate of the size of the fundamental gap from the temperature dependence of the resistivity measurements [3].

It is the purpose of the present paper to provide a coherent picture of the electronic structure of YH_3 consistent with all experimentally known data without introducing any unknown parameters. We will argue that the fundamental band gap of YH_3 is only 1.0 eV and that vanishing electric dipole matrix elements prevent this transition from being seen in the optical experiments performed up till now. Our conclusions are based on calculations of the single-particle excitation spectrum within the dynamically screened GW approximation [4].

There is a huge discrepancy between the measured gap of 2.8 eV and the value calculated using the local density approximation (LDA) of density functional theory (DFT). These calculations predict band *overlaps* of about 1.3 eV [5,6] for YH_3 in the experimentally observed, so-called HoD_3 structure [7,8]. LDA calculations are known to severely underestimate the band gaps of many materials [9,10], but the present discrepancy is exceptionally large. Because this discrepancy is comparable to what is found in transition metal oxides such as NiO , where a strong Coulomb interaction between the transition metal d electrons plays an important role and is poorly de-

scribed by the LDA, it has been suggested that a similarly strong Coulomb interaction between the electrons on hydrogen sites may be responsible for the large gap in YH_3 . On the basis of parameterized model Hamiltonians for LaH_3 and YH_3 , respectively, Ng *et al.* [11] and Eder *et al.* [12] showed that such correlated models can indeed lead to the formation of large band gaps. These authors adopt an atomic-like viewpoint in which the metal ions donate their outer three electrons to the hydrogen atoms, and view these materials essentially as lattices of H^- ions perturbed by the metal ion sublattice. They argue that large correlation effects in a H^- ion are not well accounted for in an LDA calculation causing the H-derived valence bands in YH_3 to overlap with the Y-derived conduction bands.

Apart from the issue of strong correlations, there is an obvious problem associated with the LDA description of atomic hydrogen even on the single-particle level. Although the LDA total energy of the single electron H^0 is very close to the exact value, the $1s$ eigenvalue of the Kohn-Sham (KS) equation is only roughly half the exact $1s$ electron binding energy [13]. As a result, the position of the LDA bands derived from the atomic $1s$ state may differ considerably from the true position of the corresponding one-electron levels. It is also well known that, in general, the KS eigenvalues - the conventional one-electron band structure - if interpreted as one-electron excitations, severely underestimate the electronic band gap, even for materials such as Si or Ge which are not strongly correlated [14,15]. In order to examine the one-particle excitation energies, one should solve Dyson's equation for the single-particle Green's function expressed in terms of the self-energy operator Σ . The self-energy operator can be expanded as a perturbation series in the Green's function G and the dynamically screened Coulomb interaction W . The so-called GW approximation introduced by Hedin [4] includes only the first term in this series, which is symbolically written as GW . In addition, one usually assumes a quasi-particle (QP) expression for the Green's function G . For a large number of semiconductors and insulators such calculations produce band gaps which are very close to experimental single-particle band gaps [9,10,16]. Even for transition metal oxides such as NiO [17] and MnO [18] where electron correlations play a considerable role, GW calculations produce gaps which are much closer to experiment than the values obtained in LDA calculations. The large discrepancy between the LDA and experimental band gaps in YH_3 make it particularly challenging to perform a GW calculation for this system.

In our GW calculations we use the space-time approach suggested by Rojas *et al.* [19] and essentially follow the implementation described by van der

Horst *et al.* [20]; details will be published separately later. Input data for the GW calculation consist of the electronic wave functions and energies obtained from LDA calculations [21]. For an Y_2H_6 unit cell with the so-called LaF_3 structure (see below) we used a $(6 \times 6 \times 4)$ \mathbf{k} -set, an $(8 \times 8 \times 14)$ real-space grid, and a total of 200 bands in the GW calculation. By varying the size of the real space and reciprocal space grids we estimate that QP energies are converged within 0.1 eV. The convergence with respect to the time and frequency grids, and with respect to the number of unoccupied bands included in the calculation, is even better. For the Y_6H_{18} unit cell (the HoD_3 structure, see below) we used a $(4 \times 4 \times 4)$ \mathbf{k} -set, a $(12 \times 12 \times 12)$ real-space grid, and 300 bands. We have studied the effect of including the nondiagonal matrix elements of the self-energy operator (using the LDA wave functions as a basis set) when solving the QP equation. This does not significantly change the results as compared to a calculation in which only the diagonal elements of Σ are included, except in the case of the broken symmetry structure to be discussed later. This means that the QP wave functions are practically identical to their LDA counterparts. We iterate the GW scheme by updating the QP energies in both G and W .

The crystal structure of YH_3 extracted from experiment has a Y_6H_{18} unit cell, which was first found for HoD_3 [7,8]. This rather complex structure can be derived from a simple, hexagonal LaF_3 structure with a Y_2H_6 unit cell by means of a Peierls distortion which triples the unit cell in the basal plane [6]. We use our results for YH_3 in the simpler LaF_3 structure as a starting-point, because they are easier to discuss and to interpret, yet still contain the essential features of the results for the actual (HoD_3) structure. First we discuss the LDA band structures for YH_3 in the LaF_3 and HoD_3 structures and then we present our GW results.

The LDA bands for YH_3 in the LaF_3 structure are shown in Fig. 7.1(a). Throughout the Brillouin zone the bands around the Fermi level, marked by a circle and a triangle, are well separated by a direct gap. This separation is about 0.6 eV at Γ and 2.3 eV at K. However because the minimum of the upper band at K (circle) is lower than the maximum of the lower band at Γ (triangle) this leads to a semimetal. The indirect band overlap is about 1.3 eV. The unit cell of the HoD_3 structure is three times larger than that of the LaF_3 structure in the basal ab plane. When the LaF_3 unit cell is tripled, the LDA bands originally at Γ of course remain at Γ . In addition, two new bands appear at Γ which result from folding in the bands from K in the original larger Brillouin zone (BZ). The result of this folding is shown in Fig. 7.1(b) for the bands near Γ , using symbols as in Fig. 7.1(a).

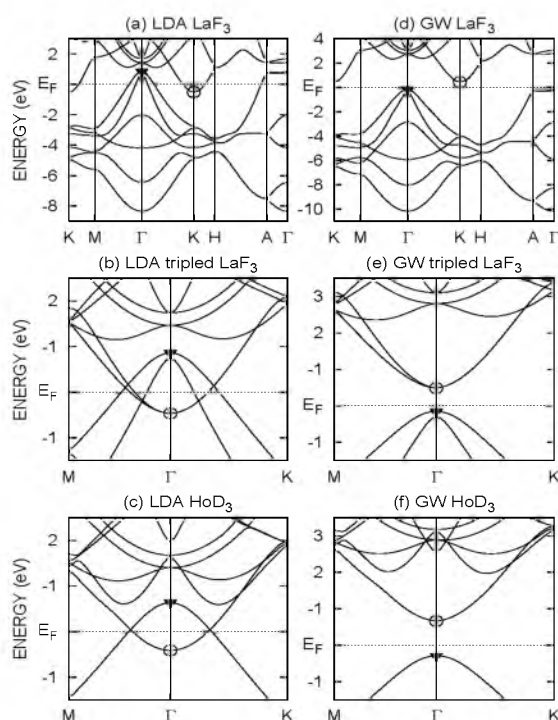


Figure 2.1: LDA electron bands for YH_3 in (a) the LaF_3 structure, (b) the tripled LaF_3 structure, and (c) the HoD_3 structure. The corresponding GW band structures (d-f) are obtained from the LDA bands by linear interpolation of the calculated QP corrections found for the \mathbf{k} -points included in the GW calculation. The circles refer to the bands which are folded back from K to Γ when the Y_2H_6 unit cell is tripled. The triangles mark bands which are originally at Γ

The indirect band overlap between Γ and K in the LaF_3 unit cell becomes a direct overlap at Γ in the BZ of the tripled unit cell. In the actual HoD_3 structure small displacements of the hydrogen atoms lead to a lowering of the symmetry in the tripled unit cell. These symmetry-breaking hydrogen displacements move one pair of bands, which overlap at Γ , away from the Fermi level. The remaining symmetry in the HoD_3 structure still allows for an overlap between the other pair of bands (which differ in symmetry). The result is shown in Fig. 7.1(c).

The results of our GW calculation for YH_3 in the LaF_3 structure are shown in Fig. 7.1(d). Compared to the LDA results of Fig. 7.1(a), the most promi-

nent feature is that the separation between the valence and the conduction bands is increased and an indirect band gap of 0.6 eV opens between Γ and K. The GW calculation thus predicts YH_3 to be semiconducting in the LaF_3 structure in contrast to the semimetal obtained in LDA. The small indirect band gap (0.6 eV) is not easily measured in an optical experiment since the strongest optical transitions are \mathbf{k} -conserving. The calculated direct gap at Γ is 2.9 eV, which corresponds very well to the experimentally observed optical gap. (This result is in fact quite similar to what is found for silicon, which has an indirect band gap of 1.2 eV but a direct optical gap of about 3 eV.) The QP corrections to the valence bands obtained from this GW calculation are largest for the lowest valence bands. As a result of this the total valence band width actually increases by about 9% as compared to the LDA calculation, to 10 eV. In the Brillouin zone of the tripled unit cell the small indirect ΓK gap is folded into a direct gap at Γ as shown in Fig. 7.1(e). In the absence of any structural change, the dipole matrix elements connecting the folded highest valence and lowest conduction bands vanish identically, so that the optical gap of 2.9 eV is between the highest valence band and the third conduction band at the Γ point in the reduced Brillouin zone, cf. Fig. 7.1(e).

We next perform a GW calculation for YH_3 in the HoD_3 structure, the results of which are shown in Fig. 7.1(f). As before, compared to the LDA calculation (Fig. 7.1(c)) we find that the conduction bands are shifted upwards and the valence bands are shifted downwards in energy. The overall valence band width is about 10 eV, as for the LaF_3 structure. This is in contrast with the results for model calculations by Ng *et al.* [11] who find a large decrease of the valence band width in LaH_3 . The GW calculation gives a direct gap at Γ of 1.0 eV for YH_3 in the HoD_3 structure, which is substantially larger than the 0.6 eV found for the LaF_3 structure (part of this difference is already present in the LDA calculation; the overlap of the corresponding LDA bands is 1.1 eV for the HoD_3 and 1.3 eV for the LaF_3 structure). Again, the symmetry-breaking hydrogen displacements in the HoD_3 structure push some of the GW bands away from the Fermi level; compare Figs. 7.1(e) and 7.1(f). The QP wave functions are practically identical to the LDA wave functions, which implies that, in the absence of strong electron hole interaction (i.e. strong excitonic effects), the matrix elements for optical transitions are unchanged. The symmetry-breaking hydrogen displacements induce additional oscillator strength between some pairs of bands but, crucially for YH_3 , not between the highest valence and the lowest conduction band. Between these two bands electric dipole tran-

sitions remain forbidden. The optical gap will therefore be given by the energy separation between the highest valence and the *second* conduction band, between which an electric dipole transition is allowed. This optical gap is 2.9 eV at Γ ; the gap is probably a few tenths of an eV smaller along the ΓM direction [21]. Our *GW* calculation then produces an optical gap which is in excellent agreement with experiment. The fundamental band gap of 1.0 eV is much smaller than the optical gap. Experimentally, this may be verified by means of a combination of photoemission and inverse photoemission spectroscopy.

Previous LDA total energy calculations predicted the existence of yet another structure in which additional displacements of the hydrogen atoms result in a further lowering of the symmetry of the HoD_3 structure, without increasing the size of the unit cell [22]. The additional hydrogen displacements lower the total energy slightly and open up a band gap of 0.8 eV in the LDA band structure [22]. So far no evidence for this broken symmetry structure has been found experimentally [2,23,24]. At the same time, however, the HoD_3 structure does not account for all details of the experimental structure determination of YH_3 [25,26] so that the relevance of the structure found in Ref. [22] remains unclear. In order to test the sensitivity of our results to the structure, we have also performed a *GW* calculation for this broken symmetry structure. We find that in this case it is important to include non-diagonal elements of the self-energy Σ in the LDA basis functions when solving the QP equation. Apparently, in order to describe the QP wave functions properly, one has to involve a substantial mixing of the LDA basis functions. Accompanying this mixing is a qualitative change in the shape of the highest valence band and the lowest conduction band going from the LDA to the *GW* band structure. The additional hydrogen displacements break the symmetry in such a way that an avoided crossing is introduced at the Fermi level in the LDA band structure between the highest valence and the lowest conduction bands in Fig. 7.1(c), see Ref. [22]. The *GW* bands of the broken symmetry structure around the Fermi level however resemble the ones shown in Fig. 7.1(f), showing - correctly - no sign of an avoided crossing. The *GW* calculation yields a fundamental band gap at Γ with a value of 1.4 eV. Breaking the symmetry will, in general, induce a finite oscillator strength between states for which it vanished by symmetry in the HoD_3 structure. So compared to the latter, the broken symmetry structure has a larger fundamental, and a smaller optical gap. Because of the lack of experimental evidence for this structure, we have refrained from a (very expensive) calculation of the detailed optical spec-

trum. Since the GW calculations result in gaps for both the HoD_3 and the broken symmetry structures, the latter no longer plays the pivotal role in the MI transition assigned to it by the LDA calculations [22].

Model calculations by Eder *et al.* focus on the (de)localization of the hydrogen orbital, which strongly depends upon the local charge or occupancy. Within a mean-field model this so-called “breathing” of the hydrogen orbitals results effectively in a downward shift of the on-site hydrogen levels [12]. At the mean-field level this breathing effect is already included in the LDA calculations (indeed it is included in any calculation that treats local charges/occupancies self-consistently). In our GW calculation, which incorporates a more accurate treatment of exchange and correlation, we find that the wave functions are not significantly changed as compared to LDA. We conclude that the quasi-particle band structure adequately describes the band gap in YH_3 and we do not need to invoke additional strong local correlations [11,12].

Roughly half of the large discrepancy between LDA calculations and the experimentally observed band gap is a consequence of the fact that in YH_3 the optical and the fundamental gap are not the same due to vanishing matrix elements for optical transitions in the range between 1 and 3 eV (an effect which is neglected in References 11 and 12). The origin of the remaining discrepancy, which is well resolved by the GW method, can be traced to the failure of LDA to describe the $1s$ eigenvalue of the neutral hydrogen atom. This is a well-understood artifact arising from the incomplete cancellation of the (fictitious) electron self-interaction by the local exchange-correlation potential [13]. We attribute the opening of a gap in YH_3 by GW to the correction of this artifact.

The picture of YH_3 which we derive from our parameter-free calculations is that of a simple compound semiconductor. We construct the solid with neutral H^0 and Y^0 atoms. Because the ionization energy of atomic H^0 is twice as large as that of Y^0 , charge is transferred from Y to H when the interaction between the neutral atoms is switched on. As a result, H acquires a negative charge (in agreement with electromigration experiments [27]). This causes the levels derived from the H $1s$ states to shift upwards in energy and the Y-derived levels to move downwards. Overlap of the valence orbitals on neighboring atoms leads to covalent interaction and the atomic levels broaden into bands. The charge transfer to hydrogen also causes the atomic orbital to delocalize leading to increased band width. These effects must be taken into account by a self-consistency procedure. However, because the LDA calculation for atomic H^0 places the $1s$ eigenvalue at -0.5 Rydberg

rather than at -1 Rydberg the difference between the Y and H on-site energies is severely underestimated to start with. As a result the band centers of the valence and conduction bands are too close and the bands overlap.

Future research should focus upon the role of point defects (such as hydrogen vacancies) and their effect on the metal-insulator transition. We note, however, that electron correlations which are small in the host material, cannot be automatically ignored when considering defects. For example, the states belonging to a vacancy in silicon are found to be very localized [28,29] and their charge dependent behavior is described well by an Anderson (negative-U) model Hamiltonian with U approximately equal to 0.3 eV [28]. This value of U is comparable in size to the bandgap of Si and the energy change associated with the local lattice distortions. However, it can be safely ignored for bulk silicon because it is negligible compared to the valence bandwidth of 12 eV.

Note added: After this work was accepted for publication we became aware of similar calculations for YH_3 in the cubic BiF_3 and hexagonal LaF_3 structures by Miyake *et al.* [30].

References

- [1] J.N. Huiberts, R. Griessen, J.H. Rector, R.J. Wijngaarden, J.P. Dekker, D.G. de Groot, and N.J. Koeman *Nature (London)* **380**, 231 (1996).
- [2] A.T.M. van Gogh E.S. Kooij and R. Griessen, *Phys. Rev. Lett.* **83**, 4614 (1999).
- [3] J.N. Huiberts, R. Griessen, R.J. Wijngaarden, M.Kremers, and C. van Haesendonck *Phys. Rev. Lett.* **79**, 3724 (1997).
- [4] L. Hedin, *Phys. Rev.* **139** A796 (1963).
- [5] J.P. Dekker, J. van Ek, A. Lodder, and J.N. Huiberts, *J. Phys. Condens. Matter* **5**, 4805 (1999).
- [6] Y. Wang and M.Y. Chou, *Phys. Rev. Lett.* **71**, 1226 (1993); *Phys. Rev. B* **51**, 7500 (1995).
- [7] N.F. Miron, V.I. Shcherbak, V.N. Bykov, and V.A. Levдик, *Sov. Phys. Crystallog.* **17**, 342 (1972).
- [8] T.J. Udovic, Q. Huang, and J.J. Rush, *J. Phys. Chem. Solids* **57**, 423 (1996).

- [9] M.S. Hybertsen, and S.G. Louie, Phys. Rev. Lett. **55**, 1418 (1985); Phys. Rev. B **34**, 5390 (1988).
- [10] R.W. Godby, M. Schlüter, and L.J. Sham, Phys. Rev. Lett. **56**, 2415 (1986); Phys. Rev. B **37**, 10159 (1988).
- [11] K.K. Ng, F.C. Zhang, V.I. Anisimov, and T.M. Rice, Phys. Rev. Lett. **78**, 1311 (1997); Phys. Rev. B **59**, 5398 (1999).
- [12] R. Eder, H.F. Pen, and G.A. Sawatzky, Phys. Rev. B **56**, 10115 (1997).
- [13] O. Gunnarsson, B.I. Lundqvist, and J.W. Wilkins, Phys. Rev. B **10**, 1319 (1974).
- [14] L.J. Sham, M. Schlüter, Phys. Rev. Lett. **51**, 1888 (1983); Phys. Rev. B **32**, 3883 (1983).
- [15] J.P. Perdew, M. Levy, Phys. Rev. Lett. **51**, 1884 (1974).
- [16] For recent reviews of the *GW* method and its applications see F. Aryasetiawan and O. Gunnarsson, Rep. Prog. Phys. **61**, 237 (1998) or L. Hedin, J. Phys. Condens. Matter **11**, R489 (1999).
- [17] F. Aryasetiawan and O. Gunnarsson, Phys. Rev. Lett. **74**, 3221 (1995).
- [18] S. Massidda *et al.*, Phys. Rev. Lett. **74**, 2323 (1995).
- [19] H.N. Rojas, R.W. Godby, and R.J. Needs, Phys. Rev. Lett. **74**, 1827 (1995).
- [20] J.-W. van der Horst, P.A. Bobbert, P.H.L. de Jong, M.A.J. Michels, G.Brocks, and P.J. Kelly, Phys. Rev. B **61**, 15817 (2000)
- [21] In the real-space, imaginary-time implementation of the *GW* method we include only a limited number of \mathbf{k} -points on a grid for which we calculate QP corrections to the LDA energies. If we interpolate linearly the QP corrections in between these \mathbf{k} -points, we find a minimum gap of 2.6 eV between bands 18 and 20 along ΓM .
- [22] P.J. Kelly, J.P. Dekker, and R. Stumpf, Phys. Rev. Lett. **78**, 1315 (1997).
- [23] T.J. Udovic, Q. Huang, and J.J. Rush, Phys. Rev. Lett. **79**, 2920 (1997).
- [24] A. Remhof *et al.*, Phys. Rev. B **59**, 6689 (1999).
- [25] T.J. Udovic, Q. Huang, and J.J. Rush, Mat. Res. Soc. Symp. Proc. **513**, 197 (1998).
- [26] J.J. Balbach *et al.*, Phys. Rev. B **58**, 14823 (1998).
- [27] F.J.A. den Broeder *et al.*, Nature **394**, 656 (1998)

- [28] J. Bernholc, N.O. Lipari, and S.T. Pantelides, Phys. Rev. B **21**, 3545 (1980)
- [29] G.A. Baraff, E.O. Kane, and M. Schlüter, Phys. Rev. B **21**, 5662 (1980)
- [30] T. Miyake, F. Aryasetiawan, H. Kino, and K. Terakura, Phys. Rev. B **61**, 16491 (2000).

Chapter 3

GW calculations for YH_3

ABSTRACT

In recent optical experiments for YH_3 , a large band gap of almost 3 eV has been observed. In contrast, calculations within the local density approximation (LDA) result in a semimetallic band structure with a band overlap near the Fermi level of more than 1 eV. This unusually large discrepancy between the LDA results and experiment has led to suggestions that strong local correlation effects, similar to those found in transition metal oxides, are important in YH_3 . Here we conclude from parameter-free quasi-particle calculations within the GW approximation that YH_3 is essentially a conventional semiconductor. We argue that the experimental results can be fully understood in band structure terms without invoking strong local correlations. The unusually large error in the band structure made by LDA is traced to its poor description of the electronic structure of the hydrogen atom. Our GW results predict a fundamental band gap of only 1 eV and an optical gap of 2.6 eV, the difference being due to vanishing matrix elements for optical transitions at lower energies. Our prediction of a small fundamental gap could be experimentally confirmed by a combination of photoemission and inverse photoemission experiments.

This chapter is based on: *Single-particle electronic excitations in YH_3* , P. van Gelderen, P.A. Bobbert, P.J. Kelly, G.Brocks, and R. Tolboom, submitted to Phys. Rev. B.

3.1 Introduction

Of the reversible effects recently found on exposing various metals to hydrogen [1,2], the most striking must surely be the “switchable mirror” effect discovered by Huiberts *et al.* [3]. The “mirror” essentially consists of a thin layer of yttrium (or lanthanum, or any rare earth metal) on top of a transparent (glass) substrate, which can be loaded with hydrogen by exposing it to hydrogen gas [3] or by electrochemical techniques [4]. The switching effect was first discovered in yttrium, which is probably still the material studied in most detail experimentally. On exposure to hydrogen, yttrium dihydride is easily formed. Like yttrium, YH_2 is a metal and it reflects light in the visible spectrum. If the amount of hydrogen in the yttrium film is increased, YH_x exhibits a metal-insulator (MI) transition at a hydrogen-to-yttrium ratio x of about 2.8. The material becomes transparent to visible light and its resistivity increases by at least two orders of magnitude [5]. The MI transition is reversible in the sense that the metallic dihydride phase can be readily recovered (for instance, by reducing the hydrogen pressure), hence the name “switchable mirror”. It has attracted a lot of interest as a very spectacular example of a metal-insulator transition and for its technological application potential.

Before the effect can be used in practical applications, a number of properties must be improved. Since the initial discovery of the effect, switching times have been reduced by using multilayer configurations [6]. The colour neutrality as well as the contrast ratios between transparent and reflecting phases have been improved by using alloys which contain magnesium [7]. This considerable progress has been achieved largely empirically. A better understanding of the principles underlying the MI transition in the switchable mirror films should help efforts to improve their switching properties. Yttrium dihydride in its bulk crystalline form has been studied in detail. Its optical and electrical properties were measured by Weaver *et al.* [8,9] and have been successfully interpreted on the basis of first-principles band structure calculations by Peterman *et al.* [10]. Much less is known about the trihydride phase since bulk samples disintegrate on absorbing the additional, third hydrogen. Indeed, it was the mechanical stability of thin film samples that was the key to Huiberts’ discovery [1]. Moreover it is very difficult to obtain truly stoichiometric YH_3 because this requires enormous hydrogen pressures. So far, samples could only be loaded up to $\text{YH}_{3-\delta}$ with $\delta \approx 0.01$ [4]. From the position of the absorption edge and its dependence on δ it was concluded that YH_3 has a large *optical* gap of about 2.8 eV [11,12]. Revised values were recently reported: 2.66 eV by Lee and

Shin [13] and 2.63 ± 0.03 by van Gogh *et al.* [14]. However, the size of the *fundamental* band gap is not known to date. There is a large increase in the resistivity upon formation of the trihydride phase which is inversely proportional to δ [15]. From this and from the increase of the resistivity with decreasing temperature (negative temperature coefficient), it could be concluded that YH_3 was a semiconductor. However, whereas for ordinary semiconductors the size of the fundamental band gap can be extracted from temperature-dependent resistivity measurements, such experiments are difficult to interpret for yttrium-hydride because hydrogen tends to be lost from the thin films when the temperature is increased [5]. The measurements by Huiberts *et al.* [15] actually show an unexpected logarithmic temperature dependence. Such a temperature dependence is characteristic of weak localization in two dimensions, albeit at much lower temperatures. In the present case it has been attributed to the temperature induced formation of hydrogen vacancies which order in defect-rich planes and form a modulated structure. In this scenario, the weak localization occurs in the conducting hydrogen-deficient phase sandwiched between insulating trihydride planes.

In YH_x the MI transition is accompanied by a structural phase change; YH_2 is cubic and YH_3 is hexagonal (as is pure yttrium metal). Since its discovery in YH_x , the MI transition has been observed in other metal-hydride materials, where it is *not* accompanied by a structural phase change. For example, LaH_x also exhibits a MI transition when x is increased from 2 to 3, but the material is cubic in both dihydride and trihydride phases. This suggests that the structural phase change from cubic to hexagonal in YH_x is not essential for the MI transition to occur, and that the origin of the latter is likely to be of an electronic nature.

A simplified picture of the electronic structure of YH_x is constructed as follows. The atomic configuration of yttrium is $[\text{Kr}] 5s^2 4d^1$. In solid metallic yttrium the three valence electrons occupy bands which are derived from the atomic $5s$ and $4d$ states and these valence bands are only partially occupied. Hydrogen introduces additional bands and since it is more electronegative than yttrium one might expect these hydrogen bands to be lower in energy than the yttrium valence bands. Each hydrogen atom brings with it only one electron, so each hydrogen band can accommodate an extra electron. In YH_2 two of the three yttrium valence electrons are transferred to the lower lying ‘hydrogen’ bands. The third yttrium electron stays in an ‘yttrium’ band and YH_2 is a metal. In YH_3 the third yttrium electron is also transferred to the hydrogen bands and there is an energy

gap if the hydrogen bands are separated in energy from the yttrium valence bands. This basically ionic model is appealing but too naive. Considering the chemistry of hydrogen more generally, the ionic species H^- is rarely observed and one would expect the bond to a hydrogen atom to involve a considerable covalent component. In the solid state this would result in hybridization between the hydrogen and yttrium bands, which spoils the simple ionic model discussed above.

Indeed this simple model of the electronic structure of YH_3 was not found in recent state-of-the-art band structures calculated with the local density approximation (LDA) of density functional theory (DFT). DFT-LDA calculations for YH_3 in the so-called HoD_3 structure, which is the lattice structure deduced from experiment [16-18], predict a (large) overlap of the yttrium and the hydrogen bands at the Fermi level [19,20]. Similarly, the best LDA calculations available for LaH_3 at the time predicted a tiny indirect band gap of 3 meV and a direct gap of 0.17 eV [21] or a small band overlap [20]. These calculations clearly contradict the experimental results. The failure of LDA calculations to predict gaps for the trihydrides motivated theorists to propose alternative explanations for the band gaps found in YH_3 and LaH_3 whereby two basically different mechanisms were put forward. The “weak correlation” proposal suggested that the solution should be sought in an improved treatment of the electronic excitations based on standard electron gas theory combined with electron-phonon coupling. The “strong correlation” proposal suggested that the description of the electron-electron interaction on an atomic length scale was the key to understanding the insulating state of the trihydrides.

In their “weak correlation” proposal [22] Kelly *et al.* argued that the zero-value band gap found for LaH_3 made it very similar to Ge which also has a vanishing gap in LDA. The reason for this discrepancy is well understood: it results from an unjustified interpretation of the Kohn-Sham eigenvalues of DFT as excitation energies. LDA band structures are known to systematically underestimate the band gaps of semiconductors and insulators - the so-called “band gap” problem [23,24] and can even predict a material to be a metal rather than a semiconductor as in the case of germanium. To calculate single-particle excitation energies, a quasiparticle equation should be solved in which the local, energy independent exchange-correlation potential of DFT is replaced by a non-local, energy dependent self-energy. Approximations based on electron-gas theory - such as the GW approximation to be discussed below - reproduce the experimental band gaps of semiconductors and insulators very well. By analogy with conventional

semiconductors, Kelly *et al.* argued that such a correction should result in a band gap for LaH₃ but would by itself be insufficient to resolve the much larger discrepancy found for YH₃. Therefore, in addition to the quasiparticle correction, they suggested that electron-phonon coupling played a role in YH₃. LDA total energy calculations in which the lattice structure is optimized predict that a symmetry lowering of the HoD₃ structure leads to a slightly lower total energy (without increasing the size of the unit cell). This Jahn-Teller like distortion leads to a band gap which would qualitatively agree with the experimental data [22]. However, the calculated symmetry-breaking hydrogen displacements have not been confirmed by diffraction experiments, neither for bulk powder samples [25] nor for thin films [26,27] although establishing the positions of all atoms uniquely from the diffraction data has proved to be a difficult task which has still not been resolved satisfactorily [28-30]. To further complicate matters, we have in the meantime shown that neutron vibrational spectroscopy data can be more easily interpreted in terms of a broken symmetry structure than in terms of the HoD₃ structure [31]. Very recent Raman effect studies of optical phonons in YH₃ and YD₃ provide the first clearcut experimental support for symmetry breaking [32].

The second explanation for the large gap in YH₃ and LaH₃ involves strong local electron-electron interactions. The discrepancy between the calculated band overlap and the observed optical gap of YH₃ is almost 4 eV. This is comparable to what is found in transition metal oxides like NiO. In the latter material strong on-site correlations between localized *d*-electrons play an important role and are poorly described by the LDA. Based on this analogy, it was suggested that YH₃ is a strongly correlated system with strong on-site interactions between two electrons on a hydrogen site. A number of groups have pursued this idea and have studied model Hamiltonians of a nearest neighbor tight-binding type, modified by on-site and/or nearest neighbor two-electron terms. The parameters in these models are then fitted to results obtained from (constrained) LDA calculations, and/or from molecular calculations that incorporate correlation explicitly, or have been simply estimated. Most of the focus has been on LaH₃ because its cubic structure makes it much easier to treat.

Wang and Chen considered a lattice of hydrogen atoms including on-site (Hubbard) and nearest neighbor two-electron Coulomb interactions, which suppress the accumulation of electrons on hydrogen sites [33]. Exact diagonalization of this Hamiltonian for a cluster of hydrogen atoms does not produce a gap, so they concluded that LaH₃ cannot be viewed as a Hubbard-

type correlation-driven insulator.

Ng *et al.* [34] adopted a quite different point of view and proposed a model which starts from doubly occupied hydrogen sites, i.e. H⁻ ions. As well as the hydrogen *s*-states, they include the La *5d* states and the nearest neighbor hybridization of these metal atom states with hydrogen. Correlation is essentially introduced by excluding doubly *unoccupied* hydrogen sites (H⁺ configurations). Within a Gutzwiller approach they show that this leads to a substantial narrowing of the valence bands. Furthermore, they lower the on-site energies of the hydrogen sites by 0.7 eV, which is the electron affinity of a free hydrogen atom, since it is well-known that LDA calculations do not give a positive electron affinity. The combination of this on-site shift and the reduced band widths produces a large band gap of 2.1 eV [34].

The model of Eder *et al.* [35] for YH₃ is also essentially a hydrogen-lattice model. Besides an on-site Hubbard term it includes a two-electron term which describes the hopping between a hydrogen and a nearest neighbor yttrium site and depends upon the occupation number of the hydrogen site. Exact diagonalization of this Hamiltonian for a one-dimensional cyclic cluster yields a band structure that can be fitted rather well by a mean-field approximation to the same Hamiltonian. The mean-field averaged hopping between adjacent hydrogen and yttrium sites lowers the effective on-site potential on the hydrogen sites. This has the effect of shifting the valence bands down and opening up a band gap of about 2 eV for YH₃ in the simplified LaF₃ structure used in this study. In general one expects such a shift of the on-site potential to be very model and parameter dependent. For instance *all* the two-electron terms discussed by Eder *et al.* are included in a mean-field way in a self-consistent (parameter-free) LDA calculation yet the latter fails to produce a gap.

In all of these model approaches a crucial role is assigned to rather different forms of electron correlation. Because only a very limited number of the two-electron terms can be included in any calculation, the final results of the calculations rely heavily on the choice of parameters in the model. Since the main goal of these calculations is to improve upon the LDA calculations, it is surprising that not more attention is paid to the more obvious shortcomings of an LDA calculation. In the first place there is a well-known problem with the LDA lowest Kohn-Sham level in the single electron hydrogen atom [36]. Although the total energy of H⁰ is near the expected value of -1 Ry, the one-electron energy level lies at ~ -0.5 Ry instead of at -1 Ry. In an LDA calculation one therefore expects the bands derived from the atomic hydrogen 1s state to be positioned too high in

energy. Correcting for this artefact might by itself produce a gap in YH_3 . The size of the correction would depend of course on the effective valence of hydrogen in YH_3 and the shift of 0.7 eV proposed by Ng *et al.* [34] seems to be only a lower bound. In the second place there is the “band gap” problem of LDA calculations discussed above. Finally, we note that the quoted experimental gap is deduced from optical experiments so that, depending on the optical matrix elements the optical gap may be very different from the fundamental band gap deduced from a band structure. As an example, the fundamental gap in silicon is 1.2 eV, whereas the direct optical gap is 3.4 eV.

Quasi-particle calculations within the so-called GW approximation are a practical means to obtain accurate band structures without using arbitrary fit parameters [37,38] and accurate band gaps have been obtained for a wide range of semiconductors and insulators using this scheme [37,38]. Remarkably, GW calculations even produce not unreasonable gaps for materials with strong on-site interactions such as NiO [39] and MnO [40]. In this paper we apply the GW method to the band gap problem in YH_3 giving a fuller account of calculations recently presented in letter form [41]. In Sec. 3.2 the GW method and the computational techniques are explained. Sec. 3.3 contains the results of the GW calculations for the various possible structures of YH_3 . Finally, in Sec. 3.4 we compare our work to the results of another recent theoretical study also based on the GW approximation [42].

3.2 Theory

3.2.1 GW calculations

Recent reviews of the GW method can be found in Refs. [37] and [38]; here we give only as much detail as is needed to reproduce the calculations and make the paper self-contained.

Single particle excitation energies can be obtained from the one-particle Green’s function which describes the propagation of an extra particle (electron or hole) added to a system of particles in its ground state. Since calculating wave functions for a many particle system is a formidable, and in general an impossible task, the Green’s function is usually approximated via a many-body perturbation expansion. The electron-electron Coulomb interaction V is treated as a perturbation to a reference system of (effectively) non-interacting electrons. The latter defines a non-interacting Green’s function G_0 , which is easily calculated, and the Green’s function

G of the interacting system can be found by solving Dyson's equation

$$G(\mathbf{r}_1, \mathbf{r}_2, \omega) = G_0(\mathbf{r}_1, \mathbf{r}_2, \omega) + \int d\mathbf{r}_3 d\mathbf{r}_4 G_0(\mathbf{r}_1, \mathbf{r}_3, \omega) \Sigma(\mathbf{r}_3, \mathbf{r}_4, \omega) G(\mathbf{r}_4, \mathbf{r}_2, \omega) \quad (3.1)$$

where $\mathbf{r}_1, \mathbf{r}_2$ are space variables and ω is a frequency (or energy) variable (Hartree atomic units are used throughout this paper). The self-energy Σ is known only in terms of a perturbation series in G_0 and the electron-electron Coulomb interaction V . The latter interaction is strong and the perturbation series contains terms that individually are divergent. This difficulty can only be avoided by applying a scheme in which such terms are carefully (re)summed to obtain a convergent (partial) result. One such scheme was given by Hedin [37] as a set of equations in which the self-energy Σ is expressed as an expansion in the Green's function G and the *dynamically screened* electron-electron interaction W . The first term in the expansion for Σ is the screened exchange interaction, and is symbolically denoted by GW . In practical calculations the expansion is usually cut off after this first term. As the reference system of non-interacting electrons one normally uses the results of a DFT-LDA calculation, since important parts of the electron-electron interaction, such as the Hartree potential, are then already included. In most GW calculations reported in the literature, both G and W are also constructed at the LDA level, where the random phase approximation (RPA) is used for setting up W . Quite often most of the spectral density ($\sim \text{Im } G$) of the interacting electron system can be represented by a set of relatively sharp peaks, each of which has a one-to-one correspondence to a peak in the spectral density of the non-interacting reference system. If this is the case, then each such peak can be identified with a particle-like excitation and is called a quasi-particle peak. In the quasi-particle approximation (QPA) one assumes that the spectral density can be approximated by the quasi-particle peaks only.

Initially only applied to model systems such as the homogeneous electron gas, the GW method was first applied to real materials in the mid 80's, to silicon by Hybertsen and Louie [43], and by Godby, Schlüter and Sham [44], to germanium by von der Linden and Horsch [45]. In all of these cases GW predicted band gaps in close agreement with the experimental values. At that stage GW calculations were computationally very demanding and only applicable to relatively simple materials with small unit cells and high symmetries, such as silicon and germanium. In the meantime, computational resources have increased enormously and considerable progress has

been made in developing more efficient computational algorithms, which has enabled parameter-free GW calculations to become feasible for more complex systems with large unit cells.

3.2.2 Implementation

An efficient implementation of the GW scheme was introduced by Rojas *et al.* [46] and described recently in detail by Rieger *et al.* [47] In this so-called real-space imaginary-time method each computational step is performed either in real or reciprocal space, depending on which representation allows that particular step to be carried out most efficiently and Fast Fourier Transforms (FFT) are used to switch between real and reciprocal space representations. The method uses the fact that the relevant quantities are smooth functions of imaginary time or frequency, whereas they are non-analytic along the real axis and thus tedious to represent numerically. Most numerical operations are thus performed along the imaginary axis and only in the final stage is the result analytically continued to the real axis.

We have developed a GW code for 3D crystals, which efficiently exploits lattice periodicity and the full space group symmetry of a particular solid. It is essentially based upon the real-space imaginary-time method, along with the mixed-space representation for nonlocal operators. [48] In the QPA the Green's function is approximated by

$$G(\mathbf{r}, \mathbf{r}', \omega) = \sum_{n\mathbf{k}} Z_{n\mathbf{k}} \frac{\Psi_{n\mathbf{k}}(\mathbf{r}) \Psi_{n\mathbf{k}}^*(\mathbf{r}')}{\omega - E_{n\mathbf{k}}} \quad (3.2)$$

Using this expression, the quasi-particle wave functions $\Psi_{n\mathbf{k}}(\mathbf{r})$ and energies $E_{n\mathbf{k}}$ can be obtained from Dyson's equation, Eq. 3.1, which simplifies to the so-called quasi-particle equation (QPE)

$$\left(-\frac{1}{2} \nabla^2 + V_{ext}(\mathbf{r}) + V_H(\mathbf{r}) \right) \Psi_{n\mathbf{k}}(\mathbf{r}) + \int d\mathbf{r}' \Sigma(\mathbf{r}, \mathbf{r}', E_{n\mathbf{k}}) \Psi_{n\mathbf{k}}(\mathbf{r}') = E_{n\mathbf{k}} \Psi_{n\mathbf{k}}(\mathbf{r}) \quad (3.3)$$

where $V_{ext}(\mathbf{r})$ is the “external” potential due to the nuclei, and $V_H(\mathbf{r})$ is the Hartree potential; $Z_{n\mathbf{k}}$ are the quasi-particle (QP) or spectral weights given by the usual expression $Z_{n\mathbf{k}} = [1 - \partial \text{Re} I(\omega) / \partial \omega |_{\omega=E_{n\mathbf{k}}}]^{-1}$ with $I(\omega) = \int \int d\mathbf{r} d\mathbf{r}' \Psi_{n\mathbf{k}}^*(\mathbf{r}) \Sigma(\mathbf{r}, \mathbf{r}', \omega) \Psi_{n\mathbf{k}}(\mathbf{r}')$. Since the self-energy Σ is non-hermitian, the “eigenvalues” $E_{n\mathbf{k}}$ are in general complex. Their real parts give the positions of the QP peaks in the spectral density ($\sim \text{Im } G$) which constitute

the usual band structure (the imaginary parts give the peak widths or QP lifetimes). The self-energy Σ is approximated by the screened exchange interaction, which becomes a simple multiplication of G (or G_0) and W in the real-space imaginary-time domain (see Eq. 3.9 below).

As the reference system of noninteracting electrons we use the results of a DFT-LDA calculation. The latter are obtained using a pseudopotential/plane wave Car-Parrinello type code [49]. The LDA wave functions $\phi_{n\mathbf{k}}$ and Kohn-Sham eigenvalues $\epsilon_{n\mathbf{k}}$ are used to set up the Green's function G_0 and the screened interaction W from which the self-energy Σ is calculated. In order to solve the QPE, Eq. 3.3, it is transformed into a matrix "eigenvalue" equation using the LDA wave functions as a basis set in which the QP wave functions are expanded. The resulting matrix is usually almost diagonal, which simplifies solving the QPE considerably. However, Σ still depends explicitly upon the QP energies so the QPE has to be solved iteratively.

In more detail, the LDA Green's function in the imaginary time domain is given by

$$G(\mathbf{r}, \mathbf{r}', i\tau) = \begin{cases} i \sum_{n\mathbf{k}}^{occ} \phi_{n\mathbf{k}}(\mathbf{r}) \phi_{n\mathbf{k}}^*(\mathbf{r}') e^{-(\epsilon_{n\mathbf{k}} - \epsilon_F)\tau}, & \tau < 0 \\ -i \sum_{n\mathbf{k}}^{unocc} \phi_{n\mathbf{k}}(\mathbf{r}) \phi_{n\mathbf{k}}^*(\mathbf{r}') e^{-(\epsilon_{n\mathbf{k}} - \epsilon_F)\tau}, & \tau > 0 \end{cases} \quad (3.4)$$

where ϵ_F is the Fermi level and we have dropped the subscript "0" on G for convenience. In setting up this Green's function, we need to truncate the summation over the unoccupied bands. This is valid since the exponent becomes very small for unoccupied states with high energies. N_{band} is the total number of (occupied and unoccupied) bands included and it is one of the parameters that determines the numerical convergence. Later on we will be using numerical Fast Fourier Transforms (FFTs) to transform from real to reciprocal space so both \mathbf{r} and \mathbf{r}' are chosen on a regular real-space grid that is commensurate with the unit cell of the system. The time τ is sampled on an exponential grid whose spacing increases with increasing time. The use of an exponential grid is efficient because it has a high density of sampling points where there is most structure and a lower density where the functions are smoother.

The dynamically screened interaction is obtained in terms of the polarization propagator P in the RPA approximation, constructed in real space and

imaginary time,

$$P(\mathbf{r}, \mathbf{r}', i\tau) = -2iG(\mathbf{r}, \mathbf{r}', i\tau)G(\mathbf{r}', \mathbf{r}, -i\tau) \quad (3.5)$$

This non-local quantity has translational symmetry if the same lattice vector \mathbf{R} is added to both \mathbf{r} and \mathbf{r}' . In the mixed-space representation, we use a fully periodic quantity $P_{\mathbf{k}}(\mathbf{r}, \mathbf{r}', i\tau)$, defined by

$$P_{\mathbf{k}}(\mathbf{r}, \mathbf{r}', i\tau) = \sum_{\mathbf{R} \in \text{IC}} P(\mathbf{r} + \mathbf{R}, \mathbf{r}', i\tau) e^{-i\mathbf{k} \cdot (\mathbf{r} + \mathbf{R} - \mathbf{r}')} \quad (3.6)$$

which has the property $P_{\mathbf{k}}(\mathbf{r} + \mathbf{R}, \mathbf{r}' + \mathbf{R}', i\tau) = P_{\mathbf{k}}(\mathbf{r}, \mathbf{r}', i\tau)$. In principle, the sum over \mathbf{R} runs over all lattice vectors; in practice we can assume that $P(\mathbf{r}, \mathbf{r}', i\tau)$ vanishes beyond a maximum distance $|\mathbf{r} - \mathbf{r}'|$. This distance defines a supercell called the interaction cell (IC). The sum over \mathbf{R} can thus be restricted to the $N_{\mathbf{R}}$ lattice vectors within the interaction cell. The interaction cell defines a corresponding \mathbf{k} -grid in the first Brillouin Zone (which is of course determined by the true unit cell of the system). $P_{\mathbf{k}}(\mathbf{r}, \mathbf{r}', i\tau)$ only needs to be evaluated for these \mathbf{k} -grid points and for both \mathbf{r} and \mathbf{r}' within the unit cell. The inverse transformation is given by

$$P(\mathbf{r}, \mathbf{r}', i\tau) = \frac{1}{N_{\mathbf{R}}} \sum_{\mathbf{k} \in \text{BZ}} P_{\mathbf{k}}(\mathbf{r}, \mathbf{r}', i\tau) e^{i\mathbf{k} \cdot (\mathbf{r} - \mathbf{r}')} \quad (3.7)$$

In the next step the polarization propagator in the mixed-space representation is Fourier transformed numerically to reciprocal space and to imaginary frequencies $P_{\mathbf{k}}(\mathbf{r}, \mathbf{r}', i\tau) \rightarrow P_{\mathbf{k}}(\mathbf{G}, \mathbf{G}', i\omega)$. In order to perform the Fourier transform the exponential time grid is interpolated onto a linear grid with double the number of grid points; the latter grid is characterized by the number of points N_t and their spacing Δt . The Coulomb interaction is Fourier transformed in a similar way, $|\mathbf{r} - \mathbf{r}'|^{-1} \rightarrow V_{\mathbf{k}}(\mathbf{G}, \mathbf{G}')$, and the screened interaction W is constructed from

$$W_{\mathbf{k}}(\mathbf{G}, \mathbf{G}', i\omega) = \left[V_{\mathbf{k}}^{-1}(\mathbf{G}, \mathbf{G}') - P_{\mathbf{k}}(\mathbf{G}, \mathbf{G}', i\omega) \right]^{-1} \quad (3.8)$$

Additional technical details concerning the treatment of the Coulomb and the screened interaction can be found in Ref. [50]. The screened interaction is then transformed back to the real-space and imaginary time domains and multiplied by G in order to obtain the self-energy operator Σ in the GW -approximation, according to

$$\Sigma(\mathbf{r}, \mathbf{r}', i\tau) = iG(\mathbf{r}, \mathbf{r}', i\tau)W(\mathbf{r}, \mathbf{r}', i\tau) \quad (3.9)$$

Subsequently, the matrix elements of Σ on the basis of the LDA wave functions are calculated, $\Sigma_{\mathbf{k}n n'}(i\tau) = \int \int d\mathbf{r} d\mathbf{r}' \phi_{n\mathbf{k}}^*(\mathbf{r}) \Sigma(\mathbf{r}, \mathbf{r}', i\tau) \phi_{n'\mathbf{k}}(\mathbf{r}')$. Each of these matrix elements is Fourier transformed to the imaginary frequency domain, fitted to an analytical function and continued to the real axis. Simple two-pole expressions are used for these fits. The QPE, Eq. 3.3, in its matrix representation is then solved iteratively to obtain the QP energies and wave functions.

The accuracy of the numerical procedure is determined by (a) N_{band} , the total number of bands used to calculate the Green's function, Eq. 3.4, (b) $N_t, \Delta t$, the number of grid points in the time domain and their spacing, (c) the spacing of the grid points \mathbf{r} in real space, (d) the size of the interaction cell and (e) the accuracy of the analytical fit to the matrix elements of Σ .

3.2.3 Self-consistency

Hedin formulated his equations as a self-consistent scheme [37]. This means that in principle *GW* calculations can be iterated until the G which is obtained as the solution of Dyson's equation, Eq.3.1, is identical to the G which is used in the construction of Σ , Eq. 3.9. The common experience however is that the results of a fully self-consistent *GW* calculation are poorer than those of a "single shot" procedure in which Σ is constructed from G and W at the LDA level. This has been demonstrated in detail for the electron gas [51], for a model one-dimensional semiconductor [52] and recently also for silicon [53]. Use of the complete, self-consistent G (without invoking the QPA of Eq.3.2) leads to a disappearance of the plasmon satellite peak, which is unphysical, and yields band gaps that are severely overestimated. It is believed that incorporating higher order diagrams in the many-body perturbation series by vertex corrections will overcome these shortcomings, but at present this is computationally too demanding for calculations on real materials. From a formal point of view a "single shot" *GW* calculation is not entirely satisfactory, since the LDA calculation represents a fairly arbitrary reference system. Although the QP wave functions $\Psi_{n\mathbf{k}}(\mathbf{r})$ are very often practically identical to the LDA wave functions $\phi_{n\mathbf{k}}(\mathbf{r})$, the QP energies $E_{n\mathbf{k}}$ are certainly different from the Kohn-Sham eigenvalues $\epsilon_{n\mathbf{k}}$, which means that the QP Green's function, Eq. 3.2, certainly differs from its LDA counterpart. More disturbing from a practical point of view is that the LDA calculation can wrongly produce a metallic state for a material which is an insulator [42]. The LDA results then severely overestimate the screening and produce a screened interaction W that is too weak. This ultimately results in a band gap from a "single shot" *GW* calculation that

is severely underestimated [42].

The commonly adopted procedure is called “best G , best W ” and is based upon a partial inclusion of self-consistency effects. The QPA is used for G , Eq. 3.2. To calculate Σ , Eq. 3.9, G is further approximated by setting the QP weights to unity, $Z_{n\mathbf{k}} = 1$, in order to obey the sum rule for the spectral density, and by using only the real part of the (generally complex) QP energies $E_{n\mathbf{k}}$. This “best G ” now has the same form as the G extracted from an LDA calculation. It can easily be updated by replacing the LDA $\phi_{n\mathbf{k}}(\mathbf{r})$ and $\epsilon_{n\mathbf{k}}$ in Eq. 3.4 by the solutions $\Psi_{n\mathbf{k}}(\mathbf{r})$ and $\text{Re } E_{n\mathbf{k}}$ of the QPE, Eq. 3.2. Once the updated Σ has been constructed using Eq. 3.9, the QPE, Eq. 3.2, can be solved again. This whole process can be iterated until self-consistency is reached. The “best G ” now describes a reference system of non-interacting electrons that is “closest” to the interacting electron system. This procedure presents a solution for describing a system where LDA does not give a good reference system for the reasons explained above.

Sometimes it is sufficient to update the energies $\text{Re } E_{n\mathbf{k}}$ only, as in the pioneering work of Hybertsen and Louie [43]. If the QP wave functions differ considerably from the LDA wave functions they must be updated as well. Aryasetiawan and Gunnarsson have found NiO to be a material where this is required and have treated the required self-consistency using some extra approximations [39]. The reference system is modified by introducing an additional potential in the LDA calculation which anticipates the changes in the wave functions and energy spectrum resulting from the GW calculation. They iterate their combined scheme of LDA and GW calculations until the band gap is identical in both calculations. This criterion for convergence is somewhat arbitrary since states with energies which do not define the gap may still change considerably in subsequent iterations. Very recently Miyake *et al.* [42] have used the same approach for YH_3 .

Updating W via Eqs. 3.4-3.8 is unavoidable if LDA calculations wrongly predict a material to be metallic. Sometimes this problem has been circumvented by using a model screened interaction constructed from experimental instead of LDA data. This approach has been used for InSb and InAs, which both have a negative gap in LDA, and the results are satisfactory [54]. Alternatively one may use the approach of Aryasetiawan and Gunnarsson [39]. We opt for an approach in which the QP energies and if necessary the QP wave functions, are updated both in G and in W in each cycle until self-consistency is reached. This approach embodies the “best G , best W ” idea for the case in which LDA incorrectly gives a metallic state without losing the advantages of the QPA in practical calculations. Our scheme re-

quires more computational effort than the approach of Aryasetiawan and Gunnarsson, because we need to recalculate the full QP spectrum (i.e. all the N_{band} occupied and unoccupied bands) in each cycle, but it avoids some of the approximations of the latter approach.

3.3 Results

We have tested our code and self-consistent procedure on silicon because its properties have been studied extensively both experimentally and theoretically. The main results of these tests are summarized in the Appendix. From neutron diffraction experiments it has been concluded that YH_3 has the HoD_3 structure. This is a complicated lattice structure with 24 atoms in the unit cell. It can be viewed as originating from the much simpler so-called LaF_3 structure by a distortion of the hydrogen sublattice which triples the size of the unit cell [19]. We use the simple LaF_3 unit cell, which contains only 8 atoms, as a convenient starting point for our GW calculations. We then modify the lattice structure step by step to the HoD_3 structure and explain how the GW results change accordingly. DFT-LDA calculations predict that another structure, which can be obtained from the HoD_3 structure by additionally breaking a symmetry in the hydrogen sublattice, is lower in energy. We shall also discuss GW calculations for YH_3 in this broken symmetry structure [22].

3.3.1 The lattice structures

The yttrium atoms in YH_3 form a hexagonal lattice and two out of every three hydrogen atoms occupy positions close to the ideal tetrahedral interstitial sites in this lattice. The remaining hydrogen atoms reside in or close to the planes formed by the yttrium atoms; these atoms are usually called the metal-plane hydrogen atoms. Fig. 5.1 (a-d) shows a simplified scheme of the relevant lattice structures in terms of planes which intersect the crystal perpendicular to the metal planes and contain the c axis. These planes are chosen so that they contain the metal-plane hydrogen atoms. The yttrium atom planes are represented by straight horizontal lines, the open circles indicate the positions of the metal-plane hydrogen atoms with respect to the yttrium planes. The hydrogen atoms at the tetrahedral sites are not shown in this simplified representation. Finally, the rectangular boxes denote the unit cells of the different structures. Fig. 5.1(a) represents the LaF_3 structure, in which the unit cell contains Y_2H_6 with two metal-plane hydrogen atoms. Fig. 5.1(b) shows exactly the same structure

in a unit cell which is tripled in the basal ab -plane. The size of the Brillouin zone corresponding to this tripled cell is three times smaller, and the bands are folded back accordingly. We will return to this point later on. The distortion of the hydrogen lattice, which transforms the LaF_3 structure into the HoD_3 structure, takes place in this tripled cell. One third of the metal-plane hydrogens move to positions slightly above the metal planes, and another third to positions below the plane. The remaining hydrogen atoms stay exactly in the metal planes. The space group of the resulting HoD_3 structure, shown schematically in Fig. 5.1 (c), is $P\bar{3}c1$ (number 165 in the International Tables). Finally, in the broken symmetry structure *all* hydrogen atoms are displaced out of the metal planes. This is indicated in Fig. 5.1 (d). One third of the hydrogen atoms is only slightly displaced out of the metal plane and the other hydrogens are roughly twice as far away from these planes. The size of the corresponding unit cell is identical to that of the HoD_3 structure but the symmetry is lower. The space group of the broken symmetry structure is $P6_3$ (number 173 in the International Tables).

3.3.2 Computational details

Apart from using a plane wave kinetic energy cutoff of 36 Ry, the computational details of the LDA calculations for YH_3 were the same as in Ref. [22]. In the GW calculations for YH_3 in the LaF_3 structure we used a real-space grid of $(8 \times 8 \times 12)$ points in the unit cell and the number of bands was taken to be $N_{\text{band}} = 200$ (see the discussion following Eq. 3.4). An interaction cell of $(6 \times 6 \times 4)$ unit cells was used and the time grid parameters were set at $N_t = 40$ and $\Delta t = 0.3$ (see the discussion following Eq. 3.6). By varying these numerical parameters systematically, we estimated that our QP energies are converged to within 0.1 eV. The inclusion of nondiagonal elements of the self-energy operator in the basis of LDA states was not crucial for YH_3 in the LaF_3 structure; it changes the gap by less than 0.05 eV. In this case the LDA wave functions are thus a good approximation to the QP wave functions.

For the GW calculations on YH_3 in the HoD_3 and in the broken symmetry structure we used a $(12 \times 12 \times 12)$ real-space grid, a $(4 \times 4 \times 4)$ interaction cell, $N_{\text{band}} = 300$, and the same time grid. Again, we estimate a convergence of the QP energies to within 0.1 eV. For the HoD_3 structure the nondiagonal elements of Σ also proved to be unimportant. However, for the broken symmetry structure some of these non-diagonal elements were large and had to be included. In this last case, particular QP wave functions were found to

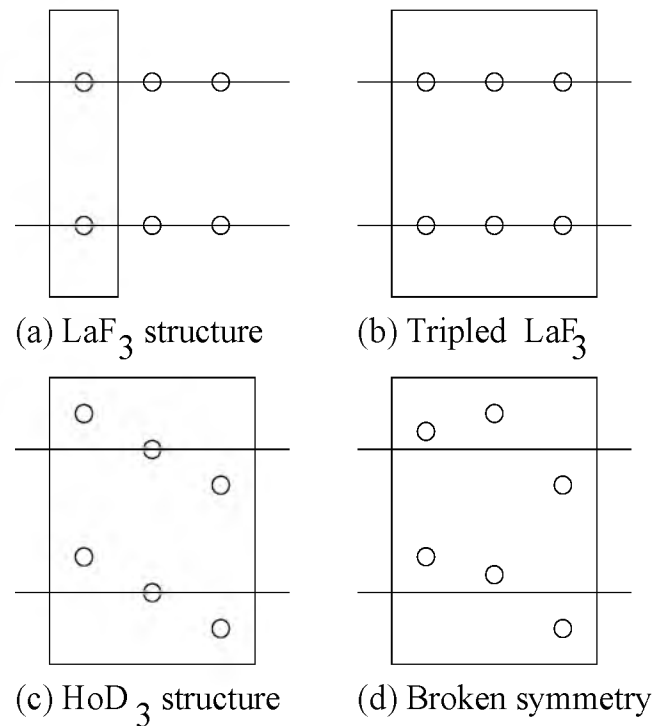


Figure 3.1: Schematic lattice structures of YH_3 . The planes of yttrium atoms are represented by straight horizontal lines, and the open circles indicate the positions of the metal plane hydrogen atoms with respect to the yttrium planes. The rectangular boxes denote the unit cells of the different lattice structures

differ significantly from their LDA counterparts, as will be discussed below.

3.3.3 The LaF_3 structure

For YH_3 in the simplified LaF_3 structure, we reproduced the LDA results of Wang and Chou in all essential details [19]. The results are shown in Fig. 7.1(a). The unit cell contains six hydrogen atoms resulting in six additional valence bands. These states overlap and interact so strongly with the yttrium s and d bands that it is no longer very meaningful to try and distinguish separate “hydrogen” and “yttrium” bands. Purely for convenience, we will call the six lowest bands in Fig. 7.1(a) “hydrogen” bands and the higher bands which are well separated from these, “yttrium” bands. The direct gap between the two groups of bands is about 0.6 eV at Γ and 2.3

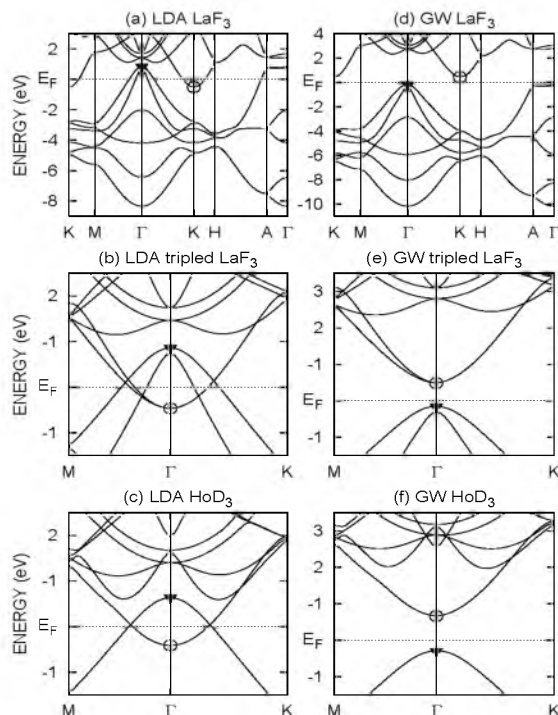


Figure 3.2: LDA electron bands for YH_3 in (a) the LaF_3 structure, (b) the tripled LaF_3 structure, and (c) the HoD_3 structure. The corresponding GW band structures (d-f) are obtained from the LDA bands by linear interpolation of the calculated QP corrections found for the \mathbf{k} -points included in the GW calculation. The circles refer to the bands which are folded back from K to Γ when the Y_2H_6 unit cell is tripled. The triangles mark bands which are originally at Γ

eV at K . However, there is indirect overlap between the highest hydrogen band at Γ (indicated by the filled triangle) and the lowest yttrium band at K (represented by an open circle). Because of this overlap (of about 1.3 eV) the Fermi level cuts through these bands and, in the LDA, YH_3 is (incorrectly) predicted to be a metal.

Calculating the GW band structure self-consistently as explained in the previous section gives us considerable freedom in choosing our starting reference system. We begin by shifting the yttrium conduction bands relative to the hydrogen valence bands so as to open a gap. The Fermi level is chosen at the center of the gap. In this way we start with a screened interaction

corresponding to a semiconductor. This leads to a large self-energy which speeds up the iteration process in the self-consistent calculation. We then iterate the GW scheme and update the QP energies in both G and W until the band energies near the Fermi level differ by less than 0.01 eV between two consecutive iterations. The converged band structure contains a considerable gap which is independent of the size of the gap chosen to begin with, as should be the case in a self-consistent procedure.

The final GW band structure for YH₃ in the LaF₃ structure is shown in Fig. 7.1 (d). For \mathbf{k} -points which were not explicitly included in the QP calculation, we linearly interpolated the calculated GW shifts for the LDA energies in order to produce comparable figures. This is reasonable because the calculated GW shifts are rather constant throughout the Brillouin zone for each band. As a result of the calculated GW shifts, the hydrogen bands become fully occupied and the yttrium bands unoccupied. An indirect band gap of 0.6 eV exists between these two sets of bands at the Γ and K points. The direct gap at Γ is 2.9 eV which agrees very well with the experimentally obtained optical gap for YH₃. Because the strongest optical excitations are \mathbf{k} -conserving, this large direct gap would dominate an optical experiment if YH₃ had the LaF₃ structure. This is then quite comparable to the situation in silicon where the fundamental gap is only 1.2 eV and the direct gap 3.4 eV.

The overall valence band width of about 10 eV in the GW calculation is slightly larger than the LDA value of about 9 eV. This increase in band width is in strong contrast to the results of the model calculation by Ng *et al.* [34] for LaH₃ which predicts a large decrease compared to the LDA valence band width. GW calculations often result in band widths which are somewhat smaller than the LDA values. However, there is no general rule that an improved treatment of correlation effects will lead to a reduction of the LDA band width. Other materials are known for which GW increases the LDA band width, two examples being LiCl [55] and CdS [56]. In any case, the fact that the band width is not drastically changed in the present GW calculation suggests that YH₃ is not strongly correlated in the sense of Ref. [34]. This suggestion is also supported by the relatively large spectral weights, indicating the strong quasi-particle character of the spectral density and thus the absence of strong correlations. The QP states of the highest valence and lowest conduction bands have spectral weights $Z_{n\mathbf{k}} \approx 0.81$. The Brillouin zone average of the spectral weight averaged over the ten lowest states is 0.84.

3.3.4 The HoD₃ structure; dielectric function

As a prelude to the *GW* calculations for YH₃ in the HoD₃ structure we first discuss the results for YH₃ in the LaF₃ structure in an artificially tripled LaF₃ unit cell (cf. Fig. 5.1(b)). The Brillouin zone corresponding to this tripled unit cell is three times smaller than the original Brillouin zone. Consequently, bands are folded back from different \mathbf{k} -points to Γ . In Fig. 7.1(b) we focus upon the LDA bands near the Fermi level around Γ . Two of the bands which were originally at K are now folded back to Γ in the smaller Brillouin zone. These bands are labeled with an open circle, while the filled triangle marks the band(s) which originated from Γ . As a result of this folding the indirect LDA band overlap in the Brillouin zone of the LaF₃ structure becomes a “direct” band overlap at Γ in the Brillouin zone of the tripled unit cell. We see that two pairs of bands cross the Fermi level around Γ .

The results of the *GW* calculation are plotted in the three times smaller Brillouin zone as well, cf. Fig. 7.1(e). The small indirect gap of YH₃ in the LaF₃ structure becomes a direct gap at Γ now. However, optical transitions between pairs of states which originate from different \mathbf{k} -points are of course still forbidden. The matrix elements for direct optical transitions between such bands vanish because of symmetry, and the optical gap at Γ in the Brillouin zone of the tripled unit cell is given by the gap between the valence band marked with the triangle, and the second lowest conduction band; it is 2.9 eV.

As discussed in Sec. 3.3.1 the HoD₃ structure results from displacing some of the metal-plane hydrogen atoms out of the metal plane (accompanied by relaxation of the tetrahedral hydrogen atoms). This lowers the symmetry and induces an interaction between one pair of the bands which overlap near the Fermi level around Γ in the LDA (cf. Fig. 7.1 (c)). The interaction moves both bands of this pair away from the Fermi level; the lower band is pushed down in energy and out of the energy range plotted in the figure. The other pair of bands remains essentially unchanged in the HoD₃ structure and the matrix elements for direct optical transitions between them still vanish. In the LDA calculation we find an overlap of about 1.1 eV between these bands at Γ . The *GW* calculation for YH₃ in the HoD₃ structure results in the opening of a direct band gap of 1.0 eV (cf. Fig. 7.1 (f)), but the optical gap at Γ is still 2.9 eV; in the ΓM direction it is a few tenths of an eV smaller [58]. The overall valence band width is 9.8 eV, close to the value of 10.0 eV in the LaF₃ structure. The limited energy resolution of experimental results [59,60] does not allow a detailed comparison to be made; the most we can

say is that there is no inconsistency in the band widths. Since the calculated QP wave functions are found to be practically identical to the LDA wave functions, we can use the latter to calculate the matrix elements for the electric dipole transitions which are needed to obtain the contribution of interband transitions to the imaginary part of the dielectric tensor, $\epsilon_2(\omega)$. An accurate calculation of these tensor elements requires a very fine \mathbf{k} -grid for the Brillouin zone integration. Such a dense \mathbf{k} -grid is computationally too expensive for a GW calculation. Instead, we have approximated the contributions of direct interband transitions to $\epsilon_2(\omega)$ using shifted LDA energies on a dense ($12 \times 12 \times 10$) \mathbf{k} -grid. The energy separation between the centers of the yttrium and hydrogen bands is increased by a constant 2 eV. This so-called “scissors operator” is a somewhat crude approximation to the actual QP spectrum but is quite good for the states close to the Fermi level. Since it is these states that almost exclusively contribute to $\epsilon_2(\omega)$ at low energies, this procedure is quite reasonable. The results are shown in Fig. 3.3; the curves correspond to the xx and zz part of the dielectric tensor respectively. In optical experiments on polycrystalline films only a superposition of the two components of the dielectric tensor can be measured.

From Fig. 3.3 it can be seen that the matrix elements for optical transitions are very small in the energy range roughly between 1 and 3 eV and the optical gap of about 2.6 eV can be clearly identified. However, there is some structure in the calculated $\epsilon_2(\omega)$ at energies below the optical gap; $\epsilon_2(\omega)$ has a tail extending downwards in energy to about 1.3 eV. This feature is related to transitions between states close to Γ which belong to the highest valence band and the lowest conduction band. Exactly at Γ transitions are symmetry forbidden but at \mathbf{k} -points near Γ without any symmetry they become weakly allowed. These transition probabilities will become more important when the high symmetry of the HoD₃ structure is broken, either statically or dynamically, whereby the large zero point motion of the hydrogen atoms should be considered in addition to the normal thermal motion. Very recently Van Gogh *et al.* have studied the dielectric functions of YH₃ experimentally and have observed weak absorption below an optical gap of 2.6 eV [14]. We speculate that this weak absorption results from such static or dynamic symmetry breaking.

3.3.5 The broken symmetry structure

Finally, we discuss the results of GW calculations for YH₃ in the broken symmetry structure. This structure has the lowest total energy within the

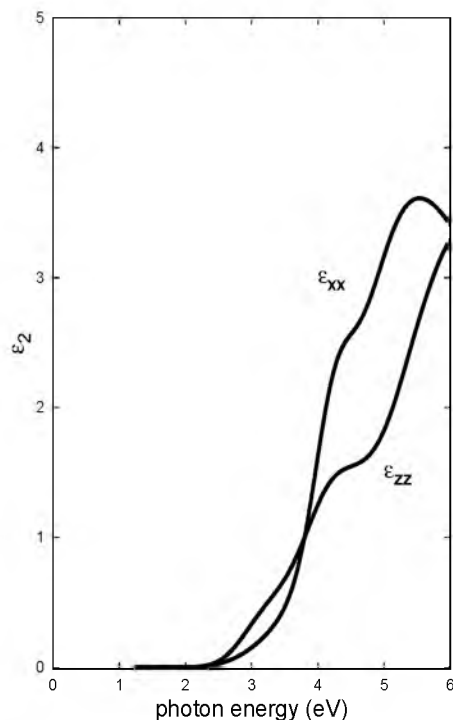


Figure 3.3: $\epsilon_2(\omega)$ calculated using the LDA wave functions and the shifted LDA energies, where the band separation between the yttrium and hydrogen band has been increased by 2 eV. The curves correspond to the xx and zz part of the dielectric tensor respectively, and have been broadened.

LDA and the LDA spectrum has a band gap [22]. However, so far this lattice structure has not been directly confirmed by e.g. diffraction experiments but there has recently been some evidence of symmetry lowering [31,32]. In Figs. 3.4 (a-b) we compare the LDA bands along the $\text{A}\Gamma$ direction for the HoD_3 structure and for the broken symmetry structure. The latter can be obtained from the HoD_3 structure by displacing the hydrogen atoms as discussed in Sec. 3.3.1. Breaking the symmetry of the HoD_3 structure introduces additional interactions between bands. As can be observed in Figs. 3.4 (a-b) the bands near the Fermi level which cross in the HoD_3 structure, show an avoided crossing in the broken symmetry structure. This opens up a band gap in the LDA spectrum. For other bands the changes are much smaller.

We have applied our self-consistent GW procedure to the broken symmetry

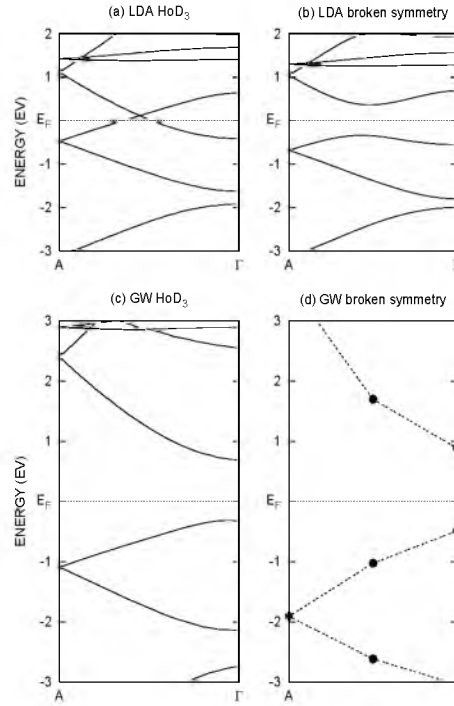


Figure 3.4: LDA band structures along $A\Gamma$ for YH_3 in (a) the HoD_3 structure and (b) the broken symmetry structure. The corresponding GW band structures are given in (c) for YH_3 in the HoD_3 structure where the calculated energy shifts have been interpolated in between \mathbf{k} -points which are not included in the GW calculation, and (d) for YH_3 in the broken symmetry structure, where the dashed lines are guides to the eye.

structure, updating the QP energies in both G and W . The resulting GW bands along $A\Gamma$ near the Fermi level are given in Fig. 3.4 (d); for comparison we have plotted the corresponding GW bands for YH_3 in the HoD_3 structure in Fig. 3.4 (c). Besides an increase in the band gap of the broken symmetry structure as a result of the GW corrections, we also find important changes in the shapes of the bands near the Fermi level compared to the LDA bands. The avoided crossing between the highest occupied and lowest unoccupied bands which is so evident in Fig. 3.4 (b) is absent in Fig. 3.4 (d). Because the QP corrections of these bands are very \mathbf{k} -dependent the interpolation scheme used to plot the GW bands for YH_3 in the HoD_3 structure can not be used. Therefore, the dashed lines which connect the calculated QP energies

in Fig. 3.4 (d) only serve as a guide to the eye. Since the GW calculation for YH_3 in the HoD_3 structure already opens up a gap, the symmetry breaking as such is no longer needed to do this. The GW bands of the broken symmetry structure actually quite closely resemble the GW bands of the HoD_3 structure. The change in the shape of the bands near the Fermi level in the broken symmetry structure going from the LDA to the GW results is accompanied by a change in the corresponding wave functions. For example, at Γ there is a significant mixing of the wave functions of the lowest unoccupied and highest occupied LDA bands in the corresponding QP wave functions. The lowest QP conduction wave function contains more than 20 % of the highest LDA valence wave function, and conversely. The final band gap in the broken symmetry structure is about 1.4 eV and the total valence band width is 10.1 eV which is comparable to the results for both the simplified LaF_3 structure and the HoD_3 structure. Breaking the symmetry will, in general, also induce a finite oscillator strength between states for which it vanished by symmetry in the HoD_3 structure. Therefore we expect that the calculated low energy tail in $\epsilon_2(\omega)$ (cf. Fig. 3.3) will be more pronounced in the case of a broken symmetry structure. Since other states are much less affected by the symmetry breaking the higher energy part of $\epsilon_2(\omega)$ will remain largely unchanged.

3.4 Discussion

In view of the failure of LDA calculations to predict a band gap for YH_3 in the HoD_3 lattice structure, strong electron-electron correlation models were proposed to explain the large gap observed in this material. The present results call into question the pivotal role of such strong correlations in opening a gap in YH_3 . Ng *et al.* [34] introduced a model in which large on-site correlation on the hydrogen atoms results in a large decrease of the valence band width and opens up a substantial gap. We do not find such a decrease of the band width in our GW calculations. On the contrary, our calculated band width increases slightly compared to the LDA result, which suggests rather extended hydrogen-related states.

The model of Eder *et al.* focuses on a correlation term describing the interplay between the hydrogen on-site occupancy and the delocalization of the hydrogen orbital by hybridization with nearest-neighbor yttrium orbitals. Already at the mean-field level this so-called “breathing” of the hydrogen orbitals results effectively in a downward shift of the on-site hydrogen levels [35]. However, at the mean-field level this breathing effect is already

included in LDA calculations, in contrast to the assertion made by Eder *et al.* As such it can *not* be used to improve upon the LDA results.

There is a much more prosaic reason why on-site hydrogen energies are not described very well within LDA. It can be traced to the failure of LDA to describe the $1s$ eigenvalue of the neutral hydrogen atom. This is a well-understood artefact arising from the incomplete cancellation of the electron self-interaction by the local exchange-correlation potential [36]. As a result, the LDA places the $1s$ eigenvalue of atomic hydrogen at -0.5 Ry rather than at -1 Rydberg [61]. The difference between the Y and H on-site energies is then severely underestimated which results in the band centers of the valence and conduction bands being too close and in an overlap of the bands. This is corrected for in the GW calculation. In addition there is the conventional problem in LDA band structures that semiconductor band gaps are too small. For these conventional semiconductors quasi-particle calculations within the GW approximation give quite accurate results without introducing fitting parameters. Such parameter-free calculations for YH₃ in the experimentally obtained lattice structure predict a substantial fundamental band gap of 1 eV. Because the dipole matrix elements for transitions between the highest valence and lowest conduction states vanish, the optical gap is much higher in energy, namely 2.6 eV. This difference between fundamental and optical gaps is neglected in Refs. [34] and [35].

Very recently, Miyake *et al.* [42] also studied the quasi-particle spectrum of YH₃ by a GW calculation. Their main results were obtained for YH₃ in the hypothetical cubic BiF₃ structure and only a limited set of calculations was performed for YH₃ in the simplified LaF₃ structure making a detailed comparison difficult. Their main conclusion, like ours, is that weak correlation as described in the perturbative GW approximation is sufficient to open a gap. Our optical gap is in agreement with experimental (optical) data. In addition, we predict a smaller fundamental gap which could be verified by a combination of photoemission and inverse photoemission experiments.

The picture of YH₃ which we derive from our parameter-free calculations is that of a simple compound semiconductor in which on-site Coulomb correlations play a minor role and can be treated within the GW formulation of many-body perturbation theory. This interpretation is supported by the relatively large spectral weights ($Z_{n\mathbf{k}} \sim 0.8$) of the quasi-particle peaks. We can think of constructing the solid starting with neutral H⁰ and Y⁰ atoms. Because the ionization energy of atomic H⁰ is twice as large as that of Y⁰, charge is transferred from Y to H when the atoms interact [61]. As a result, H acquires a negative charge, which is in agreement with the interpreta-

tion of electromigration experiments given in Ref. [62]. This charge transfer causes the levels derived from the H $1s$ states to shift upwards in energy and the Y levels to move downwards. As usual, overlap of the valence orbitals on neighboring atoms leads to a covalent interaction and the atomic levels broaden into bands. In addition, the charge transfer to hydrogen causes the atomic orbital to delocalize and leads to increased band width. These effects are fully accounted for by a self-consistent band model.

The present results show that symmetry-breaking hydrogen displacements are not needed to open a band gap in YH_3 . Whether or not such symmetry-breaking plays a role in YH_3 is still a subject of debate [31,32].

Now that we have obtained a coherent picture of the host material YH_3 , future research could profitably address the role of point defects, such as hydrogen vacancies, and their effect on the transport and optical properties. We note that although on-site electron correlation is small compared to the valence or conduction band width of YH_3 , it is not necessarily small compared to the band gap and almost certainly plays an important role in determining the charge states of hydrogen vacancies. In silicon for example, the gap states of lattice vacancies are found to have atomic-like localization [63,64], and consideration of on-site correlation effects is essential for understanding the behaviour of vacancies. Nonetheless, these effects are not considered to play any role in determining the properties of defect-free crystalline silicon.

Appendix

In order to test our GW code and to study the effect of self-consistency at different levels, we performed calculations for crystalline silicon which has been studied extensively by Hybertsen and Louie [43] and by Godby, Schlüter and Sham [44], who found excellent agreement with experiment. More recently, very good results were also obtained by Rieger *et al.* [47] and by Fleszar and Hanke [57]. We will compare our results with those obtained recently by Rieger *et al.*; other comparisons can be found in Ref. [47]. We have used a Troullier-Martins pseudopotential, [65] a plane wave kinetic energy cutoff of 25 Ry and an adequate \mathbf{k} -point sampling to obtain well-converged LDA results. An LDA calculation for silicon predicts a one-electron spectrum with a band gap of about 0.5 eV, whereas the experimental gap is close to 1.2 eV.

In our GW calculations we find that the QP energies near the Fermi level are converged within 0.03 eV or better with respect to these numerical

band	present		Rieger	
	LDA	$G_0 W_0$	LDA	$G_0 W_0$
Γ_{1v}	-11.94	-11.52	-11.89	-11.57
Γ'_{25v}	0.00	0.00	0.00	0.00
Γ_{15c}	2.56	3.15	2.58	3.24
Γ'_{2c}	3.17	3.76	3.28	3.94
X_{1v}	-7.80	-7.61	-7.78	-7.67
X_{4v}	-2.84	-2.79	-2.82	-2.80
X_{1c}	0.64	1.33	0.61	1.34
L'_{3v}	-9.60	-9.33	-9.57	-9.39
L_{1v}	-6.96	-6.78	-6.96	-6.86
L'_{3v}	-1.19	-1.17	-1.17	-1.17
L_{1c}	1.44	2.06	1.46	2.14
L_{3c}	3.33	4.00	3.33	4.04
band gap	0.51	1.17	0.49	1.20

Table 3.1: LDA and GW energies and band gaps in silicon from the present method and the results by Rieger *et al.* [47].

parameters if we use a $(6 \times 6 \times 6)$ real-space grid, a $(4 \times 4 \times 4)$ interaction cell, $N_{\text{band}}=145$, $N_t=40$, and $\Delta t=0.3$. The QP energies agree very well with those reported by Rieger *et al.* [47], as can be seen in Table 3.1. The small deviations which occur already at the level of the LDA calculation come from using a slightly different pseudopotential.

In principle, when solving the QP equation, one must also include nondiagonal elements of the self-energy operator in the LDA basis wave functions. For silicon it is known that these elements are small, and that the eigenfunctions of the QP equation are practically identical to the LDA wave functions. We have specifically tested this by including all nondiagonal elements between the lowest 30 bands, and find that the results for the tabulated QP energies change by less than 0.01 eV. The LDA and QP wave functions overlap by more than 99.9 percent. In order to test our code for hexagonal systems (YH₃ has a hexagonal unit cell) we studied bulk silicon in an artificial hexagonal unit cell containing 6 atoms, with its c -axis along the (111) (cubic) crystal direction. The QP energies agreed very well with those obtained for the cubic unit cell.

The effect of a self-consistent Green's function is first tested by iterating the GW scheme, replacing the LDA energies in G by the calculated real

band	$G_0 W_0$	$G_1 W_0$	$G_2 W_0$	GW
Γ_{1v}	-11.52	-11.54	-11.56	-11.82
Γ'_{25v}	0.00	0.00	0.00	0.00
Γ_{15c}	3.15	3.24	3.25	3.47
Γ'_{2c}	3.76	3.86	3.87	4.09
X_{1v}	-7.61	-7.63	-7.65	-7.81
X_{4v}	-2.79	-2.80	-2.80	-2.85
X_{1c}	1.32	1.40	1.41	1.61
L'_{2v}	-9.33	-9.35	-9.37	-9.58
L_{1v}	-6.78	-6.80	-6.81	-6.96
L'_{3v}	-1.17	-1.18	-1.18	-1.20
L_{1c}	2.06	2.14	2.15	2.35
L_{3c}	4.00	4.08	4.09	4.32
band gap	1.17	1.25	1.26	1.46

Table 3.2: Calculated QP energies for silicon at special \mathbf{k} -points when W is kept at the LDA level (W_0) while G is updated, and the self-consistent result (indicated by GW).

parts of the QP energies from the previous iteration. The results of the first three iterations when only G is updated are shown in Table 3.2. W_0 means that we keep W fixed at the LDA level. The QP energies change by about -0.01 eV and about 0.1 eV for the occupied and unoccupied states respectively, after the first update of G . After the second update the changes are much smaller and after the third update (not shown here) the QP energies of interest change by less than 0.01 eV. We have used the latter as a convergence criterion for the self-consistent GW calculation. The band gap is increased by about 0.1 eV by this partial self-consistent procedure, in agreement with Ref. [47].

If the LDA calculation wrongly predicts a metallic state as in YH_3 , one has to update W as well for reasons discussed in Sec. 3.2.3. The effect of updating the QP energies in W is tested for silicon. We find that now more iterations are required to achieve self-consistency; starting from the LDA spectrum the QP energies are converged in 6 iterations (within 0.01 eV). The final self-consistent results when updating the energies in both G and W are also given in Table 3.2 in the column headed by GW . These self-consistent QP energies shift by up to 0.2 eV as compared to the partial self-consistent results, downwards for the occupied states and upwards for

the unoccupied states. The band gap increases by approximately 0.2 eV leading to poorer agreement with experiment.

References

- [1] F. Klose, C. Rehm, D. Nagengast, H. Maletta, and A. Weidinger, *Phys. Rev. Lett.* **78**, 1150 (1997).
- [2] B. Hjörvarsson, J.A. Dura, P. Isberg, T. Watanabe, T.J. Udovic, G. Andersson, and C.F. Majkrzak, *Phys. Rev. Lett.* **79**, 901 (1997).
- [3] J.N. Huiberts, R. Griessen, J.H. Rector, R.J. Wijngaarden, J.P. Dekker, D.G. de Groot, and N.J. Koeman, *Nature (London)* **380**, 231 (1996).
- [4] P.H.L. Notten, M. Kremers, and R. Griessen, *J. Electrochem. Soc.* **143**, 3348 (1996).
- [5] The presence of a thin protective metallic Pd layer on top of the yttrium used to prevent oxidation and enhance hydrogen absorption makes it difficult to accurately determine the resistivity of the insulating trihydride phase.
- [6] P. van der Sluis, *Appl. Phys. Lett.* **73**, 1826 (1998).
- [7] P. van der Sluis, M. Ouwerkerk, and P.A. Duine, *Appl. Phys. Lett.* **70**, 3356 (1997).
- [8] J.H. Weaver, R. Rosei, and D.T. Peterson, *Phys. Rev. B* **19**, 4855 (1979).
- [9] J.H. Weaver, D.T. Peterson, and R.L. Benbow, *Phys. Rev. B* **20**, 5301 (1979).
- [10] D.J. Peterman, B.N. Harmon, J. Marchiando, and J.H. Weaver, *Phys. Rev. B* **19**, 4867 (1979).
- [11] R. Griessen, J.N. Huiberts, M. Kremers, A.T.M. van Gogh, N.J. Koeman, J.P. Dekker, and P.H.L. Notten, *J. Alloys Compd.* **253-254**, 44 (1997).
- [12] A.T.M. van Gogh, E.S. Kooij, and R. Griessen, *Phys. Rev. Lett.* **83** 4614 (1999).
- [13] M.W. Lee and W.P. Shin, *J. Appl. Phys.* **86**, 6798 (1999).
- [14] A.T.M. van Gogh, *Probing the Metal-Insulator Transition in Rare-Earth Based Switchable Mirrors*, Ph.D. Thesis, Vrije Universiteit, Amsterdam (2001) and to be published.

-
- [15] J.N. Huiberts, R. Griessen, R.J. Wijngaarden, M. Kremers, and C. van Haesendonck, *Phys. Rev. Lett.* **79**, 3724 (1997).
- [16] T.J. Udovic, Q. Huang, and J.J. Rush, *J. Phys. Chem. Solids* **57**, 423 (1996).
- [17] N.F. Miron, V.I. Shcherbak, V.N. Bykov, and V.A. Levdik, *Sov. Phys. Crystallog.* **17**, 342 (1972).
- [18] M. Mannsmann and W.E. Wallace, *J. Phys. (Paris)* **25**, 454 (1964).
- [19] Y. Wang and M.Y. Chou, *Phys. Rev. Lett.* **71**, 1226 (1993); *Phys. Rev. B* **51**, 7500 (1995).
- [20] J.P. Dekker, J. van Ek, A. Lodder, and J.N. Huiberts, *J. Phys. Condens. Matter* **5**, 4805 (1993).
- [21] D.K. Misemer and B. Harmon, *Phys. Rev. B* **26**, 5634 (1982).
- [22] P.J. Kelly, J.P. Dekker, and R. Stumpf, *Phys. Rev. Lett.* **78**, 1315 (1997).
- [23] L.J. Sham and M. Schlüter, *Phys. Rev. Lett.* **51**, 1888 (1983); *Phys. Rev. B* **32**, 3883 (1985).
- [24] J.P. Perdew and M. Levy, *Phys. Rev. Lett.* **51**, 1884 (1983).
- [25] T.J. Udovic, J.J. Rush, Q. Huang, and I.S. Anderson, *Phys. Rev. Lett.* **79**, 2920 (1997).
- [26] A. Remhof, G. Song, K. Theis-Bröhl, and H. Zabel, *Phys. Rev. B* **56**, R2897 (1997).
- [27] A. Remhof, G. Song, Ch. Sutter, A. Schreyer, R. Siebrecht, H. Zabel, F. Güthoff and J. Windgasse, *Phys. Rev. B* **59**, 6689 (1999).
- [28] T.J. Udovic, Q. Huang, and J.J. Rush, *Mat. Res. Soc. Symp. Proc.* **513**, 197 (1998).
- [29] J.J. Balbach, M.S. Conradi, M.M. Hoffmann, T.J. Udovic, N.L. Adolphi, *Phys. Rev. B* **58**, 14823 (1998).
- [30] T.J. Udovic, Q. Huang, R.W. Erwin, B. Hjörvarsson, and R.C.C. Ward, *Phys. Rev. B* **61**, 12701 (2000).
- [31] P. van Gelderen, P.J. Kelly, and G. Brocks, *Phys. Rev. B* **63**, R100301 (2001).
- [32] H. Kierey, M. Rode, A. Jacob, A. Borgschulte, and J. Schoenes, *Phys. Rev. B* **63**, 134109 (2001).
- [33] X.W. Wang and C.F. Chen, *Phys. Rev. B* **56**, R7049 (1997).

- [34] K.K. Ng, F.C. Zhang, V.I. Anisimov, and T.M. Rice, Phys. Rev. Lett. **78**, 1311 (1997); Phys. Rev. B **59**, 5398 (1999).
- [35] R. Eder, H.F. Pen, and G.A. Sawatzky, Phys. Rev. B **56**, 10115 (1997).
- [36] O. Gunnarsson, B.I. Lundqvist, and J.W. Wilkins, Phys. Rev. B **10**, 1319 (1974).
- [37] L. Hedin, Phys. Rev. **139**, A796 (1965); L. Hedin, and S. Lundqvist in *Solid State Physics*, edited by H. Ehrenreich, F. Seitz, and D. Turnbull (Academic, New York, 1969), Vol. 23, p. 1.
- [38] For recent reviews of the *GW* method and its applications see F. Aryasetiawan and O. Gunnarsson, Rep. Prog. Phys. **61**, 237 (1998) or L. Hedin, J. Phys. Condens. Matter **11**, R489 (1999).
- [39] F. Aryasetiawan and O. Gunnarsson, Phys. Rev. Lett. **74**, 3221 (1995).
- [40] S. Massidda, A. Continenza, M. Posternak, and A. Baldereschi, Phys. Rev. Lett. **74**, 2323 (1995).
- [41] P. van Gelderen, P.A. Bobbert, P.J. Kelly, and G. Brocks, Phys. Rev. Lett. **85**, 2989 (2000).
- [42] T. Miyake, F. Aryasetiawan, H. Kino, and K. Terakura, Phys. Rev. B **61**, 16491 (2000).
- [43] M.S. Hybertsen and S.G. Louie, Phys. Rev. Lett. **55**, 1418 (1985); Phys. Rev. B **34**, 5390 (1988).
- [44] R.W. Godby, M. Schlüter, and L.J. Sham, Phys. Rev. Lett. **56**, 2415 (1986); Phys. Rev. B **37**, 10159 (1988).
- [45] W. von der Linden and P. Horsch, Phys. Rev. B **37**, 8351 (1988).
- [46] H.N. Rojas, R.W. Godby, and R.J. Needs, Phys. Rev. Lett. **74**, 1827 (1995).
- [47] M.M. Rieger, L. Steinbeck, I.D. White, H.N. Rojas and R.W. Godby, Computer Physics Communications **117** 211-228 (1999); L. Steinbeck, A. Rubio, L. Reining, M. Torrent, I.D. White, and R.W. Godby, Comput. Phys. Commun. **125**, 105 (2000).
- [48] X. Blase, A. Rubio, S.G. Louie, and M.L. Cohen, Phys. Rev. B **52**, R2225 (1995).
- [49] R. Stumpf and M. Scheffler, Comput. Phys. Commun. **79**, 447 (1994).
- [50] J.-W. van der Horst, P.A. Bobbert, P.H.L. de Jong, M.A.J. Michels, G. Brocks, and P.J. Kelly, Phys. Rev. B **61**, 15817 (2000).

-
- [51] B. Holm, and U. von Barth, Phys. Rev. B **57**, 2108 (1998).
- [52] H.J. de Groot, P.A. Bobbert, and W. van Haeringen, Phys. Rev. B **52**, 11000 (1995).
- [53] W.-D. Schöne and A.G. Eguiluz, Phys. Rev. Lett. **81**, 1662 (1998).
- [54] X. Zhu and S.G. Louie, Phys. Rev. B **43**, 14142 (1991).
- [55] M.S. Hybertsen and S.G. Louie, Phys. Rev. B **32**, 7005 (1985).
- [56] O. Zakharov, A. Rubio, X. Blase, M.L. Cohen, and S.G. Louie, Phys. Rev. B **50**, 10780 (1994).
- [57] A. Fleszar and W. Hanke, Phys. Rev. B **56**, 10228 (1997).
- [58] In the real-space, imaginary-time implementation of the *GW* method we include only a limited number of \mathbf{k} -points on a grid for which we calculate QP corrections to the LDA energies. If we interpolate linearly the QP corrections in between these \mathbf{k} -points, we find a minimum gap of 2.6 eV between the highest valence band and the second lowest conduction band along ΓM .
- [59] A. Fujimori and L. Schlapbach, J. Phys. C **17**, 341 (1984).
- [60] B. Hjörvarsson, J.-H. Guo, R. Ahuja, R.C.C. Ward, G. Andersson, O. Eriksson, M.R. Wells, C. Sâthe, A. Agui, S. M. Butorin, and J. Nordgren, J. Phys. Condens. Matter **11**, L119 (1999).
- [61] The Kohn-Sham LDA eigenvalues also underestimate the ionization energy of the free yttrium atom but by a much smaller amount than for hydrogen.
- [62] F.J.A. den Broeder *et al.*, Nature **394**, 656 (1998).
- [63] J. Bernholc, N.O. Lipari, and S.T. Pantelides, Phys. Rev. B **21**, 3545 (1980).
- [64] G.A. Baraff, E.O. Kane, and M. Schlüter, Phys. Rev. B **21**, 5662 (1980).
- [65] N. Troullier and J.L. Martins, Phys. Rev. B **43**, 1993 (1991).

Chapter 4

Phonon spectrum of YH_3

ABSTRACT

Total energy calculations for YH_3 indicate that small symmetry-breaking hydrogen displacements can lower the total energy of the structure deduced from neutron powder diffraction (NPD) experiments on YD_3 . However, such displacements were not observed in subsequent low temperature NPD experiments. Here we present the results of parameter-free lattice dynamics calculations for YH_3 performed in order to see if the hydrogen displacements might be obscured by large zero point motions. Comparison of the theoretical vibrational densities of states calculated for the HoD_3 and broken symmetry structures with the recently reported experimental spectrum determined by inelastic neutron scattering yields evidence that symmetry lowering has in fact been seen.

This chapter is based on: *Phonon spectrum of YH_3 : Evidence for a broken symmetry structure*, P. van Gelderen, P.J. Kelly, and G. Brocks, Phys. Rev. B **63**, 100301 (R) (2001).

Metal-hydrogen systems show interesting, reversible effects upon hydrogen absorption and desorption [1-3]. Huiberts *et al.* [3]. found that, when exposed to hydrogen gas, thin reflecting films of yttrium and lanthanum undergo a metal-insulator transition as a function of their hydrogen content. The transition is readily observed with the naked eye, and reversible, giving rise to the name “switchable mirrors” for the phenomenon. Switching occurs on a short time scale, at room temperature and at moderate hydrogen pressures opening up the possibility of a number of technological applications. In the yttrium-hydrogen system the transition takes place when the hydrogen-to-yttrium ratio is about 2.8; below this ratio the material is metallic and reflecting, above it the material is semiconducting and transparent.

From a theoretical point of view, the nature of this metal-insulator transition is intriguing. The properties of metallic YH_2 have been successfully interpreted on the basis of self-consistent density functional calculations [4-6]. However, straightforward application of such calculations within the Local Density Approximation (LDA) failed to produce a gap for the semiconducting YH_3 phase. Calculations for YH_3 in the HoD_3 structure [7] (found for YD_3 in early experimental work by Miron *et al.* [8]) yielded a band *overlap* of about 1.3 eV [9,10]. The failure of the LDA calculations to explain the band gap in YH_3 prompted new theoretical work into the nature of the gap in this material. Initially, two basically different mechanisms were proposed. In the first mechanism an important role is assigned to strong on-site correlation effects which are capable of opening up a large gap in the electronic spectrum of parameterized model Hamiltonians [11,12] Kelly *et al.* [13] identified strong electron-phonon coupling as a second possibility on the basis of parameter-free total energy calculations which showed that small symmetry-breaking hydrogen displacements lower the total energy and open up a substantial gap in the LDA spectrum. However, while LDA calculations usually describe ground state properties such as the equilibrium structure quite reliably, the band gaps in semiconductors are often severely underestimated. To study excitations a more sophisticated approach is necessary. It has been shown that single-particle excitation energies (including band gaps) can be predicted very accurately for a wide range of materials by quasiparticle calculations within the *GW* approximation [14,15]. We recently reported the results of such calculations for YH_3 [16] and predicted a fundamental gap of 1 eV for YH_3 in the HoD_3 structure. The optical gap is about 3 eV due to vanishing matrix elements for optical transitions at lower energies. These results explain the experimental data without invok-

ing symmetry-breaking hydrogen displacements or strong on-site electron correlation effects.

On the other hand, since the *GW* calculations also produce a large gap for YH_3 in the broken symmetry structure, symmetry-breaking hydrogen displacements are not ruled out by these calculations. The experimental evidence has tended to favor the HoD_3 structure. This structure was recently confirmed using neutron diffraction techniques both for YD_3 powders by Udovic *et al.* [17] and for epitaxially grown films by Remhof *et al.* [18]. However, Udovic *et al.* [17] found unusually large temperature factors for the motion along the *c*-axis of the deuterium atoms located in or near the metal planes when they interpreted their diffraction data in terms of the HoD_3 structure. It is precisely these deuterium (or hydrogen) atoms which are displaced along the *c*-axis from their high symmetry positions in the broken symmetry structure proposed by Kelly *et al.* [13]. However, the small additional Bragg peaks in the powder diffraction pattern predicted for a static broken-symmetry structure are not observed experimentally in low temperature neutron powder diffraction (NPD) experiments [19]. It is conceivable though that a large zero point motion of the hydrogen atoms could reconcile the measured powder diffraction pattern with the broken symmetry structure [20]. Very recent solid state nuclear magnetic resonance experiments on YD_3 powders and neutron diffraction experiments on epitaxial YD_3 films suggest that the symmetry may be lower than that of HoD_3 [21,22].

Information on the dynamics of the hydrogen atoms was obtained by Udovic *et al.* [23,24], who used high resolution neutron vibrational spectroscopy (NVS) to determine the YH_3 phonon density of states. In this paper we present the results of *ab-initio* calculations of the lattice dynamics for YH_3 both in the HoD_3 structure and in the broken symmetry structure. In the harmonic approximation the dynamics is simply given by the eigenmodes of the dynamical matrix which can be calculated if the atomic force constants are known. In the so-called direct method, the forces are calculated using a supercell geometry. One atom is displaced slightly from equilibrium and the forces on all the other atoms in the supercell are calculated from the self-consistent charge density using the Hellmann-Feynman theorem within the LDA total energy framework [13,20]. Such a calculation is repeated for an irreducible set of atomic displacements; the remaining atomic force constants are found making use of the known space group symmetry. Since an unconstrained energy minimization may result in a broken symmetry structure, calculations on the HoD_3 structure must be done by constraining

the symmetry. We use a $(2 \times 2 \times 2)$ supercell containing 192 atoms. This approach has been successfully employed for a variety of materials [25,26]. The calculated phonon densities of states of the HoD_3 structure and the broken symmetry structure are compared to the NVS data of Udovic *et al.* [24]. From the calculated eigenvectors we can identify the character of the vibrational modes which dominate each particular energy range.

In YH_3 the yttrium atoms form a hexagonal structure. Two of the hydrogen atoms occupy positions close to interstitial sites which have local tetrahedral symmetry; we shall denote these atoms by H(T). The third hydrogen atom is found in or close to an yttrium plane of the hexagonal structure; we shall denote this atom by H(M). If all H(M) atoms were exactly in the yttrium plane the unit cell would be Y_2H_6 . In the HoD_3 structure however, two out of every three H(M) atoms move slightly away from the yttrium plane, one to a position $\sim 0.07c$ above the yttrium plane, the other to a position $\sim 0.07c$ below the yttrium plane, whereas the third H(M) atom stays exactly in the yttrium plane. This displacement pattern is sketched schematically in Fig. 5.1(a) where a plane containing the c -axis and the H(M) atoms is shown. The lines represent intersections with the metal planes and the open circles represent the H(M) atoms. This modulation of the metal plane hydrogen atoms leads to a tripling of the unit cell to Y_6H_{18} . As a consequence of the out-of-plane H(M) displacements the H(T) atoms also move in a subtle way which is described in detail in references [10] and [13]. In the closely related broken symmetry structure *all* the H(M) atoms move out of the metal plane, one third of them by $\sim 0.07c$, one third by $\sim -0.07c$, and one third by $\sim 0.03c$ (see Fig. 5.1(b)). These displacements are such that the glide and inversion symmetries of the HoD_3 structure, space group $P\bar{3}c1$, are broken but a screw axis connecting the two H(M) atoms which are displaced by $\sim -0.07c$, is added. The space group of YH_3 in the broken symmetry structure becomes $P6_3$. Starting from the HoD_3 structure, this symmetry lowering can be achieved in four different but equivalent ways. The average of these four equivalent broken symmetry structures has the high symmetry of the HoD_3 structure (cf. Fig. 5.1(c)).

The calculated phonon band structure in the Y_6H_{18} unit cell of the broken symmetry structure has 72 bands in total. To a large extent the motion of the yttrium atoms is decoupled from that of the hydrogen atoms because of the large difference in mass between the two species (yttrium has an atomic weight of 89). The 18 bands in the phonon band structure with energies below 30 meV are mainly due to the low-frequency motion of yttrium. The remaining 54 bands at energies above 30 meV involve almost exclusively the

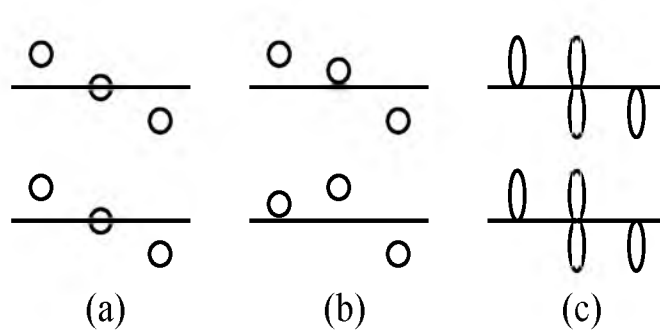


Figure 4.1: Schematic outline of (a) the HoD_3 structure, (b) the broken symmetry structure, (c) the superposition of four representations of the broken symmetry structure.

hydrogen atoms. These conclusions also hold for YH_3 in the HoD_3 structure. One major difference between the two YH_3 structures is the appearance of a soft mode ($\omega^2 < 0$) in the HoD_3 structure at Γ . This indicates that the latter structure is unstable, i.e. there are atomic displacements which can lower the energy, which is consistent with the fact that the broken-symmetry structure has a lower energy, as found earlier by explicit energy minimization [13]. In Fig. 5.5(a) the calculated phonon density of states for YH_3 in the broken symmetry structure is shown. The low frequency yttrium modes tell us little about the structure of YH_3 , so we will not discuss them in detail. The hydrogen sublattice vibrational modes are grouped in frequency bands separated by gaps. Large differences in frequencies are observed between modes corresponding to vibrations in the yttrium (ab) plane and modes in which the atoms vibrate in the c -direction. The H(M) atoms can move relatively freely in channels in the c -direction, but in the ab plane they are constrained by the yttrium atoms in that plane. The modes corresponding to vibrations of H(M) atoms in the c -direction have frequencies between 45 and 99 meV, whereas the basal plane oscillations of the H(M) atoms have frequencies around 160 meV. Vibrations of the tetrahedral hydrogen atoms H(T) have intermediate frequencies; most ab plane oscillations have frequencies between 76 and 99 meV, and between 110 and 130 meV, vibrations in the c -direction have frequencies mainly between 130 and 160 meV. We have also calculated the Debye-Waller factors, but since their influence on the calculated spectra is minor and we use a gaussian broadening anyway, we have not included them in the data given in Fig. 5.5. The calculated phonon density of states shown in Fig. 5.5(a) can be compared to the results obtained from neutron vibrational spectroscopy (NVS)

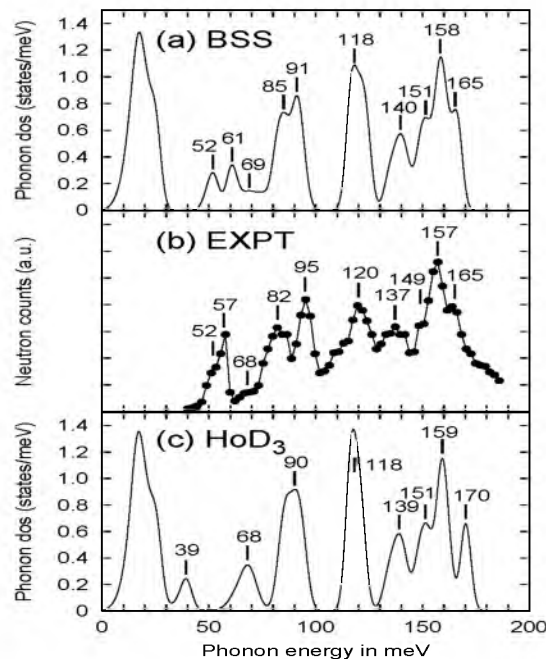


Figure 4.2: (a) Calculated total phonon densities of states for YH_3 in the broken symmetry structure. The data have been broadened with a Gaussian. (b) Experimental neutron vibrational spectroscopy where only a selected number of data points has been taken from Ref. [24]. (c) Calculated total phonon densities of states for YH_3 in the high symmetry structure. The data have been broadened with a Gaussian.

by Udovic *et al.*; these results are reproduced in Fig. 5.5(b). The numbers give the positions of the peaks in meV. We will compare the positions of the peaks and their relative intensities. The large peak at low energy in the calculated spectrum results from vibrations of yttrium atoms. This peak is not present in the experimental data. The agreement between the calculated and the experimental spectrum, though not perfect, is satisfactory. In the following we will argue that the agreement with the calculated phonon density of states derived from the HoD_3 structure is in fact significantly worse. We concentrate on the most prominent features of the spectra. In the calculations we find low energy peaks at 52, 61 and a broad peak at 69 meV, representing 6 bands in total. As discussed above, these correspond

to eigenmodes which are dominated by H(M) vibrations along the c -axis. In the broken symmetry structure these atoms occupy three different Wyckoff positions giving rise to three slightly different energies. In the NVS experiment, there seems to be a single main peak at 57 meV, with some indication of another feature at 52 meV. In the HoD₃ structure with $P\bar{3}c1$ symmetry, there are only two Wyckoff positions occupied by H(M) atoms in the ratio of 2:1. Udovic *et al.* suggested that this bimodal structure was evidence for the existence of only two Wyckoff positions, which is consistent with the HoD₃ structure [23]. We present an alternative interpretation, suggesting that the broad feature in the NVS data near 68 meV corresponds to the broad feature centered on 69 meV in the calculated density of states of the broken symmetry structure. This suggestion is supported by the phonon density of states calculated for the HoD₃ structure which is shown in Fig. 5.5(c). The overall agreement with the experimental data is much worse. Only two peaks are found, corresponding to the motion of the H(M) atoms occupying the two distinct Wyckoff positions in the HoD₃ structure. One peak has an energy of 39 meV and the other peak is found at 68 meV, representing 2 and 4 bands respectively. Although the relative intensity of these peaks is in agreement with experiment, their position is not. The first peak has an energy that is much too low. The second peak is about 10 meV higher than the experimental value.

The next two peaks in the experimental spectrum are found at 82 meV and 95 meV; they have approximately equal intensity. We argue that these peaks mainly result from vibrations of the H(T) atoms in the ab -plane. In the HoD₃ structure we basically find only one strong peak at 90 meV in this energy range, representing 12 bands, which is in clear disagreement with experiment. In the broken symmetry structure this feature around 90 meV is split into two peaks at 85 and 91 meV each representing 6 bands (cf. Fig. 5.5(a)). The splitting of the peak is caused by the existence of two different sites for H(T) atoms in the broken symmetry structure, both of which are occupied by six hydrogen atoms; in the HoD₃ structure there is only one such site for H(T) atoms. Although the size of the splitting is clearly underestimated as compared to the experimental data, the splitting itself and the asymmetric shape of the peaks can be understood in terms of a broken symmetry structure and not of a HoD₃ structure.

The high energy parts (> 100 meV) of the experimental spectrum and the calculated density of states of both the HoD₃ and the broken symmetry structures are very similar. The most prominent difference is found in the structures above 150 meV. The broken symmetry structure gives a main

peak at 158 meV and side peaks at 151 and 165 meV. In the HoD_3 structure the upper peak at 170 meV is clearly split off from the main structure. This peak is due to the motion in the ab plane of those H(M) atoms which are positioned exactly in the metal plane, right in the centre of a triangle of yttrium atoms. In the broken symmetry structure these atoms are about $0.03c$ out of the metal-plane. The tighter confinement of the H(M) atoms in the ab plane in the HoD_3 structure shifts their vibrational modes to a higher frequency. Since these sidepeaks are present for both lattice structures, their observation cannot serve to discriminate unequivocally between both structures. However, again the experimental data are in better agreement with the broken symmetry structure.

Although the agreement between the calculated density of states and the experimental NVS data is reasonably good, it is obviously not perfect. Apart from the usual sources of error in the calculation (the local density approximation, a finite supercell, etc.), one can expect that the most severe approximation is that of assuming harmonic motion for all the atoms. The calculated amplitudes of the zero point motions are particularly large for the H(M) atoms involved in the symmetry lowering when going from the HoD_3 to the broken symmetry structure. The energy difference between the HoD_3 structure and the broken symmetry structure is small and comparable to the zero point energy of about 30 meV of the modes associated with the motion of the H(M) atoms in the c -direction. It is quite possible therefore that the system is not confined to the broken symmetry structure, but that the H(M) atoms sample a large part of configuration space. The symmetry of the HoD_3 structure can be broken in four different but equivalent ways and thus the system could be in a superposition of such structures. This would lead to the picture given schematically in Fig. 5.1(c). At present the huge temperature factors found from the NPD experiments are the only experimental support for such a picture. In a quantum-averaged picture the ground state electronic properties are given by the statistical weight of the electronic structures of the ionic configurations encountered during zero point motion. Since we obtain large gaps in recent GW calculations for YH_3 for both the HoD_3 structure and the broken symmetry structure, the weighted average must have a large gap as well. The lattice dynamics beyond the harmonic approximation can be studied in an *ab-initio* molecular dynamics simulation which incorporates the quantum character of the hydrogen atoms. Although possible in principle, [27] and feasible for simple molecules [28], such calculations are computationally too demanding for a solid with such a large unit cell as YH_3 .

References

- [1] F. Klose, Ch. Rehm, D. Nagengast, H. Maletta, and A. Weidinger, Phys. Rev. Lett. **78**, 1150 (1997).
- [2] B. Hjörvarsson, J.A. Dura, P. Isberg, T. Watanabe, T.J. Udovic, G. Andersson, and C.F. Majkrzak, Phys. Rev. Lett. **79**, 901 (1997).
- [3] J.N. Huiberts, R. Griessen, J.H. Rector, R.J. Wijngaarden, J.P. Dekker, D.G. de Groot, and N.J. Koeman, Nature (London) **380**, 231 (1996).
- [4] J.H. Weaver, R. Rosei, and D.T. Peterson, Phys. Rev. B **19**, 4855 (1979).
- [5] J.H. Weaver, D.T. Peterson, and R.L. Benbow, Phys. Rev. B **20**, 5301 (1979).
- [6] D.J. Peterman, B.N. Harmon, J. Marchiando, and J.H. Weaver, Phys. Rev. B **19**, 4867 (1979).
- [7] M. Mansmann and W.E Wallace, J. Phys. (Paris) **25**, 454 (1964).
- [8] N.F. Miron, V.I. Shcherbak, V.N. Bykov, and V.A. Levдик, Sov. Phys. Crystallogr. **17**, 342 (1972).
- [9] J.P. Dekker, J. van Ek, A. Lodder, and J.N. Huiberts, J. Phys. Condens. Matter **5**, 4805 (1993).
- [10] Y. Wang and M.Y. Chou, Phys. Rev. Lett. **71**, 1226 (1993); Phys. Rev. B **51**, 7500 (1995).
- [11] R. Eder, H.F. Pen, and G.A. Sawatzky, Phys. Rev. B **56**, 10115 (1997).
- [12] K.K. Ng, F.C. Zhang, V.I. Anisimov, and T.M. Rice, Phys. Rev. Lett. **78**, 1311 (1997); Phys. Rev. B **59**, 5398 (1999).
- [13] P.J. Kelly, J.P. Dekker, and R. Stumpf, Phys. Rev. Lett. **78**, 1315 (1997).
- [14] L. Hedin, Phys. Rev. **139**, A796 (1965).
- [15] Recent reviews of the *GW* method are F. Aryasetiawan and O. Gunnarsson, Rep. Prog. Phys. **61**, 237 (1998); L. Hedin, J. Phys. Condens. Matter **11**, R489 (1999).
- [16] P. van Gelderen, P.A. Bobbert, P.J. Kelly, and G. Brocks, Phys. Rev. Lett. **85**, 2989 (2000).
- [17] T.J. Udovic, Q. Huang, and J.J. Rush, J. Phys. Chem. Solids **57**, 423 (1996).

- [18] A. Remhof, G. Song, Ch. Sutter, R. Siebrecht, H. Zabel, F. Güthoff, and J. Windgasse, *Phys. Rev. B* **59**, 6689 (1999).
- [19] T.J. Udovic, Q. Huang, and J.J. Rush, *Phys. Rev. Lett.* **79**, 2920 (1997).
- [20] P.J. Kelly, J.P. Dekker, and R. Stumpf, *Phys. Rev. Lett.* **79**, 2921 (1997).
- [21] J.J. Balbach, M.S. Conradi, M.M. Hoffmann, T.J. Udovic, N.L. Adolphi, *Phys. Rev. B* **58**, 14823 (1998).
- [22] T.J. Udovic, Q. Huang, R.W. Erwin, B. Hjörvarsson, and R.C.C. Ward, *Phys. Rev. B* **61**, 12701 (2000).
- [23] T.J. Udovic, J.J. Rush, Q. Huang, and I.S. Anderson, *J. Alloys and Compounds* **253-254**, 241 (1997).
- [24] T.J. Udovic, Q. Huang, and J.J. Rush, *Mat. Res. Soc. Symp. Proc.* **513**, 197 (1998).
- [25] W. Frank, C. Elsässer, and M. Fähnle, *Phys. Rev. Lett.* **74**, 1791 (1995).
- [26] G. Kresse, J. Furthmüller, and J. Hafner, *Europhys. Lett.* **32**, 729 (1995).
- [27] D. Marx and M. Parrinello, *Z. Phys. B* **95**, 143, (1995).
- [28] D. Marx and M. Parrinello, *Science*, **271**, 179 (1996).

Chapter 5

Structure and dynamics of YH_3

ABSTRACT

Total energy calculations for YH_3 have predicted that small displacements of hydrogen atoms can lower the total energy of the high symmetry structure deduced from neutron powder diffraction (NPD) experiments on YD_3 . Such symmetry-breaking displacements were however not observed in subsequent low temperature NPD experiments. Recent analysis of the phonon modes obtained from Raman spectroscopy do present evidence for a symmetry breaking. A full phonon density of states has been determined by inelastic neutron scattering experiments, or neutron vibrational spectroscopy (NVS) Here we present the results of parameter-free lattice dynamics calculations for YH_3 for each of the three proposed structures. The results are obtained within the harmonic model starting from a force field which is calculated from first principles in a supercell geometry. Comparison of the calculated phonon densities of states with the experimental NVS spectrum gives clear evidence for a symmetry broken structure. The Debye-Waller factors for certain hydrogen atoms are exceptionally large however. We speculate on the importance of these large zero-point motions on the structure of YH_3 .

This chapter is based on: *Structural and dynamical properties of YH_3* , P. van Gelderen, P.J. Kelly, and G.Brocks, submitted to Phys. Rev. B.

5.1 Introduction

Interest in metal-hydrogen systems has been rekindled by the discovery of reversible effects which occur when hydrogen is absorbed and desorbed [1-3]. Huiberts *et al.* [3] found that, when exposed to hydrogen gas, thin films of yttrium, lanthanum and rare earth metals exhibit a metal-insulator transition as a function of the hydrogen content. The transition occurs at room temperature and is readily observed with the naked eye leading to the name “switchable mirrors” to describe this phenomenon [3]. The films are grown on a glass substrate and covered with an optically thin layer of palladium to protect them against oxidation. Unlike bulk samples which disintegrate when the trihydride phase is formed [4] the switchable mirror films are usually stable against hydrogen “loading”. This allows for a detailed study of the metal-insulator transition, for example by measuring simultaneously the transmission of light through the film and its electrical resistivity. The β - YH_2 phase is formed when sufficient hydrogen has been absorbed to form a dihydride. The resistivity of this phase is about a factor five lower than that of pure metallic yttrium and YH_2 is a good reflector for visible wavelengths. Further increase of the hydrogen content leads to nucleation of the γ - YH_3 phase. At a hydrogen-to-yttrium ratio of about 2.8 the resistivity increases sharply and the film becomes transparent to visible light. From the position of the absorption edge in substoichiometric $\text{YH}_{3-\delta}$ with $\delta \sim 0.1$ an optical gap of about 3 eV was deduced [5,6] for YH_3 . The large increase in the resistivity when the trihydride phase is formed, as well as its negative temperature coefficient and its inverse proportionality to δ in $\text{YH}_{3-\delta}$ suggest that YH_3 is a true semiconductor. However, so far the size of the fundamental gap has not been determined experimentally. If the H_2 -pressure is reduced sufficiently, hydrogen desorbs until the dihydride phase is recovered. Since the process of switching between the reflecting dihydride and the transparent trihydride phase is reversible, takes place on a relatively short time scale, and occurs at room temperature, the switchable mirrors may become suitable for a number of different applications.

From a more fundamental point of view the switchable mirrors are intriguing because at the time of their discovery a good understanding of the mechanism underlying the metal-insulator transition was lacking. The properties of YH_2 had been studied by Weaver *et al.* [7,8] and successfully interpreted on the basis of self-consistent electronic structure calculations by Peterman *et al.* [9]. However, straightforward application of band theory to YH_3 failed to produce a gap. Using one-electron band structure calculations based upon the Local Density Approximation (LDA) to Density

Functional Theory (DFT), Dekker *et al.* [10] and Wang and Chou [11] considered a number of possible lattice structures for YH_3 but did not succeed in finding a structure with a band gap. At the time the only evidence that YH_3 had the structure first determined for HoD_3 by Mannsmann and Wallace [12] was a rather brief early report of a neutron diffraction structure determination for YD_3 by Miron *et al.* [13] This quite complicated HoD_3 structure has 24 atoms in a hexagonal unit cell which is tripled in the basal *ab*-plane. The HoD_3 structure of YD_3 was recently confirmed by Udovic *et al.* [14] in neutron powder diffraction (NPD) experiments and even more recently by Remhof *et al.* [15] for epitaxially grown films of the type used in the switching experiments [16]. For the HoD_3 structure, both theoretical studies found a band structure characteristic of a semimetal with a large band overlap of about 1.3 eV [11] at the center of the Brillouin zone.

The failure of DFT-LDA calculations to explain the large band gap in YH_3 and LaH_3 prompted theoretical work into the nature of the band gap in these materials. Two different mechanisms were proposed to explain the large gap. The first suggestion was inspired by a comparably large discrepancy between LDA calculations and experiment for transition metal oxides like NiO. In that case strong on-site Coulomb interactions between *d*-electrons play an important role and are poorly described in an LDA calculation. In the case of the hydrides, the interaction between two electrons on a hydrogen atom and/or the interaction between an electron on a hydrogen site and an electron on a neighboring metal site is then assumed to be very strong and inadequately described by the LDA. Parameterized model Hamiltonians were postulated which invoke such strong electron correlation effects and it was shown that for a certain choice of parameters such correlations can indeed open up a large gap in the electronic spectrum of YH_3 and LaH_3 [17,18]. Kelly *et al.* proposed a “weak correlation” approach, in which they suggested that the solution to the band gap problem should be sought in an improved treatment of the electronic excitations based on standard electron gas theory. [19,20]. They argued that the zero-value band gap found by LDA in LaH_3 , for instance, made the problem similar to Ge, which also has a vanishing gap in LDA. In fact it is well-known that DFT-LDA severely underestimates band gaps in general [21,22] and that in order to calculate single-particle excitation energies, a quasiparticle equation should be solved in which a non-local, energy dependent self-energy should be used (instead of the local, energy independent exchange-correlation potential of DFT). Approximations based on electron-gas theory - more specific the *GW* approximation [23,24] - reproduce experimental band gaps of semiconduc-

tors and insulators very well [21,25,26]. Remarkably, even for the transition metal oxides NiO [27] and MnO [28] GW calculations predict band gaps which are much closer to the experimental values than DFT-LDA does. Our recent GW calculations predict a fundamental gap of 1 eV for YH_3 in the HoD_3 structure [20]. The optical gap is much larger (3 eV) due to vanishing matrix elements for optical transitions at lower energies. These results are in general agreement with experiments on the yttrium hydrides and a more detailed discussion can be found in Ref. [29].

Meanwhile, whereas DFT-LDA is not very well suited to calculate a spectrum, it does give accurate ground state properties, such as the charge density and the structure as results from a total energy calculation. Kelly *et al.* found from such a calculation that small displacements of hydrogen atoms in YH_3 which break the symmetry of the HoD_3 structure, lower the total energy and open up a gap already in the LDA band structure [19]. A GW calculation of the quasiparticle spectrum also produces a large gap for YH_3 in the broken symmetry structure. Its band structure looks quite similar to that of YH_3 in the HoD_3 structure, so from optical experiments it might be quite difficult to distinguish between the two structures [5].

From NPD experiments by Udovic *et al.* on YD_3 [14], which were refined using the HoD_3 structure, unusually large anisotropic temperature factors are found for the deuterium atoms, in particular for the so-called “metal-plane” deuterium atoms located in or close to the planes containing the yttrium atoms. Udovic *et al.* proposed a measure of disorder on the “metal-plane” deuterium sublattice. They incorporated this in their refinement by defining additional, fractionally occupied sites for these atoms. The atoms involved in this “fractional disorder” are exactly those atoms which are displaced from their high symmetry positions in the proposed broken symmetry structure. Small additional Bragg peaks due to the proposed symmetry lowering however are not found in low temperature NPD experiments [30]. It is conceivable though that large hydrogen zero point motion could reconcile the measured powder diffraction pattern with the broken symmetry structure [31]. In addition, solid state Nuclear Magnetic Resonance (NMR) experiments [32] which probe the local symmetry of the deuterium sites, could not be interpreted using the HoD_3 structure which may be an indication for symmetry breaking. In a new paper on neutron diffraction experiments on thin epitaxial YD_3 films it was suggested that the diffraction data are not only consistent with the $P\bar{3}c1$ space group of the HoD_3 structure, but also with less symmetric $P6_3cm$ space group [33]. These results have reopened the discussion on the lattice structure of YH_3 [34]. Recently Kierey

et al. [35] have performed Raman spectroscopy experiments on YH_3 ; from a symmetry analysis Raman active phonon modes they have concluded that their YH_3 films must have either $\text{P6}_3\text{cm}$ or P6_3 symmetry. The latter is the space group the “broken symmetry structure”, which is the structure with the lowest total energy from the LDA calculations. LDA calculations on YH_3 with lattice structure constrained to have $\text{P6}_3\text{cm}$ symmetry results in a total energy which is between that of the HoD_3 and the P6_3 broken symmetry structures; its band structure is almost identical to that of the HoD_3 structure [36].

In the present work we reconsider the prediction of the LDA total energy calculations that YH_3 has the structure with P6_3 symmetry, and give full account of our previously reported results [37]. We present the results of *ab-initio* calculations of the phonon dispersion curves of YD_3 and YH_3 in the HoD_3 structure (P3c1 symmetry), in the broken-symmetry structure (P6_3 symmetry) and in the recently proposed lattice structure with $\text{P6}_3\text{cm}$ symmetry. We calculate the root mean square displacements of the atoms in each of the cartesian directions, the Debye-Waller factors, as well as the ellipsoids of thermal and zero point motion using the eigenvalues and eigenvectors of the dynamical matrix. The Debye-Waller factors can be compared directly to the values derived from the NPD experiments for YD_3 . They may reveal whether the additional peaks expected for a broken symmetry structure have escaped detection as a result of large zero point motions.

We also compare the calculated eigenvalues of the dynamical matrix directly to the energies and symmetries of the observed optical modes in the Raman experiments. In addition we interpret neutron vibrational spectroscopy (NVS) data for YH_3 obtained by Udovic *et al.* [38]. From the calculated eigenvectors we can identify the modes of vibration which predominate in particular energy ranges. Some of the features observed experimentally appear to be better matched by corresponding features calculated for a broken-symmetry structure. For example, we will suggest that particular features of the experimental vibrational density of states are related to the splitting of the 12 tetrahedral hydrogen sites in Y_6H_{18} into two different Wyckoff positions. Where there is such splitting, this may be an indication of symmetry-breaking. In the HoD_3 structure the tetrahedral hydrogen atoms correspond to only one Wyckoff position. This splitting is also suggested by the NMR experiments, and may provide a direction for additional experimental studies in order to resolve all details of the structure and dynamics of YH_3 .

5.2 Calculation of lattice vibrations

Most textbooks on solid state physics contain a discussion of lattice dynamics in the harmonic approximation (see e.g. Madelung [39]). More detailed accounts can be found in a large number of more specialized works (see e.g. Brüesch [40]). The crystal potential energy is expanded in displacements $u_{n\alpha i}$ of the atoms from their equilibrium positions $R_{n\alpha i}$, where n labels the unit cells, α the atoms in the unit cell, and i the three cartesian directions. In the harmonic approximation, this expansion is carried out to second order as

$$U = U_0 + \sum_{n\alpha i n'\alpha' i'} \frac{\partial^2 U}{\partial R_{n\alpha i} \partial R_{n'\alpha' i'}} u_{n\alpha i} u_{n'\alpha' i'} \quad (5.1)$$

where U_0 is an arbitrary constant. The first order terms in such an expansion correspond to the forces on the atoms in the equilibrium configuration which, by construction, vanish. The coefficients of the quadratic term are atomic force constants and are denoted compactly as $\Phi_{n\alpha i}^{n'\alpha' i'}$. They describe the reaction force on atom α in the n -th cell in the i -th direction when atom α' in cell n' is displaced in direction i' . Atomic force constant tensors are symmetric under interchange of the atomic indices, and satisfy symmetry relations imposed by the lattice symmetry.

The equations of motion for the atoms are those of a system of coupled harmonic oscillators. Making use of the lattice periodicity, the solutions can be labeled by a wave vector \mathbf{q} . They are the eigenmodes of the dynamical matrix whose elements are given by

$$D_{\alpha i}^{\alpha' i'}(\mathbf{q}) = \frac{1}{\sqrt{m_\alpha m_{\alpha'}}} \sum_n \Phi_{n\alpha i}^{0\alpha' i'} e^{i\mathbf{q} \cdot (\mathbf{R}_{0\alpha'} - \mathbf{R}_{n\alpha})} \quad (5.2)$$

m_α is the atomic mass of atom α , and $\mathbf{R}_{n\alpha}$ gives the position of atom α in unit cell n in real space. Unit $\|0$ is chosen as the principal unit cell. In principle the summation in Eq. 5.2 extends to unit cells at infinity, but in practice it can be truncated since the reaction forces become negligibly small at large distances. The eigenvalues of this matrix correspond to the squared eigenfrequencies, $\omega_j^2(\mathbf{q})$, of the oscillators. The index j is the band index which combines the indices α and i , and labels the $3r$ branches of the phonon band structure of a solid with r atoms in the unit cell. The eigenvector $Q_{j\alpha i}(\mathbf{q})$ describes the contribution from the j^{th} phonon mode with wave vector \mathbf{q} to the displacement of atom α in the direction i .

To describe the lattice dynamics of particular materials, empirical models have been developed (see e.g. Bilz [41]) in which the force constants were

mostly determined by fitting to experimental phonon dispersion curves. With modern computers it is now possible to determine atomic force constants reliably from calculations within the framework of DFT-LDA without introducing any arbitrary fitting parameters. There are basically two ways of doing this. The linear response method approaches the problem by calculating the inverse of the dielectric matrix [42,43] and has been successfully applied to a number of semiconductors [44,45], and metals [46]. It can be used to calculate the dynamical matrix for general \mathbf{q} -vectors. In the so-called direct method, the force constants are calculated using a supercell geometry. This method is a natural extension of the *frozen phonon* method [47] in which the frequency of specific phonons that fit within the finite geometry of a supercell are determined. Within the supercell, the atoms are then displaced, e.g. as in an optical phonon mode, and the energy change is calculated as a function of the amplitude of the displacement. Only phonon frequencies at particular high-symmetry \mathbf{q} -points can be calculated in this way. This method was later extended for solids with high-symmetry geometries in which planes of atoms vibrate as a whole [48-50] and shown to be successful for determining e.g. the lattice dynamics of superstructures in selected directions in \mathbf{q} -space [51]. Recently, planar force constants obtained in this way could be mapped out to obtain force tensors between single atoms as well [52]. In principle, if the supercell can be made so large that the force constants vanish on the surface of the supercell (assuming that the displaced atom is at the centre of the supercell) then the direct method is exact for any \mathbf{q} .

In the direct method used here, we displace a specific atom in a specific direction and calculate the forces on all the other atoms in the supercell from the self-consistent charge density of the disturbed system via the Hellmann-Feynman theorem (see e.g. Ref. [53]). This calculation is repeated for each symmetry independent atom and direction. The self-consistent charge density is calculated within DFT-LDA. This approach relies upon the Born-Oppenheimer approximation which assumes that the electrons are in their instantaneous ground state for any ionic configuration. The direct method was used for simple metals [54,55], for semiconductors [56], and for insulators [57,58]. Calculated phonon frequencies are usually very accurate and agree with the experimental data within a few percent. In semiconductors and insulators with nonvanishing Born effective charges (Z^*) the longitudinal optical (LO) modes at $\mathbf{q} = 0$ are not obtained correctly within a finite supercell. The reason for this is the incomplete electrostatic screening in such systems, which leads to long-range interatomic force constants

[58]. With knowledge of the Born effective charge tensors and the dielectric constant ϵ_∞ the effect of long-range interactions can be included in the dynamical matrix [58-60]. These quantities can be obtained using linear response theory [61,62,45]. From the interplanar force constants obtained in supercell calculations Kunc and Martin [48] have used an alternative way to calculate the correct frequencies for the LO vibrations. Kern *et al.* [63] have recently described its application in detail; we will use their approach.

subsectionProjected phonon densities of states
From the phonon bands $\omega_j(\mathbf{q})$ it is straightforward to find the corresponding density of states. The eigenvectors contain information about which atoms are moving in which direction for each mode. This makes it possible to calculate densities of states which tell us how particular atoms move in particular directions as a function of phonon energy, which is very useful for the interpretation of inelastic neutron scattering experiments. The phonon density of states for displacement of atom α in direction i is given by

$$G_{\alpha i}(\omega) = \frac{V}{(2\pi)^3} \sum_j \int_{BZ} |Q_{j\alpha i}(\mathbf{q})|^2 \delta(\omega - \omega_j(\mathbf{q})) d\mathbf{q} \quad (5.3)$$

where V is the unit cell volume.

5.2.1 Motion of single atoms

In the quantum mechanical solution of the coupled harmonic oscillator problem, each oscillator with frequency $\omega_j(\mathbf{q})$ can have an occupation of $n_{j\mathbf{q}}$ phonons. The total vibrational energy is

$$E = \sum_{j\mathbf{q}} (n_{j\mathbf{q}} + \frac{1}{2}) \hbar \omega_j(\mathbf{q}) \quad (5.4)$$

where $n_{j\mathbf{q}}$ depends on the temperature T and $\frac{1}{2}\hbar\omega_j(\mathbf{q})$ is the zero point energy. For a solid in thermal equilibrium with a heat bath at temperature T the mean number of excited phonons with energy $\hbar\omega_j(\mathbf{q})$ is given by the Bose-Einstein distribution

$$n_{j\mathbf{q}}(T) = \frac{1}{\exp(\hbar\omega_j(\mathbf{q})/k_B T) - 1} \quad (5.5)$$

The mean square displacement of a single quantum mechanical harmonic oscillator, $\langle u^2 \rangle = \frac{\hbar}{m\omega} (n + \frac{1}{2})$, is easily generalized to that of a single atom α in the direction i as

$$\langle u_{\alpha i}^2 \rangle = \frac{V}{(2\pi)^3} \frac{\hbar}{m_\alpha} \sum_j \int_{BZ} |Q_{j\alpha i}(\mathbf{q})|^2 \frac{(n_{j\mathbf{q}}(T) + \frac{1}{2})}{\omega_j(\mathbf{q})} d\mathbf{q} \quad (5.6)$$

It is evident from this expression that light atoms, such as hydrogen, vibrating at low frequencies exhibit large zero point motions. To calculate Eq. 5.6 we use Eq. 5.3 to transform the sum over modes j and \mathbf{q} -vectors into an integral which includes the partial density of states $G_{\alpha i}(\omega)$. The off-diagonal elements $\langle u_{\alpha i} u_{\alpha j} \rangle$ can be calculated in an analogous fashion.

5.2.2 Ellipsoids of vibration

The thermal and zero point motion of the atoms is often described using the matrix of anisotropic temperature factors \mathbf{B} (see e.g. Willis and Pryor [64]). For atom α it is defined by

$$B_{ij}(\alpha) = 8\pi^2 \langle u_{\alpha i} u_{\alpha j} \rangle. \quad (5.7)$$

Diagonalizing this symmetric matrix yields the lengths and directions of the main axes of the ellipsoid of thermal or zero point motion. Evidently, the form of \mathbf{B} is restricted by the symmetry of the atomic site in the crystal. For example, the full cubic symmetry in silicon restricts the ellipsoids of vibration of the atoms to spheres. Moreover, equivalent atoms, the positions of which are related by a symmetry operation, have ellipsoids related by symmetry. These symmetries of \mathbf{B} provide a way to check the internal consistency of the calculations.

5.2.3 Debye-Waller factors

The relative intensity of a diffraction peak corresponding to reciprocal lattice vector \mathbf{K} in a powder diffraction pattern can be obtained from

$$I(\mathbf{K}) \sim \left| \sum_{\alpha} \exp(i\mathbf{K} \cdot \mathbf{R}_{\alpha}) f_{\alpha}(\mathbf{K}) \exp(-W_{\alpha}(\mathbf{K})) \right|^2 \quad (5.8)$$

where \mathbf{R}_{α} is the position of atom α in the unit cell. The atomic scattering factors for neutron scattering $f_{\alpha}(\mathbf{K})$ are \mathbf{K} -independent and can be found in standard tables. The Debye-Waller factor $W_{\alpha}(\mathbf{K})$

$$W_{\alpha}(\mathbf{K}) = \frac{1}{16\pi^2} \sum_{ij} K_i K_j B_{ij}(\alpha) \quad (5.9)$$

describes the reduction of the scattered intensity at \mathbf{K} resulting from the thermal vibration of atom α . Consequently, the intensity of the peaks in the diffraction spectra that correspond to large \mathbf{K} in combination with large B_{ij} are most affected by atomic motions.

5.3 Results for YH_3

In order to estimate the accuracy of the calculated phonon spectra test calculations were made for silicon using the direct supercell method with supercells containing 54 and 250 atoms. The results show a good agreement with experiment and are summarized in the appendix. Very reasonable dispersion curves are already obtained using the smaller supercell indicating the short range of the force constants. In this section we present our results for YH_3 in the HoD_3 and broken symmetry structures. We begin by describing these structures in more detail.

5.3.1 The proposed lattice structures for YH_3

The HoD_3 and broken symmetry structures are closely related. They are best described by starting with a hexagonal lattice consisting of $ABAB\dots$ stacked planes of yttrium atoms. In our unit cells we choose one yttrium “metal” plane at $z = +\frac{c}{4}$ and the other at $z = -\frac{c}{4}$. The hexagonal lattice contains three interstitial sites per metal atom which have high local symmetry, two with a tetrahedral and one with an octahedral symmetry. Additional atoms such as hydrogen are usually assumed to occupy such high symmetry sites and indeed, out of every three hydrogen atoms in YH_3 two are to be found close to the tetrahedral sites. We shall denote these atoms by $\text{H}(\text{T})$. However, instead of occupying the octahedral site, the third hydrogen atom prefers to descend into the metal plane. This give rise to the so-called LaF_3 structure with a Y_2H_6 unit cell where two hydrogen atoms, which we shall denote $\text{H}(\text{M})$, are found in the metal-plane while the $\text{H}(\text{T})$ atoms repel one another and move slightly away from the ideal tetrahedral positions and from the metal planes. The four $\text{H}(\text{T})$ atoms are located in planes at about $z = \pm 0.09c$ and $z = \pm 0.41c$. The equilibrium unit cell is about 15 % larger than the unit cell volume of pure metallic yttrium in the hexagonal close packed structure, almost entirely as a result of elongation of the c -axis. Compared to an “ideal” structure in which the hydrogen atoms all occupy tetrahedral and octahedral symmetry sites, all of the displacements just described lead to substantial lowering of the total energy [11].

We now take this so-called LaF_3 structure and triple it in the basal ab -plane such, that there are three metal-plane hydrogen atoms in each metal plane in each unit cell. In the HoD_3 structure, two of these three atoms move slightly away from the metal plane. One moves to a position about $0.07c$ above the metal plane, the other to a position about $0.07c$ below the metal

plane. The third H(M) stays exactly in the metal plane. This displacement is sketched schematically in Fig. 5.1 where a plane containing the c -axis and the H(M) atoms is shown. The lines represent intersections with the metal planes and the open circles represent the H(M) atoms. The plane shown is a glide plane with a translation vector of $c/2$ in the z -direction. As a consequence of the out-of-plane H(M) displacements the H(T) atoms also move slightly, as described in detail in references [11] and [19]. The tripled hexagonal unit cell contains 24 atoms with a stoichiometry Y_6H_{18} .

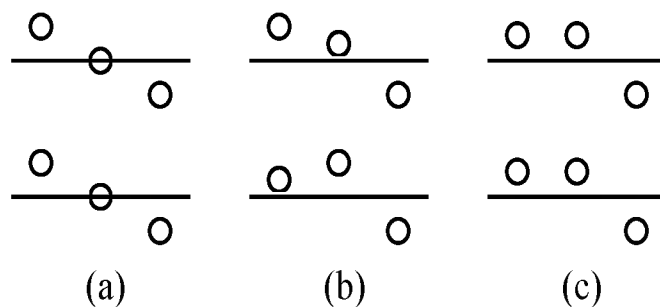


Figure 5.1: Schematic outline of the proposed lattice structures for YH_3 , with (a) the HoD_3 structure with $P\bar{3}c1$ symmetry, and the broken symmetry structures with (b) $P6_3$ and (c) $P6_3cm$ symmetry respectively. The horizontal lines indicate the planes formed by the yttrium atoms in the ab plane direction. The c -axis is in the plane of the paper and the open circles denote the H(M) hydrogen atoms; the H(T) atoms are not shown.

In the broken symmetry structure which corresponds to the lowest total energy in LDA calculations the unit cell is also tripled with respect to the LaF_3 structure. But now *all* the H(M) atoms move out of the metal plane, one third of them by about $0.07c$, one third by about $-0.07c$, and the rest by about $0.03c$ (see Fig. 5.1). The displacements are *different* for H(M) atoms which are related by a translation over $c/2$ in the z -direction. When for instance a H(M) atom in the lower metal plane moves up by about $+0.07c$, the related atom in the upper metal plane moves up by about $0.03c$ and vice versa. However, the remaining related pair of H(M) atoms that are displaced by the same amount with respect the metal planes, i.e. by about $-0.07c$. Comparing this structure to the HoD_3 structure we observe that the glide and inversion symmetries of the HoD_3 structure (space group $P\bar{3}c1$) are broken. They are replaced by a screw axis through the H(M) atoms that are displaced by $-0.07c$. The space group for this broken symmetry structure is $P6_3$. The H(T) atoms are also slightly displaced as compared to

their positions in the LaF_3 structure due to the H(M) displacements [19]. Recently a new lattice structure has been proposed that has $P6_3cm$ symmetry, in which also all the H(M) atoms are displaced out of the metal plane. Like in the HoD_3 structure the displacements are identical for H(M) atoms which are related by a translation over $c/2$ in the z -direction. Two out of every three H(M) atoms are displaced by about $0.05c$ and the remaining H(M) atoms by about $-0.07c$. Since all the H(M) atoms are displaced out of the metal plane this structure has no inversion centre. Instead, there is both a screw axis through the H(M) atoms that are displaced by $-0.07c$, and a glide plane, which is the plane containing the c -axis and the H(M) atoms. Again the H(T) atoms are displaced from the positions they have in the LaF_3 structure. In Table 5.1 we summarize the details of the three proposed lattice structures for YH_3 .

In the following discussion we shall mainly focus upon the positions and the zero point motion of the H(M) atoms in the c -direction. These atoms play a key role in the symmetry lowering when going from the HoD_3 structure to either of the broken symmetry structures. We note that, starting from the HoD_3 structure, a symmetry lowering can be achieved in four different but equivalent ways. For example, the four representations of the $P6_3$ broken symmetry structure can be transformed into each other by applying those symmetry elements of the HoD_3 structure which no longer apply to this broken symmetry structure (glide and inversion). The “average” of these four equivalent broken symmetry structures has the high symmetry of the HoD_3 structure.

5.3.2 Computational details

We use the direct supercell method for calculating the phonon dispersion curves for YH_3 within the harmonic approximation for the three lattice structures described above. The supercell is defined by doubling the unit cell in each of the three lattice directions; this $(2 \times 2 \times 2)$ cell contains 192 atoms. The inequivalent atoms in the principal unit cell are displaced one at a time by 0.1 a.u. (0.052916 \AA) in each of the three cartesian directions and the self-consistent charge density is recalculated for each perturbed structure. Using this new charge density we determine the Hellmann-Feynman forces on all other atoms in the supercell. The atomic force constant between the displaced atom and an arbitrary atom in the supercell is then given by the ratio of the force in a particular direction on the atom in the supercell and the amplitude of the given displacement. In order to remove (small) contributions from third order (and higher odd order) terms in the

	$P\bar{3}c1$	$P6_3$	$P6_3cm$
Y	6f x= 0.663	6c x= 0.667 y=-0.003 z= 0.250	6c x= 0.669 z= 0.250
$H_1(T)$	12g x= 0.348 y= 0.025 z= 0.093	6c x= 0.345 y=-0.015 z= 0.093	6c x= 0.306 z= 0.091
$H_2(T)$		6c x=-0.308 y=-0.042 z=-0.093	6c x=-0.354 z=-0.092
$H_1(M)$	4d z= 0.181	2a z=-0.316	4b z= 0.200
$H_2(M)$	2a	2b z= 0.184	2a z= 0.324
$H_3(M)$		2b z=-0.216	

Table 5.1: Wyckoff positions of the yttrium (Y), tetrahedral hydrogen ($H(T)$) and the metal-plane hydrogen ($H(M)$) atoms in the proposed lattice structures of YH_3 in the HoD_3 structure with $P\bar{3}c1$ symmetry, and the broken symmetry structures with $P6_3$ and $P6_3cm$ symmetries. The numbers are obtained upon optimizing these structures in a $(2 \times 2 \times 2)$ supercell using Γ -point only sampling of the Brillouin zone.

crystal potential, we use displacements in positive and negative direction and average the force constants. The full space group symmetry of the solid is used to keep the number of required supercell calculations to a minimum. Having generated all the force constants we symmetrize the force tensors by applying the symmetry elements to all atoms and averaging the resulting force fields. Once the time-consuming self-consistent supercell calculations have been performed and the force constants have been obtained, the dynamical matrix can be constructed for any \mathbf{q} and diagonalized. Since this is only a 72×72 matrix for a solid with 24 atoms in the unit cell, this last step is not computationally demanding. Following Parlinski *et al.* [57] we construct an extended supercell which includes images of atoms that lie on the boundary of the supercell. Each image of these atoms is included in the calculation with a fractional weight which depends upon the geometry of the supercell. We include all the generated force constants in our calculation of the phonon bands, also if shells of atoms are incomplete as a consequence of the shape of the supercell. In this way we almost perfectly obey the translational sum rule, which demands that the sum of all the forces in the supercell vanishes.

$$\sum_{n\alpha} \Phi_{n\alpha i}^{0\alpha' i'} = 0 \quad (5.10)$$

This sum rule should hold for each direction i , and for each atom α' displaced in each cartesian direction i' . Small deviations from the sum rule due to nonharmonic contributions or numerical errors result in the frequencies of the acoustic modes not going to zero exactly at $\mathbf{q} = 0$. We correct for this unphysical behavior by changing for each i and for each α' and i' the force constant $\Phi_{0\alpha' i}^{0\alpha' i'}$ by the difference between the force on the displaced atom and the sum of all forces on the atoms which were not displaced. This difference should be exactly zero according to the sum rule. The corrections we have to make are small but ensure that the acoustic modes behave physically near $\mathbf{q} = 0$. The other bands show negligible changes.

The ground state properties of the supercells described in this work are conveniently calculated using a Car-Parrinello type electronic structure code [65-67]. For reasons of efficiency we sample only the Γ -point of the Brillouin zone. We comment upon this in the next subsection. The one-electron wave functions within DFT-LDA are expanded in a plane wave basis, including functions up to a kinetic energy cutoff of 30 Rydberg. Soft Troullier-Martins pseudopotentials were used [68], and generated as described in Refs. [11] and [69]. We include nonlinear core corrections for yttrium following Louie *et al.* [70].

5.3.3 Supercell and Brillouin zone sampling

The accuracy of the calculated phonon eigenvectors and eigenfrequencies depends on the size of the supercell used to calculate the atomic force constants. Ideally it should be so large that all forces vanish at the boundaries of the cell but this is never fully achieved in practice. As a result of this, atoms inside the supercell experience forces not only from the displacement of the atom inside their own cell but also from the periodic images of that displaced atom. Atoms outside the supercell on the other hand, are considered not to experience any forces. Both of these effects contribute to systematic errors in the dispersion curves. Phonon frequencies of modes that fit within the supercell geometry do not suffer from this type of error. A problem related to the use of a finite supercell is the approximation of the Brillouin zone summation in the calculation of the self-consistent charge density and the total energy by a single \mathbf{k} -point, in our case the Γ -point. Making explicit use of time-reversal symmetry in the Car-Parrinello algorithm means that a Γ -point calculations is relatively efficient. Since the Γ -point approximation becomes better as the supercell size is increased, and we need a large supercell to calculate the force constants anyway, we have not attempted to calculate the forces with an improved \mathbf{k} -point sampling. We have carried out a number of tests of the BZ summation in order to estimate the reliability of the Γ -point sampling for the $\text{Y}_{48}\text{H}_{144}$ supercell ($= 2 \times 2 \times 2 \times \text{Y}_6\text{H}_{18}$) used in most of our calculations.

We compare a number of highly converged total energy differences, calculated with primitive unit cells and dense BZ sampling [11,19], with those obtained with the $\text{Y}_{48}\text{H}_{144}$ supercell and Γ -point sampling. As a reference we use the Y_2H_6 lattice in which the hydrogen atoms are located in the tetrahedral H(T) and octahedral H(O) positions of the hexagonal yttrium lattice. Increasing the nearest-neighbor H(T)-H(T) distance from $0.25c$ to $0.30c$, and moving the H(O) atoms into the metal planes to become H(M) atoms we find from our supercell calculations a decrease in the total energy of $985 \text{ meV}/\text{YH}_3$ which is to be compared to the values of $980 \text{ meV}/\text{YH}_3$ reported by Wang and Chou [11], and $965 \text{ meV}/\text{YH}_3$ reported by Kelly *et al.* [19]. The total energy difference between the HoD_3 structure and the broken symmetry structure with P6_3 symmetry is $16 \text{ meV}/\text{Y}_6\text{H}_{18}$, as compared to 40 meV found by Kelly *et al.* [71]. For the Γ -only $\text{Y}_{48}\text{H}_{144}$ supercell find calculate that total energy of the lattice structure with $\text{P6}_3\text{cm}$ symmetry is in between the total energies of the HoD_3 structure and that of the broken symmetry structure with P6_3 symmetry.

We conclude from these tests that the Γ -point sampling is quite good. We

can understand this in terms of the very low and vanishing density of states at the Fermi level for the HoD_3 and broken-symmetry structures, respectively. For a (near) semiconductor a special-point type of sampling should be quite good and this is achieved using the supercell.

5.3.4 Phonon band structures

The calculated phonon band structure for YH_3 in the broken symmetry structure ($P6_3$ symmetry, Fig. 5.1) is shown in Fig. 5.2 along some high symmetry directions in the Brillouin zone. With 24 atoms in the unit cell there are in total 72 bands. The lowest 18 branches are dominated by the low frequency motions of yttrium which, with an atomic weight of 89, are essentially decoupled from the hydrogen motion. The hydrogen atoms are well separated from one another by the large yttrium atoms. This and the tripling of the unit cell leads to a large number of almost dispersionless hydrogen-related phonon bands. Unfortunately there are no experimental \mathbf{q} -resolved spectra with which we can compare, since bulk YH_3 crystals of the type needed for neutron scattering measurements disintegrate into powder because of the large volume change associated with the hydrogen absorption. However, from the eigenvectors $Q_{j\alpha i}(\mathbf{q})$ we know for each frequency $\omega_j(\mathbf{q})$ which atoms are moving in which direction. We will use this information in the next section to interpret NVS data, which can be measured with powder samples.

The nearly complete decoupling of the eigenmodes of the yttrium and hydrogen sublattices and the fact that pure yttrium is also hexagonal allows for comparison of the calculated low frequency modes with dispersion curves which have been measured for pure yttrium [72]. The energies and dispersions are found to be quite comparable and the differences can to a large degree be attributed to the substantial elongation of the c -axis in YH_3 .

For YH_3 in the broken symmetry structure which corresponds to a band structure with a gap, we have checked in detail the relevance of long-range force constants by explicitly using the correction method described by Kern *et al.* [63] for the dispersions along ΓA . The planar force constants between a central displaced atom and the plane of atoms on the edge of the supercell give an upper bound for the effect of long-range forces. Including such corrections only slightly modifies the frequencies of the LO modes at Γ . It does not change the frequencies of other special \mathbf{q} -points which fit exactly in our supercell geometry. As the dispersions of the optical modes are very small anyway, we have neglected these corrections in further calculations.

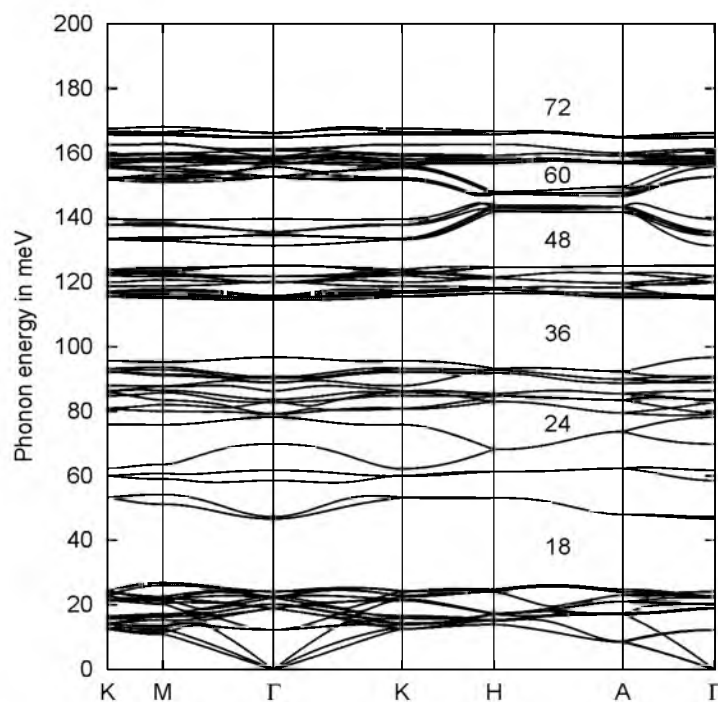


Figure 5.2: *Calculated phonon dispersion curves for YH_3 in the broken symmetry structure with $P6_3$ symmetry. The numbers between H and A give the total number of bands starting from 0 meV.*

We have also calculated the lattice dynamics for YH_3 in the HoD_3 structure ($P\bar{3}c1$ symmetry, Fig. 5.1); the corresponding phonon band structure is shown in Fig. 5.3. Since both structures are very similar, so are their phonon bands. However, there is one major difference. For the HoD_3 structure we find a soft mode close to Γ where, because $\omega^2 < 0$, we plot the real quantity $i\omega$. This shows that the HoD_3 structure is unstable, i.e. there are atomic displacements which can lower the energy, contrary to the assumption that the unperturbed lattice was in equilibrium. The position of the minimum of ω^2 is at $\mathbf{q} = 0$. This implies that a lower total energy structure exists in the same unit cell. Inspection of the calculated eigenvector of the soft mode reveals that it moves both H(M) atoms which are exactly in the plane in the HoD_3 structure, out of this plane. This is indeed the essential difference between the HoD_3 and broken symmetry ($P6_3$) structures. The soft mode for YH_3 in the HoD_3 structure is a restatement of the earlier finding by

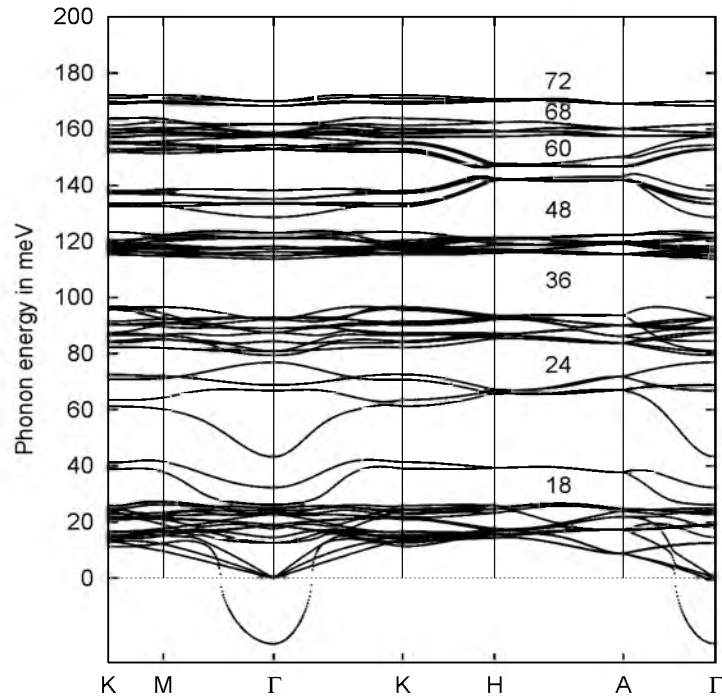


Figure 5.3: As the previous figure for YH_3 in the HoD_3 structure. For the soft mode solutions with $\omega^2 < 0$ we plot the real quantity $i\omega$.

explicit energy minimization that the broken symmetry structure has a lower total energy [19].

For YH_3 in the lattice structure with $\text{P6}_3\text{cm}$ symmetry, Fig. 5.1, we obtain the band structure shown in Fig. 5.4. The phonon band structure is quite similar to that of the P6_3 symmetry structure of Fig. 5.2. There is no soft mode in Fig. 5.4 although YH_3 in the P6_3 structure has a lower total energy. This is because the displacements needed to transform the $\text{P6}_3\text{cm}$ structure into the P6_3 structure do not simply correspond to an eigenmode of YH_3 in the $\text{P6}_3\text{cm}$ structure. In detail there are important differences between the calculated lattice dynamical properties of the $\text{P6}_3\text{cm}$ and P6_3 structures, which are discussed in the section dealing with the calculated phonon densities of states.

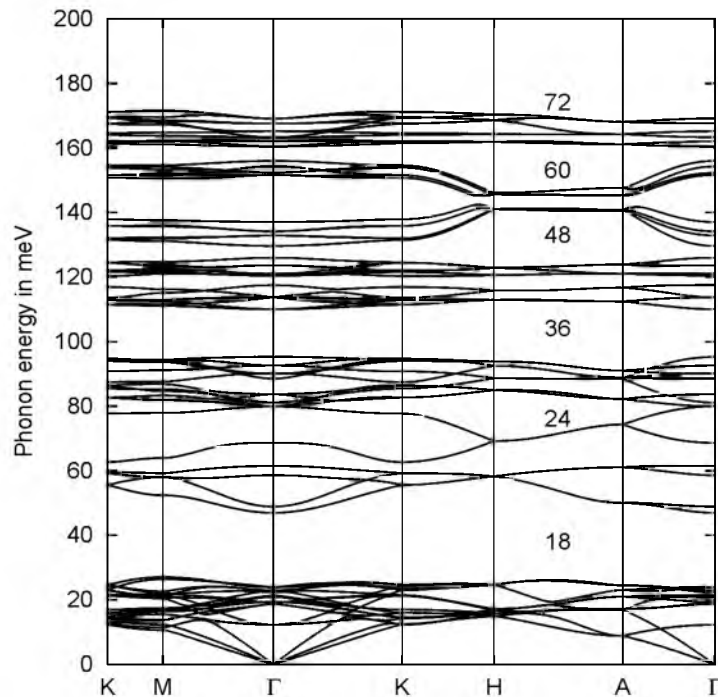


Figure 5.4: As the previous figure for YH_3 in the broken symmetry structure with $P6_3cm$ symmetry.

5.3.5 Raman and infrared spectra

The calculated phonon eigenfrequencies and eigenmodes at Γ can be compared to the results of the Raman experiments by Kierey *et al.* [35]. From a symmetry analysis of the experimentally observed modes Kierey *et al.* concluded that there is no inversion symmetry in the YH_3 lattice. The HoD_3 structure has $P\bar{3}c1$ symmetry which includes an inversion centre. Consequently, on the basis of these Raman experiments the HoD_3 structure was ruled out as a possible lattice structure for YH_3 . In Table 5.2 we compare our calculated phonon frequencies with the frequencies obtained from the Raman experiments, labeled with their point group symmetry at Γ . We omit the results we have obtained for the HoD_3 structure because these have an incorrect symmetry, as discussed. Both for the $P6_3cm$ structure and the $P6_3$ structure the calculated and experimental frequencies agree reasonably well, one would perhaps have a slight preference for the $P6_3cm$ structure from these data. This conclusion however is based upon the fact

Symmetry	Raman	Th.P6 ₃	Th.P6 ₃ cm
E ₁	19.0	18.8	18.7
A ₁	23.3	24.0	22.9
A ₁	54.9	58.5	58.6
A ₁	60.5	61.7	61.6
A ₁	76.9	78.1	80.0
A ₁	81.2	83.6	80.7
E ₁	90.0	88.8	89.8
E ₂	92.2	90.3	92.4
A ₁	97.2	96.7	95.0
E ₁	112.3	115.7	113.5
E ₁	161.2	161.0	162.0

Table 5.2: Comparison of the experimentally observed Raman frequencies by Kierey [35] with the calculated frequencies of the correct symmetry, for the broken symmetry structures with P6₃ and P6₃cm symmetry. The energies are in meV.

that of the many modes of the system only a limited number appear in the experimental Raman spectrum. Additional modes are required in order to really distinguish between P6₃cm and P6₃ symmetry.

A few vibrational modes were also identified by Lee and Shin [6] in optical experiments on $\text{YH}_{3-\delta}$; their corresponding frequencies are 77, 112, and 156 meV. They can be identified from the list of calculated frequencies of both the P6₃cm and P6₃ symmetry structures, cf. Table 5.2, but again the data are insufficient to distinguish between these two structures.

5.3.6 Densities of states and NVS experiments

The phonon density of states for YH_3 in the P6₃ broken symmetry structure is shown in Fig. 5.5 (a). From the partial densities of states for yttrium (not plotted) we find that the yttrium atoms largely dominate the low frequency vibrations as might be expected on account of their large mass. There is no clear distinction between the frequencies of motion in the basal ab plane and along the c -direction. Hydrogen atoms hardly participate in the motions at energies below 30 meV. The yttrium motions account for the lowest 18 bands, compare Fig. 5.2. The vibrations at energies above 40 meV (the remaining 54 bands) involve almost exclusively motions of hydrogen atoms.

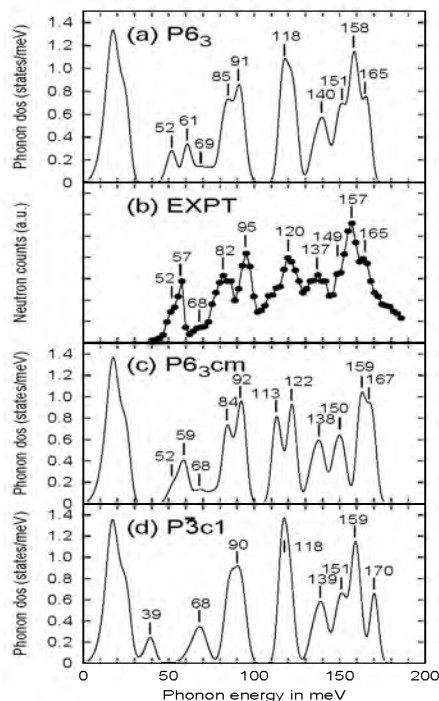


Figure 5.5: (a) Calculated total phonon densities of states for YH_3 in the broken symmetry structure with $P6_3$ symmetry. The data have been broadened using a Gaussian lineshape. The numbers indicate the maxima, or peak positions. (b) Experimental neutron vibrational spectroscopy data taken from Ref. [34]. (c) Calculated total phonon densities of states for YH_3 in the structure with $P6_3cm$ symmetry and (d) the HoD_3 structure with $P\bar{3}c1$ symmetry respectively.

The frequencies of the latter vibrations are grouped in bands separated by gaps, which results in well-defined peaks in the phonon density of states, cf. Fig. 5.5 (a). We observe large differences between the frequencies of modes corresponding to vibrations in the ab plane and those in which the atoms oscillate in the c -direction. This can be observed very clearly in Fig. 5.6 where the partial densities of states is plotted for the H(T) and H(M) atoms, projected onto motions in the basal plane and along the c -axis. The difference between those two motions is most striking for the H(M)-atoms. These can move relatively freely in open channels along the c -direction but are laterally constrained in the ab plane by the metal atoms in that plane. The former motions lead to low frequency modes with energies mainly between 50 meV and 70 meV, whereas the ab plane oscillations of the H(M)

atoms give high frequency modes with energies between 150 and 170 meV. The separation in energy between basal plane and longitudinal vibrations of the H(T) sublattice is smaller. The corresponding ab plane oscillations have energies between 80 and 100 meV, and between 110 and 130 meV. The vibrations of the H(T) atoms in the c -direction have frequencies mainly between 130 and 160 meV. In the following we will analyze the phonon density of states in detail. As it turns out the pattern of splitting and relative intensities of the peaks can sometimes be rationalized reasonably well on account of the symmetry independent (Wyckoff) positions of the hydrogen atoms and their occupation ratio.

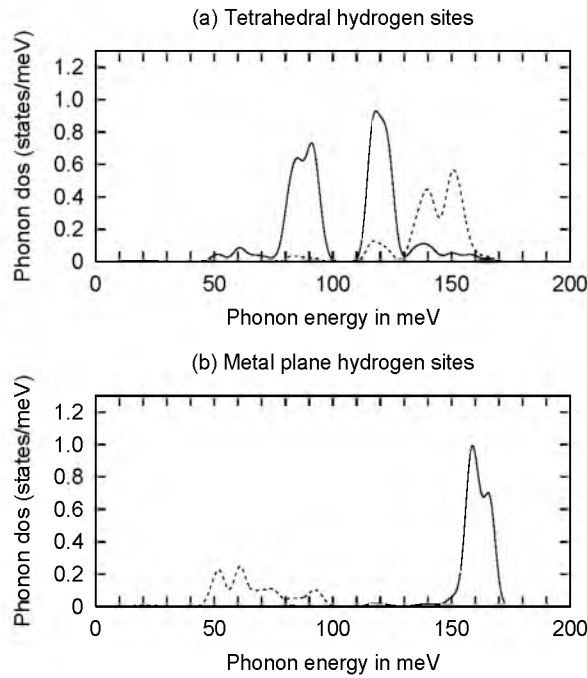


Figure 5.6: *Partial phonon densities of states calculated by projecting on (a) the H(T) and (b) the H(M) atoms, and oscillations in the basal ab -plane (solid lines) and in c -axis directions (dashed lines) respectively.*

In NVS experiments for YH_x and LaH_x powders with x ranging from 0 to 3, Udovic *et al.* [34,38] have measured the energy loss of neutrons as a result of inelastic scattering. This is closely related to our calculated total phonon density of states. The experimental high resolution data are plotted

$P6_3$	$P\bar{3}c1$	$P6_3cm$	Exp.	vibrations
52	39	52	52	H(M) $\parallel c$
61		59	57	H(M) $\parallel c$
69	68	68	68?	H(M) $\parallel c$
85		84	82	H(T) $\perp c$
91	90	92	95	H(T) $\perp c$
118	118	122	120	H(T) $\perp c$
140	139	138	137	H(T) $\parallel c$
158	159	159	157	H(M) $\perp c$

Table 5.3: Positions of calculated peaks in the (broadened) phonon density of states for the three possible structures. The experimental data are obtained from the NVS spectrum of Udovic *et al.* [34]. The energies are in meV.

in Fig. 5.5 (b). In Table 5.3 we compare the peak positions in the calculated phonon density of states of the broken symmetry structure ($P6_3$) to the peak energies obtained from the NVS experiments for YH_3 (Exp). Most calculated peaks have energies that compare very well to the experimental data, but there are differences in the details. We will discuss these differences starting from the low frequency eigenmodes which are dominated by H(M) vibrations along the c -direction. In the $P6_3$ broken symmetry structure the H(M) atoms are divided over three different Wyckoff positions, cf. Fig. 5.1 (b), which gives rise to three peaks at slightly different energies. Each of these peaks represents 2 bands, see Fig. 5.2 the bands 19 up to and including 24. In the calculations we find peaks at 52, 61 and a broad peak at 69 meV. The fact that these peaks indeed correspond H(M) vibrations along the c -direction can be observed in Fig. 5.6. In the NVS experiment, there is a single strong peak at 57 meV and a shoulder at 52 meV. In the HoD_3 structure with $P\bar{3}c1$ symmetry there are only two Wyckoff positions for the H(M) atoms with an occupation ratio of 2:1. Udovic *et al.* suggested that the two experimental peaks and their relative intensity are evidence for the existence of only two Wyckoff positions, which would agree with the HoD_3 structure [33]. We would suggest the presence of a broad feature in the NVS data near 68 meV, which could correspond to the broad peak at 69 meV in the calculated density of states of the $P6_3$ broken symmetry structure.

We can also compare the experimental results to the phonon density of states of the other two structures; the main results are collected in Table 5.3

and Fig. 5.5 (c) and (d). In the low energy range 40-70 meV, the calculated density of states of the $P6_3cm$ symmetry structure of Fig. 5.5 (c) gives a very good agreement with experiment. In the $P6_3cm$ symmetry again only two H(M) Wyckoff positions are present which are occupied according to a ratio 2:1. The singly occupied Wyckoff site corresponds to the atoms which are slightly further displaced from the metal plane. Consequently, these atoms are somewhat more confined along the c -axis by the yttrium atoms which leads to the higher frequency of 68 meV for modes involving motions of these atoms along the c -axis.

The calculated phonon density of states for the HoD_3 structure ($P\bar{3}c1$) is shown in Fig. 5.5 (d) where we have ignored the soft mode and its imaginary frequency. The agreement with experiment is much poorer. The peak corresponding to the motion along the c -axis of the H(M) atoms located *exactly* in the yttrium plane, cf. Fig. 5.1 (c), which corresponds to the bands 19 and 20 in Fig. 5.3, is has an energy of 39 meV, which is too low compared to the experimental feature at 52-57 meV. It even partially overlaps with the highest frequency yttrium vibrations. Part of its intensity is lost to the soft mode at imaginary frequencies. The peak related to the vibrations along the c -axis of the out-of-plane H(M) atoms (the 4 bands 21 up to and including 24 in Fig. 5.3) is at 68 meV, which is about 10 meV higher than the experimental feature.

The next feature in the experimental spectrum are two relatively strong peaks at 82 and 95 meV. All three lattice structures give strong peaks in their phonon density of states in this energy range, but the shape and splitting of the peaks differ. The peaks correspond to bands 25 up to including 36 in Figs. 5.2-5.3. These bands are mainly composed of vibrations of the H(T) atoms moving in the ab -plane, cf. Fig. 5.6. In the HoD_3 ($P\bar{3}c1$) structure all 12 bands lead to essentially one peak at 90 meV, Fig. 5.5 (d), whereas in the $P6_3cm$ and $P6_3$ broken symmetry structures we find two peaks at 84, 92 and 85,91 meV, respectively, each of which correspond to 6 bands. In the experimental spectrum there is a clear splitting between two peaks at 82 meV and 95 meV with approximately equal intensity. It will be obvious that this agrees reasonably well with the broken symmetry structures, but poorly with the HoD_3 structure. In simple terms the splitting into two peaks is related to the two different Wyckoff positions for the H(T) atoms in both broken symmetry structures, both of which are equally occupied by six hydrogen atoms. In the HoD_3 all 12 tetrahedral hydrogens correspond to a single Wyckoff position. In the broken symmetry structures all of the metal-plane H(M) hydrogens are displaced out of the metal planes.

As a result of this also the H(T) atoms above the metal planes experience a different local environment than the H(T) atoms below the metal planes. These two different types of H(T) atoms thus also experience a slightly different local force fields. Although the size of the splitting of the two peaks is apparently underestimated in our calculations, the peak splitting itself can be easily understood in terms of a broken symmetry structure.

The peak around 120 meV in the experimental spectrum is seen to correspond to the bands 37 up to and including 48, cf. Figs. 5.2-5.3 and Fig. 5.5. These also are mainly composed of vibrations of the H(T) atoms in the ab plane, cf. 5.6. All three structures give this peak rather well. Only the $\text{P6}_3\text{cm}$ structure gives a clearly split feature with maxima at 113 meV and 122 meV. It is not clear to us whether a low energy shoulder below 120 meV is present in the experimental spectrum, cf. Fig. 5.5 (b). Bands 49 up to and including 60 correspond to vibrations of the H(T) atoms along the c -axis with energies roughly in the range 140-150 meV. Again all three structures give a density of states in this range which agrees rather well with experiment.

The high energy range >150 meV is dominated by vibrations of the H(M) atoms in the ab plane corresponding to bands 61 up to and including 72 in Figs. 5.2-5.3. The highest frequency peak is due to vibrations in the ab plane direction of the H(M) atoms that are in or closest to the metal ab plane, see Fig. 5.1. In the HoD_3 structure these atoms are tightly confined exactly in the metal plane in the centre of an equilateral triangle of yttrium atoms, and these consequently have a high vibrational frequency of 170 meV. In the broken symmetry structures this effect is still present but weaker because these atoms are slightly out of the metal-plane. The vibrations H(M) atoms that are further away from the metal planes in the ab plane direction show up at a slightly lower energy around 160 meV. This peak has an intensity which is roughly twice that of the highest energy peak, which again reflects the occupancy of the corresponding hydrogen sites. In the experimental high resolution data of Ref. [34] a double peak at 157, 165 meV with the right intensity distribution can be clearly identified. The splitting agrees rather well with the broken symmetry structures and the agreement with the HoD_3 structure is slightly worse. Finally it may be observed that the high energy density of states >150 meV for the P6_3 broken symmetry structure has a better agreement with experiment than the $\text{P6}_3\text{cm}$ broken symmetry structure, cf. 5.5 (a)-(c). This is mainly due to the fact that the gap between the H(T) c -axis vibrations below 150 meV and the H(M) ab plane vibrations is too large in the latter structure.

In conclusion, whereas the agreement between the calculated phonon density of states and the experimental NVS data is rather good for the broken symmetry structures, there are discrepancies with the density of states of the HoD_3 structure, especially in the energy range below 100 meV. The distinction between both broken symmetry structures, $P6_3$ vs. $P6_3cm$ is more difficult to make. The calculated phonon density of states of the $P6_3$ structure gives a slightly better agreement with the experimental data in the energy range above 100 meV. This structure is also the one that has the lowest total energy in a DFT/LDA calculation.

5.4 Results for YD_3

Using the atomic force constants calculated for YH_3 it is trivial to recalculate the phonon bands for YD_3 in the broken symmetry structure by doubling the corresponding masses when setting up the dynamical matrix. Due to the almost perfect decoupling between the hydrogen and yttrium vibrations, the low frequency yttrium modes are almost identical to those in YH_3 . The frequencies of the deuterium modes in YD_3 differ from those of hydrogen in YH_3 almost exactly by a factor of $1/\sqrt{2}$. This is what you would get by a simple scaling of the frequencies according to the masses. We therefore refrain from showing the YD_3 phonon bands explicitly. We next calculate the anisotropic temperature factors for the broken symmetry structure, both at zero temperature and at 295 K. The experimental data at 295 K were refined in detail by Udovic *et al.* [14]. The \mathbf{B} -matrices of temperature factors, Eq. 5.7, possess the symmetry properties imposed by a particular site. \mathbf{B} -matrices of symmetry-related sites should transform into one another by applying the symmetry operations of the space group. These symmetry properties were explicitly checked and found to hold within 1 %. For the yttrium atoms we find almost isotropic temperature factors (which is not imposed by symmetry). The zero point motion results in an (almost) isotropic B of about 0.11 \AA^2 . This number increases to about 0.39 \AA^2 at 300 K which is reasonably close to the experimentally determined value of 0.34 \AA^2 found by Udovic *et al.* in their model II [14] for YD_3 . Direct comparison is difficult though, since the experimental data are refined assuming a different structure. For those atoms that vibrate in modes which are similar in both lattice structures, we do find values in good agreement with the experimental values. As before, we denote the deuterium atoms in the tetrahedral and metal plane positions by $D(T)$ and $D(M)$, respectively. For the $D(T)$ atoms, the calculated value of B_{33} is 1.08 \AA^2 , the experimen-

Atom	position	Wyckoff	B_{11}	B_{33}
theory				
D ₁ (M)	-0.07 <i>c</i>	2a	0.98	2.42
D ₂ (M)	+0.07 <i>c</i>	2b	0.97	3.14
D ₃ (M)	+0.03 <i>c</i>	2b	0.94	3.88
experiment				
D(m2)	±0.07 <i>c</i>	4d	0.84	2.8
D(m1)	0.00 <i>c</i>	2a	0.5	6.7

Table 5.4: Calculated temperature factor matrix elements in \AA^2 along the lattice axes for each of the Wyckoff positions of the H(M) atoms in YD_3 in the $P6_3$ structure. These are compared to the experimental temperature factors obtained by assuming a HoD_3 structure. By symmetry, $B_{11} = B_{22} = 2B_{21} = 2B_{12}$. The other elements are zero by symmetry.

tal value is 1.13\AA^2 . The calculated numbers in the \mathbf{B} -matrix for the D(T) atoms which correspond to an in-plane motion are about 50 % larger.

Most interesting are the D(M) atoms, for which the thermal and zero point motion is strongly anisotropic. The motion of these atoms is very much confined within the basal plane, but it has a very large amplitude in the c -direction and a correspondingly huge temperature factor. The ellipsoids of vibration (Eq. 5.7) for these atoms are cigar-shaped. The results for these motions at 295 K are given in Table 5.4. The zero point motion still dominates the root mean square displacements of these deuterium atoms at 295 K, so the results at zero temperature are very similar. Because of the three-fold rotation symmetry of this site, the \mathbf{B} -matrix elements are related by $B_{11} = B_{22} = 2B_{21} = 2B_{12}$; consequently only the symmetry independent values B_{11} and B_{33} are given in Table 5.4. In the broken symmetry structure the three different Wyckoff positions for the D(M) atoms are labeled with an index. D₁(M) and D₂(M) correspond to deuterium atoms at about $0.07 c$ from the metal plane, D₃(M) to atoms closer to the plane at about $0.03 c$. In our calculations we have chosen a representation for the broken symmetry structure in which both D₂(M) and D₃(M) are *above* the metal plane.

The calculated values of B_{33} are large, and largest for the D₃(M) atoms which are located closest to the metal planes. The numbers extracted from experiment for out-of-plane atoms [D(m2) in Ref. [14]; the D(m1) atoms are exactly in the metal plane] are also large. In particular, the value is

huge for the deuterium atom which is assumed by Udovic *et al.* to be in the metal plane. The value of 6.7 corresponds to a root mean square displacement of about 0.3 Å which is about 1.3 % of the lattice constant in the c -direction. For hydrogen it is even larger ($\sim 0.02 c$), and of the same order of magnitude as the size of the symmetry-breaking hydrogen displacements ($\sim 0.03 c$) predicted from the LDA calculations.

Udovic *et al.* [30] tried to refine the diffraction data using the broken symmetry structure suggested by Kelly. Since they do not find the small additional peaks which should be present if the high symmetry is broken, they concluded that YH_3 has the HoD_3 structure. In particular, they focused on the (103)-reflection, repeated the experiment at low temperature and took more data. They found no significant structure corresponding to the (103)-reflection. Using the broken symmetry geometry we have calculated the Debye-Waller factors at zero temperature and compare the reduction of intensity of the (103)-reflection peak to the corresponding reduction of neighboring peaks. Although the reduction for the (103)-reflection is somewhat larger than for other peaks, it is only reduced by about one third compared to the intensity in the absence of zero point motion. This is not sufficient to make this peak unobservable in the diffraction experiments. It consequently seems to rule out the possibility that the symmetry breaking is being masked in diffraction experiments by a large zero point motion. However, it does not rule out the possibility that the system is actually in a superposition of broken symmetry states. In the next section we discuss this possibility in more detail.

5.5 Discussion

We have calculated the lattice vibrational properties of YH_3 and YD_3 within the harmonic approximation for three proposed lattice structures for YH_3 . Apart from a calculated soft mode in the HoD_3 structure the phonon bands look quite similar for the three structures and are in overall agreement with the experimental NVS data [34,38]. The soft mode reflects the fact that the HoD_3 structure ($P\bar{3}c1$ symmetry) is unstable in DFT/LDA calculation [19]. The vibrational frequencies at Γ agree reasonably well with the Raman spectra of Kierey *et al.* [35] for both the other two, so-called broken symmetry structures, which have $P6_3$ and $P6_3cm$ symmetry, respectively. On account of these data there is no clear preference for one or the other structure.

The phonon bands can be divided in to groups that are reasonably well-

separated, which gives rise to distinct peaks in the phonon density of states. The latter can be compared to the experimental NVS spectrum of Udovic *et al.* [34]. Moreover, from the calculated eigenvectors we can identify for each peak in the calculated phonon density of states which atoms in which direction have a dominant contribution to the vibrations represented by that peak. The lowest frequency modes below 30 meV correspond almost exclusively to yttrium vibrations, and are comparable to the modes in pure yttrium; modes at higher energies (54 bands in total) are mainly due to motions of the hydrogen sublattice. In these modes we find distinct differences between the calculated spectra of the three suggested lattice structures. At the low energy side below 100 meV, the NVS spectrum is in poor agreement with the phonon density of states of the HoD₃ structure. The agreement with the density of states of the broken symmetry structures is clearly much better; there are only small differences between the P6₃ and P6₃cm structures. Comparison of the data in the high energy range above 100 meV gives a slightly better agreement with the P6₃ structure, which is also the lowest energy structure from a DFT/LDA calculation [19].

The agreement between the NVS experimental data and the phonon density of states is not perfect. For instance, around 90 meV two peaks are found in the experiment which are split by 13 meV. The calculated splitting is only 6 and 8 meV for the P6₃ and P6₃cm structures respectively (and next to zero for the HoD₃ P $\bar{3}$ c1 structure). This could indicate a shortcoming of the LDA in describing the energy landscape or an inaccuracy in the harmonic approximation we have used here. It could also indicate the use of an insufficiently large supercell for calculating the interatomic force constants. It is difficult to test the latter as we estimate the computational effort required for a (3 × 3 × 3) supercell to be at least an order of magnitude larger than for the (2 × 2 × 2) supercell we have used. At this stage it is not feasible to test better approximations. However, the assignments we have attached to the peaks of the NVS spectrum could be checked by measurements on single crystals, which should give more detailed information.

The calculated zero point motions for the hydrogen and deuterium atoms are very large and anisotropic. This is particularly true for the H(M)-atoms which are involved in the symmetry lowering when going from the HoD₃ structure to a broken symmetry structure. Since the high P $\bar{3}$ c1 symmetry of the HoD₃ structure can be broken in four different but equivalent ways the LDA Born-Oppenheimer surface has four global minima. The energy difference between the high symmetry structure and the P6₃ broken symmetry structure is small [71]; it is in fact smaller than the calculated total

zero point energy (~ 60 meV) of the two modes in the $P6_3$ broken symmetry structure which are relevant for the symmetry breaking. Therefore it is not unlikely that the system is not confined in a particular $P6_3$ structure but instead in a quantum superposition of broken symmetry states. This would lead to the picture given schematically in Fig. 5.7. Refining the experimental powder diffraction data using all available sites in such a superposition of four representations of the broken symmetry structure is very complicated due to the huge amount of degrees of freedom in that case. Therefore it is not easy to prove or disprove this model by a refinement of the neutron powder diffraction data [73]. The huge temperature factors are the only experimental support at present.

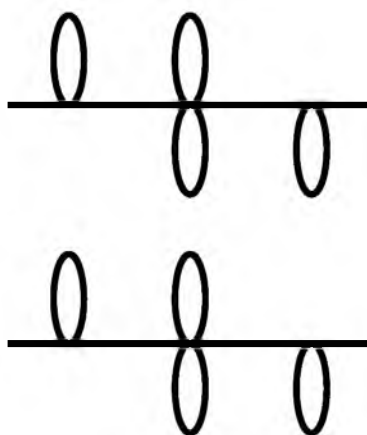


Figure 5.7: Schematic picture of the quantum averaged broken symmetry structures as in Fig.5.1. The ellipsoids give an impression of the quantum delocalization of the $H(M)$ atoms.

The recent solid state NMR experiments [32] are even more difficult to interpret. The results of these experiments for YD_3 show that deuterium sites of different local symmetry exist in the ratio of approximately 1:1:1. In the $P\bar{3}c1$ (HoD_3) structure the ratio of hydrogen sites of different symmetry is 12:4:2, which is very different from the NMR results. For the two broken symmetry structures the 12 $H(T)$ atoms are divided equally over two Wyckoff positions. The $H(M)$ atoms are distributed over two Wyckoff positions in a ratio 2:1 in the $P6_3cm$ structure and equally distributed over three Wyckoff positions in the $P6_3$ structure. This would lead to a ratio of 6:6:4:2 for the $P6_3cm$ structure and 6:6:2:2:2 for $P6_3$ structure. Thus for both these structures the splitting of the $H(T)$ sites is in agreement with

the NMR results. However for the H(M) sites the NMR results indicate the presence of more symmetry than one would expect on the basis of either of the broken symmetry structures. This may point towards a quantum averaging that leads to indistinguishable NMR features for the H(M) atoms. Due to their quantum motion all of these metal plane hydrogen atoms have a large probability to be out of the metal plane, as sketched in Fig. 5.7. This may give rise to similar resonance patterns for all the H(M) atoms. To be consistent we have to assume however that the quantum motion of the H(T) atoms is smaller, since they still give rise to two different features in the NMR data.

Recently we have calculated the band structure of YH_3 using the GW approach both for the high symmetry $\text{P}\bar{3}\text{c}1$ structure and for the $\text{P}6_3$ structure. One might wonder what the influence of the large zero point motions of the hydrogen atoms is on the band structure and, in particular, on the band gap. In a quantum averaged picture the electronic properties are given by averaging the electronic structures corresponding to the ionic configurations encountered during the zero point motion (if one assumes that the Born-Oppenheimer approximation does not break down and the electrons are always in their instantaneous ground state). In general, this electronic structure average can be different from the electronic structure corresponding to the average high symmetry lattice structure. However, since the recent GW calculations give a substantial band gap for both the HoD_3 structure and the broken symmetry structure, it is likely that the electronic structure average also has a substantial gap.

It would be very interesting to explicitly include the quantum character of the hydrogen or deuterium atoms, and to solve the Schrödinger equation for the hydrogen atoms in the potential landscape. This can be done in principle using the *ab-initio* path-integral molecular dynamics method [74]. This method was recently used to include the quantum character of hydrogen in simple molecules, and clearly showed the effect of quantum tunneling of the hydrogen atoms [75,76]. Applying this method to a solid is a formidable computational effort requiring even an order of magnitude more computer time than a “classical” Car-Parrinello molecular dynamics simulation. Unfortunately, this is at present out of reach.

Appendix

We have tested our codes by calculating phonon band structures for silicon using the direct supercell method to calculate interatomic force constants.

We use a large ($5 \times 5 \times 5$) supercell consisting of 250 silicon atoms and a smaller ($3 \times 3 \times 3$) supercell of 54 silicon atoms. In both cases only the Γ -point was used for the Brillouin zone summation. In the calculation of the phonon bands we include the force constants between the central, displaced atom, and complete shells of neighboring atoms. In the larger supercell we have neighbors up to the twelfth shell, and neighbors up to the fifth shell in the smaller supercell. Following Capaz and Joannopolis [77] we include for both supercells one more shell of atoms in which the force constants are chosen to obey the translational sum rule exactly. In figure 5.8 we plot the phonon bands for silicon using the force constants obtained in the smaller and larger supercell respectively. Using the larger supercell we are able to reproduce the experimental data in great detail.

The calculated frequencies at the zone boundaries agree within 3.5 percent with the experimental data taken from Ref. [41]. Using the much smaller ($3 \times 3 \times 3$) supercell also leads to very reasonable results. At the zone boundaries of the Brillouin zone we find discrepancies which are 6.7 percent or less. The ellipsoids of zero point motion are spheres for silicon as a result of full cubic symmetry. The calculated root mean square displacements are close to the experimental values [78], both using the smaller and the larger supercell.

References

- [1] F. Klose, C. Rehm, D. Nagengast, H. Maletta, and A. Weidinger, *Phys. Rev. Lett.* **78**, 1150 (1997).
- [2] J.A. Dura, P. Isberg, T. Watanabe, T.J. Udovic, G. Andersson, and C.F. Majkrzak, *Phys. Rev. Lett.* **79**, 901 (1997).
- [3] J.N. Huiberts, R. Griessen, J.H. Rector, R.J. Wijngaarden, J.P. Dekker, D.G. de Groot, and N.J. Koeman, *Nature (London)* **380**, 231 (1996).
- [4] J.N. Huiberts, J.H. Rector, R.J. Wijngaarden, S. Jetten, D. de Groot, B. Dam, N.J. Koeman, R. Griessen, B. Hjörvarsson, S. Olafsson, and Y.S. Cho, *J. Alloys and Compounds* **239**, 158 (1996).
- [5] A.T.M. van Gogh, E.S. Kooij, and R. Griessen, *Phys. Rev. Lett.* **83**, 4614 (1999).
- [6] M.W. Lee, and W.P. Shin, *J. Appl. Phys.* **86**, 6798 (1999).
- [7] J.H. Weaver, R. Rosei, and D.T. Peterson, *Phys. Rev. B* **19**, 4855 (1979).

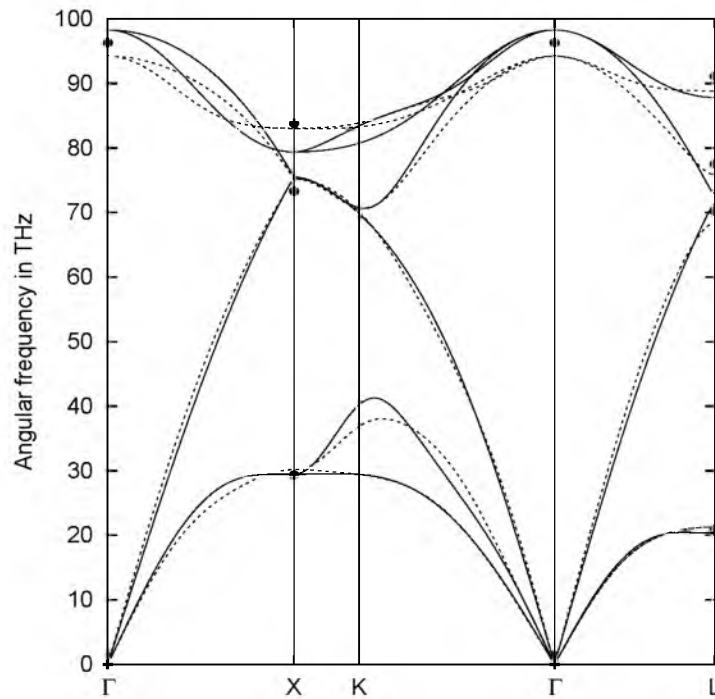


Figure 5.8: *Calculated phonon bands for silicon using force constants from the smaller supercell (solid lines) and the bigger supercell (dashed lines). Some experimental values taken from Ref. [78] are given by the filled circles.*

- [8] J.H. Weaver, D.T. Peterson, and R.L. Benbow, Phys. Rev. B **20**, 5301 (1979).
- [9] D.J. Peterman, B.N. Harmon, J. Marchiando, and J.H. Weaver, Phys. Rev. B **19**, 4867 (1979).
- [10] J.P. Dekker, J. van Ek, A.Lodder, and J.N. Huiberts, J. Phys. Condens. Matter **5**, 4805 (1993).
- [11] Y. Wang and M.Y. Chou, Phys. Rev. Lett. **71**, 1226 (1993); Phys. Rev. B **51**, 7500 (1995).
- [12] M. Mannsmann and W.E Wallace, J. Phys. (Paris) **25**, 454 (1964).
- [13] N.F. Miron, V.I. Shcherbak, V.N. Bykov, and V.A. Levдик, Sov. Phys. Crystallog. **17**, 342 (1972).

- [14] T.J. Udovic, Q. Huang, and J.J. Rush, *J. Phys. Chem. Solids* **57**, 423 (1996).
- [15] A. Remhof, G. Song, Ch. Sutter, R. Siebrecht, H. Zabel, F. Güthoff, and J. Windgasse, *Phys. Rev. B* **59**, 6689 (1999).
- [16] A. Remhof, G. Song, K. Theis-Bröhl, and H. Zabel, *Phys. Rev. B* **56**, R2897 (1997).
- [17] R. Eder, H.F. Pen, and G.A. Sawatzky, *Phys. Rev. B* **56**, 10115 (1997).
- [18] K.K. Ng, F.C. Zhang, V.I. Anisimov, and T.M. Rice, *Phys. Rev. Lett.* **78**, 1311 (1997); *Phys. Rev. B* **59**, 5398 (1999).
- [19] P.J. Kelly, J.P. Dekker, and R. Stumpf, *Phys. Rev. Lett.* **78**, 1315 (1997).
- [20] P. van Gelderen, P.A. Bobbert, P.J. Kelly, and G. Brocks, *Phys. Rev. Lett.* **85**, 2989 (2000)
- [21] L.J. Sham, and M. Schlüter, *Phys. Rev. Lett.* **51**, 1888 (1983); *Phys. Rev. B* **32**, 3883 (1985).
- [22] J.P. Perdew, and M. Levy, *Phys. Rev. Lett.* **51**, 1884 (1983).
- [23] L. Hedin, *Phys. Rev.* **139**, A796 (1965); L. Hedin, and S. Lundqvist in *Solid State Physics*, edited by H. Ehrenreich, F. Seitz, and D. Turnbull (Academic, New York, 1969), Vol. 23, p. 1.
- [24] For recent reviews of the *GW* method and its applications see F. Aryasetiawan and O. Gunnarsson, *Rep. Prog. Phys.* **61**, 237 (1998) or L. Hedin, *J. Phys. Condens. Matter* **11**, R489 (1999).
- [25] M.S. Hybertsen, and S.G. Louie, *Phys. Rev. Lett.* **55**, 1418 (1985); *Phys. Rev. B* **34**, 5390 (1988).
- [26] R.W. Godby, M. Schlüter, and L.J. Sham, *Phys. Rev. Lett.* **56**, 2415 (1986); *Phys. Rev. B* **37**, 10159 (1988).
- [27] F. Aryasetiawan and O. Gunnarsson, *Phys. Rev. Lett.* **74**, 3221 (1995).
- [28] S. Massidda, A. Continenza, M. Posternak, and A. Baldereschi, *Phys. Rev. Lett.* **74**, 2323 (1995).
- [29] P. van Gelderen, P.A. Bobbert, P.J. Kelly, G. Brocks, and R. Tolboom, submitted to *Phys. Rev. B*
- [30] T.J. Udovic, J.J. Rush, Q. Huang, and I.S. Anderson, *Phys. Rev. Lett.* **79**, 2920 (1997).

-
- [31] P.J. Kelly, J.P. Dekker, and R. Stumpf, Phys. Rev. Lett. **79**, 2921 (1997).
- [32] J.J. Balbach, M.S. Conradi, M.M. Hoffmann, T.J. Udovic, N.L. Adolphi, Phys. Rev. B **58**, 14823 (1998).
- [33] T.J. Udovic, Q. Huang, R.W. Erwin, B. Hjörvarsson, and R.C.C. Ward, Phys. Rev. B **61**, 12701 (2000).
- [34] T.J. Udovic, Q. Huang, and J.J. Rush, Mat. Res. Soc. Symp. Proc. **513**, 197 (1998).
- [35] H. Kierey, M. Rode, A. Jacob, A. Borgschulte, and J. Schoenes, Phys. Rev. B **63**, 134109 (2001).
- [36] P. van Gelderen, P.J. Kelly, and G. Brocks, to be published.
- [37] P. van Gelderen, P.J. Kelly, and G. Brocks, Phys. Rev. B **63**, R100301 (2001).
- [38] T.J. Udovic, J.J. Rush, Q. Huang, and I.S. Anderson, J. Alloys and Compounds **253-254**, 241 (1997).
- [39] O. Madelung, *Introduction to Solid State Theory*, Springer, Berlin, Heidelberg, New York, 1978.
- [40] P. Brüesch, *Phonons: Theory and Experiments I*, Springer, Berlin, Heidelberg, New York, 1982.
- [41] H. Bilz and W. Kress, *Phonon Dispersion Relations in Insulators*, Springer Verlag, Berlin, Heidelberg, New York, 1979.
- [42] R.M. Martin, Phys. Rev. **186**, 871 (1969).
- [43] S. Baroni, P. Giannozzi, and A. Testa, Phys. Rev. Lett. **58**, 1861 (1987).
- [44] P. Pavone, K. Karch, O. Schütt, W. Windl, D. Strauch, P. Giannozzi, and S. Baroni, Phys. Rev. B **48**, 3156 (1993).
- [45] P. Giannozzi, S. de Gironcoli, P. Pavone, and S. Baroni, Phys. Rev. B **43**, 7231 (1991).
- [46] S.Y. Savrasov, Phys. Rev. B **54**, 16470 (1996).
- [47] M.T. Yin and M.L. Cohen, Phys. Rev. Lett. **45**, 1004 (1980).
- [48] K. Kunc and R.M. Martin, Phys. Rev. Lett. **48**, 406 (1982).
- [49] M.T. Yin and M.L. Cohen, Phys. Rev. B **25**, 4317 (1982).
- [50] K. Kunc, and P. Gomes Dacosta, Phys. Rev. B **32**, 2010 (1985).
- [51] A. Fasolino, E. Molinari, and K. Kunc, Phys. Rev. B **41**, 8302 (1990).

- [52] S. Wei and M.Y. Chou, Phys. Rev. Lett. **69**, 2799 (1992); Phys. Rev. B **50**, 2221 (1992).
- [53] J. Ihm, A. Zunger, and M.L. Cohen, J. Phys. C **12**, 4409 (1979).
- [54] W. Frank, C. Elsässer, and M. Fähnle, Phys. Rev. Lett. **74**, 1791 (1995).
- [55] A. Eichler, K.-P. Bohnen, W.Reichardt, and J. Hafner, Phys. Rev. B **57**, 324 (1998).
- [56] G. Kresse, J. Furthmüller, and J. Hafner, Europhys. Lett. **32**, 729 (1995).
- [57] K. Parlinski, Z.Q. Li, and Y. Kawazoe, Phys. Rev. Lett. **78**, 4063 (1997).
- [58] X. Gonze, J.-C. Charlier, D.C. Allan, M.P. Teter, Phys. Rev. B **50**, 13035 (1994).
- [59] F. Detraux, Ph. Ghosez, and X. Gonze, Phys. Rev. Lett. **81**, 3297 (1998)
- [60] K. Parlinski, Z.Q. Li, and Y. Kawazoe, Phys. Rev. Lett. **81**, 3298 (1998)
- [61] X. Gonze, Phys. Rev. B **55**, 10337 (1997)
- [62] X. Gonze, and Ch. Lee, Phys. Rev. B **55**, 10355 (1997)
- [63] G. Kern, G. Kresse, and J. Hafner, Phys. Rev. B **59**, 8551 (1999)
- [64] B.T.M. Willis and A.W. Pryor, *Thermal Vibrations in Solids*, Cambridge University Press, 1975.
- [65] G.Brocks, J. Chem. Phys. **102**, 2522 (1995); J. Phys. Chem. **100**, (1996); 17327 Phys. Rev. B**55**, 6816 (1997); Theor. Chem Acc. **104**, 116 (2000).
- [66] R. Car and M. Parrinello, Phys. Rev. Lett. **55**, 2471 (1985).
- [67] I. Stich, R. Car, M. Parrinello, and S. Baroni, Phys. Rev. B **39**, 4997 (1989).
- [68] N. Troullier and J.L. Martins, Phys. Rev. B **43**, 1993 (1991).
- [69] Y. Wang and M.Y. Chou, Phys. Rev. B **44**, 10339 (1991).
- [70] S.G. Louie, S. Froyen, and M.L. Cohen, Phys. Rev. B **26**, 1738 (1982).
- [71] An unconstrained energy minimization invariably finds a broken symmetry structure. However, accurate determination of the energy gain requires a constrained symmetry energy minimization. The energy

difference of 70 meV per Y_6H_{18} unit cell between the HoD_3 and broken symmetry structure reported in Ref. [19] was too large because in the HoD_3 calculation full relaxation of the yttrium atoms was not included. Including this relaxation lowers the energy gain to about 40 meV.

- [72] S.K. Sinha, T.O. Brun, L.D. Muhlenstein, and J. Sakurai, Phys. Rev. B **1**, 2430 (1970).
- [73] T.J. Udovic, private communication
- [74] D. Marx and M. Parrinello, J. Chem. Phys. **104**, 4077 (1996).
- [75] D. Marx and M. Parrinello, Z. Phys. B **95**, 143, (1995).
- [76] D. Marx and M. Parrinello, Science, **271**, 179 (1996).
- [77] R.B. Capaz and J.D. Joannopoulos, Phys. Rev. B **54**, 13402 (1996).
- [78] P.J.E. Aldred and M. Hart, Proc. Roy. Soc. London A **332**, 223 (1973).

Chapter 6

GW calculations for LaH₃

ABSTRACT

From optical transmission experiments and electrical resistivity measurements it has been concluded that LaH₃ is a semiconductor, with an optical band gap of about 1.9 eV. Contrary to this result recent electronic structure calculations within the Local Density Approximation (LDA) predict that LaH₃ should be metallic. This discrepancy between experiment and the LDA result has led to the suggestion that the gap in LaH₃ results from strong local electron correlations, which are not included in the LDA. However, we argue on the basis of quasi-particle calculations within the so-called *GW* approximation that the gap in this material is well understood without invoking strong on-site correlation effects.

6.1 Introduction

Recent interest in the lanthanum and yttrium hydrides can be traced back to the discovery by Huiberts *et al.* [1] of so-called “switchable mirrors”. They have found that thin films of yttrium and lanthanum which are exposed to hydrogen gas absorb hydrogen atoms and exhibit a spectacular metal-insulator (MI) transition as a function of their hydrogen content. This reversible MI transition which takes place at a hydrogen-to-metal ratio of about 2.8 can be witnessed with the naked eye. The number of hydrogen atoms per metal atom in the films can easily be switched between two and three by varying the hydrogen pressure or by electrochemical techniques [2]. In the dihydride phase the switchable mirror layers are metallic and reflecting whereas the trihydrides are semiconducting and transparent. The possibility that these switchable mirrors can be used in technological applications has evidently stimulated a large amount of experimental work [3-7]. The semiconducting trihydride phases have attracted theoretical interest because a large discrepancy was found between the experimentally obtained band gaps and predictions by electronic structure calculations within the Local Density Approximation (LDA). This discrepancy is particularly large for YH_3 . For this material the experimentally determined band gap is almost 3 eV whereas LDA calculations predict band *overlap* by more than 1 eV for YH_3 in the experimentally obtained lattice structure [8,9] which is the so-called HoD_3 structure [10].

LDA calculations are essentially ground state calculations which usually produce very accurate total energies and charge densities. However, it is well known that these calculations underestimate band gaps for many semiconductors and insulators. The discrepancy between the LDA results and experiment for LaH_3 is of the same order as the discrepancy found for many other materials. However, for YH_3 the discrepancy is much larger, and for that reason alternative mechanisms have been proposed to explain the gap in these materials.

The first mechanism was suggested on the basis of LDA total energy calculations by Kelly *et al.* [11]. These calculations predict that YH_3 has a lattice structure which is slightly different from the HoD_3 structure. Small symmetry-breaking hydrogen displacements were found to lower the total energy and open up a gap of about 0.8 eV in the LDA spectrum. Along with a correction for the usual underestimation of the band gap in LDA spectra, this symmetry-breaking might explain the large gap in YH_3 . However, the predicted displacements in this strong electron-phonon coupling mechanism have not been confirmed in neutron diffraction experiments so far

[12,13]. This might be related to large hydrogen zero point motion though [14]. On the other hand, the comparison of calculated phonon densities of states to vibrational spectroscopy data by Udovic *et al.* [15,16] seems to support a symmetry breaking [17]. In the second mechanism a pivotal role is assigned to strong local electron correlations. The interactions between localized d orbitals in transition metal oxides like NiO are poorly described in the LDA, which is reflected in a severe underestimation of the band gap by about 4 eV [18]. Since this discrepancy is of the same size as the discrepancy in YH₃, it has been suggested that similar strong local correlations between two electrons on a hydrogen site may be responsible for the large gaps in LaH₃ and YH₃. Ng *et al.* [19] have postulated a parameterized model Hamiltonian for LaH₃ which includes strong local correlation terms. The excitation spectrum of LaH₃ for this model calculation has a band gap of about 2 eV if reasonable parameters are used. Using a similar model for YH₃ Eder *et al.* [20] have shown that strong local correlations can open a gap for YH₃ as well. However, starting from the LDA results, the opening of a gap is different in both model calculations. In the model by Ng *et al.* the gap opens up mainly due to a large reduction of the hydrogen valence band width as compared to the LDA band width. On the other hand, the main effect of “breathing” of the hydrogen orbitals in the model by Eder *et al.* is to lower the hydrogen on-site energies, and consequently the hydrogen band center in a band picture.

6.2 Quasi-particle calculations for LaH₃

In this work we study the importance of correlation effects in LaH₃ in parameter-free quasi-particle (QP) calculations. It is well known that the calculated Kohn-Sham eigenvalues, if interpreted as single-particle excitation energies, are often much less accurate, and band gaps are usually considerably underestimated in LDA calculations [21,22]. From QP calculations within the GW approximation [23,24] much better gaps have been obtained for a wide variety of systems [25-28]. We present the results of such GW calculations for LaH₃ which show that the gap in this material can be understood without invoking strong local correlations. Recently we have shown [29] that GW calculations predict a fundamental gap of 1 eV for YH₃ and an optical gap which is almost 3 eV - in close agreement with experiment. The situation in LaH₃ is different from that in YH₃ in three aspects. In the first place the calculated band overlap in recent LDA calculations for LaH₃ [8,19] is *indirect* and about 0.5 eV which is much smaller

than the *direct* band overlap of 1.3 eV which was found for YH₃ [8,9]. Secondly, the experimentally obtained band gap for LaH₃ (~ 1.9 eV) is about 1 eV smaller than the optical gap determined for YH₃ (~ 2.6 eV). Finally, LaH₃ has a fairly simple lattice structure with only 4 atoms in the unit cell, contrary to YH₃ which has a complicated lattice structure with 24 atoms in the unit cell. Since both LaH₂ and LaH₃ are cubic it is believed that the structural phase change found for the YH_{*x*} system when *x* increases from 2 to 3, is not related to the MI transition. Despite these differences switchable mirrors based on yttrium and lanthanum essentially work in the same way.

Our calculated single-particle excitation energies and QP wave functions result from numerically solving the so-called quasi-particle equation. The self-energy operator Σ , needed in this equation, can be expanded in a series in the single-particle Green's Function G and the dynamically screened Coulomb interaction W . In the GW approximation only the first term in this expansion, symbolically given by GW , is included. For setting up this self-energy operator we essentially use the real-space imaginary-time method suggested by Rojas *et al.* [30] and described in detail by Rieger *et al.* [31]. G and W (in the random-phase approximation) are constructed from the LDA wave functions and energies, on a real-space grid which consists of $(10 \times 10 \times 10)$ grid points in the unit cell, and $(6 \times 6 \times 6)$ unit cells in the so-called interaction cell. In the construction of the Green's Functions 200 bands are included and an exponential (imaginary) time grid with a length of 12 \hbar is used. QP energies are updated in both G and W . By systematically varying the numerical convergence parameters the convergence of the QP energies has to be tested. In particular, for the results reported here, the convergence with respect to the size of the interaction cell (or k-grid) may not be perfect. From the calculated QP energies on the $(6 \times 6 \times 6)$ \mathbf{k} -set we have constructed the QP density of states. Finally, using the QP energies along with the LDA wave functions (these are found to be practically identical to the QP wave functions) the contributions of direct interband transitions to the imaginary part of the dielectric tensor have been calculated.

The LDA wave functions and energies are obtained from a pseudopotential plane wave code [32]. For lanthanum we have generated a soft pseudopotential [33] for which cutoff radii 3.56 a.u., 3.75 a.u. and 2.09 a.u. have been chosen for the *s*, *p* and *d* parts respectively. The *s* potential was used as a local reference potential. The (experimental) lattice parameter used is 10.5946 a.u. Neutron powder diffraction experiments at room temperature have shown that LaH₃ has the high-symmetry BiF₃ structure [15,34]. This

structure is face-centered cubic, with lanthanum in the origin, and hydrogen atoms occupying the ideal tetrahedral interstitial sites at $(\frac{1}{4}\frac{1}{4}\frac{1}{4})$ and $(\frac{3}{4}\frac{3}{4}\frac{3}{4})$ and the ideal octahedral site at $(\frac{1}{2}\frac{1}{2}\frac{1}{2})$. At very low temperatures the diffraction data seem to suggest a symmetry breaking and the formation of a large supercell, because small additional peaks show up in the diffraction pattern when the samples are cooled down [15,34]. This is also predicted by LDA total energy calculations for LaH₃ [35].

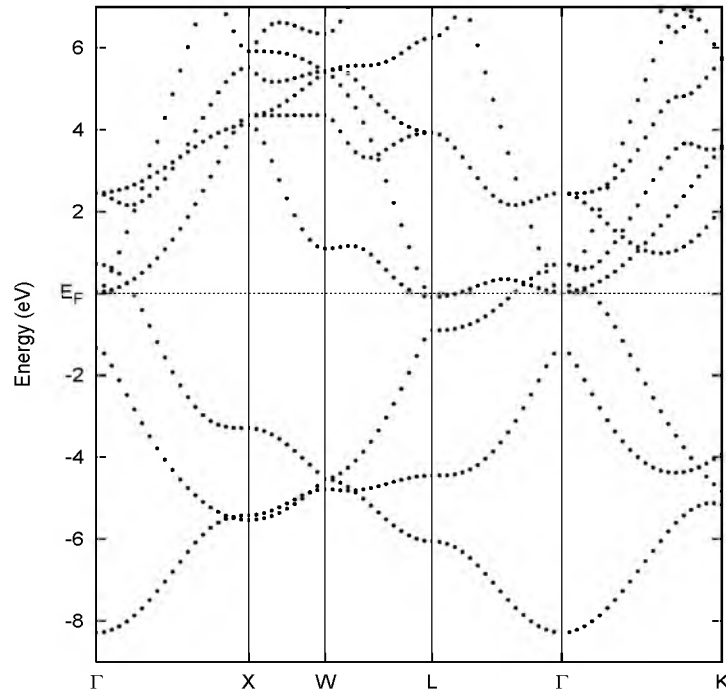


Figure 6.1: DFT-LDA band structure of LaH₃ in the BiF₃ structure.

Fig. 6.1 shows the results of the LDA calculation for LaH₃. The three bands which have the lowest energies throughout most of the Brillouin zone are hydrogen-related bands. The next bands are derived from the lanthanum 5*d* and 6*s* atomic levels. The hydrogen-derived bands partly overlap the lanthanum-derived bands near the center of the Brillouin zone. Therefore LaH₃ is a metal in this band structure calculation. The largest band overlap between the highest hydrogen-derived band and the lowest lanthanum-derived band is indirect and exists along ΓL . In the present calculation this overlap is about 0.6 eV which is comparable to other, recently obtained val-

ues for the band overlap in LaH_3 [8,19]. It is also in very good agreement with the results of calculations using the very accurate full-potential linear augmented plane wave (FLAPW) method [37]. In parts of the Brillouin zone away from Γ there is already a large energy separation between the hydrogen-related and lanthanum-related bands. Therefore, starting from the LDA band structure, a band gap could easily be opened up, either by increasing the energy separation between the hydrogen and the yttrium band centers, or by decreasing the hydrogen band width.

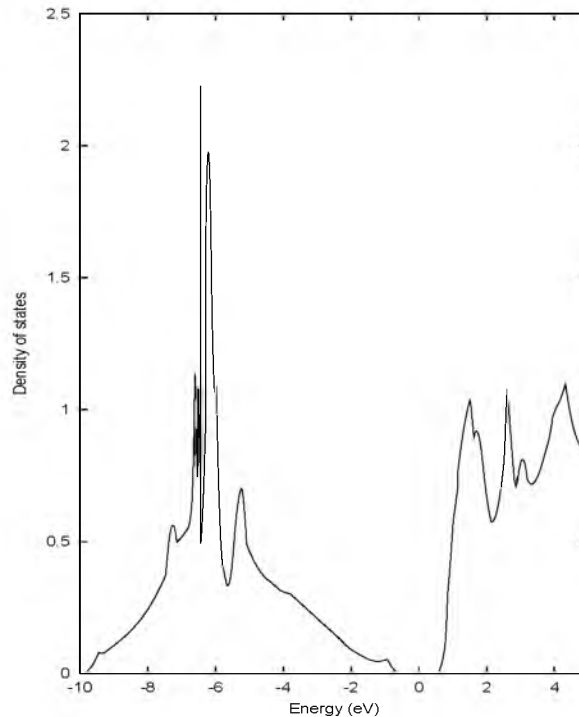


Figure 6.2: *Quasi-particle density of states for LaH_3 calculated on a $(6 \times 6 \times 6)$ \mathbf{k} -grid.*

In the calculated QP spectrum resulting from our *GW* calculation the hydrogen-derived and lanthanum-derived are fully separated in energy. The resulting band structure corresponds to a semiconductor. As a result the hydrogen-derived bands are now fully occupied whereas the lanthanum-derived bands are completely empty. The Fermi level is in between the top of the hydrogen-derived bands and the bottom of the lanthanum bands. There is an indirect fundamental band gap of about 1.3 eV, between states

at Γ and L. We can not exclude the possibility that the fundamental band gap is actually slightly smaller (along ΓL) because there is only a limited set of \mathbf{k} -points included in our GW calculation.

From the calculated QP spectrum we have constructed the QP density of states (DOS) which is shown in Fig. 6.2. The total hydrogen band width has somewhat increased over the LDA value of 9.0 eV to 9.3 eV. This is in strong contrast with the model calculation by Ng *et al.* which predicts a large reduction of the hydrogen band width. Our present results place the center of gravity of the hydrogen-related bands at a binding energy between 6 and 7 eV. The calculated density of states is very small near the band edges, so that comparison with experiment must be made carefully. In the early photoelectron experiments by Peterman *et al.* [36] the main features in the valence density of states are found at binding energies of about 5 and 7 eV, in good agreement with the present results.

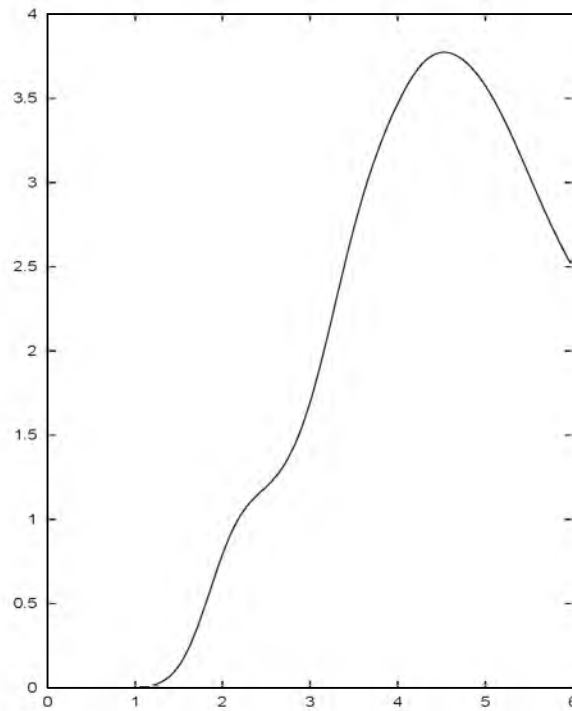


Figure 6.3: *Calculated imaginary part of the dielectric tensor using a $(6 \times 6 \times 6)$ \mathbf{k} -grid.*

In Fig. 6.3 we show the contributions of direct interband transitions to the

imaginary part of the dielectric tensor, $\epsilon_2(\omega)$, which is isotropic because of the high cubic symmetry of the system. The data have been broadened with a Gaussian. From this figure it is clear that the *optical* gap is somewhat larger than the fundamental gap. It is about 1.6 eV, which is close to the experimentally obtained value of 1.9 eV. Due to the fact that the fundamental gap is smaller but indirect, weak phonon-assisted absorptions may be expected below the optical gap in LaH_3 . In recent experiments Van Gogh *et al.* have studied the dielectric functions of LaH_3 and have indeed observed weak absorption below the optical gap [38].

The results of the *GW* calculations for LaH_3 and YH_3 have important differences. In YH_3 the fundamental gap of about 1 eV is direct between states at Γ , but optical transitions between the top of the valence band and the bottom of the conduction band are dipole forbidden by symmetry. Therefore the optical gap is 2.6 eV. Since these particular symmetry rules do not apply to states at \mathbf{k} -points away from Γ weak absorptions are likely to occur at energies between 1 eV and 2.6 eV, due to transitions between states belonging to the highest valence band and the lowest conduction band close to Γ . In LaH_3 the fundamental gap is indirect, and about 1.3 eV. The strongest optical transitions are direct interband transitions which start at photon energies of about 1.6 eV. These direct transitions at Γ in LaH_3 between the bands near the Fermi level are not dipole forbidden by symmetry. Weak phonon assisted absorptions may be expected at photon energies starting at 1.3 eV. The differences in the details of the electronic structure of YH_3 and LaH_3 may be studied in photoemission (and inverse photoemission) experiments. Such experiments should be able to identify a considerably smaller direct fundamental gap for YH_3 , and a slightly smaller indirect gap for LaH_3 .

The origin of the discrepancy between the LDA results the experimental band gaps is identical for both LaH_3 and YH_3 . The size of the calculated *GW* corrections (roughly 2 eV) to the positions of the hydrogen band centers in the LDA band structures is practically identical in both materials. This result shows that the problems in the LDA calculation are caused by the hydrogen levels, and not by states which are related to the metal atoms. Because the direct LDA band overlap in YH_3 (1.1 eV) is larger than the indirect LDA band overlap in LaH_3 (0.6 eV) the fundamental gap in the *GW* calculation for YH_3 is smaller (1.0 eV) than the fundamental gap in LaH_3 (1.3 eV). Due to vanishing matrix elements for optical dipole transitions, the optical gap in YH_3 is almost 2.6 eV. The optical gap in LaH_3 (1.6 eV) is given by the direct and symmetry allowed gap at Γ .

The *GW* method resolves the relatively large error in the lowest Kohn-Sham eigenvalue for hydrogen. This error is a well known artifact which arises from the incomplete cancellation of the LDA electron self-interaction by the local exchange-correlation potential [39]. This leads to the picture that LaH_3 (like YH_3) is a conventional compound semiconductor with charge transfer from lanthanum to hydrogen. Starting from the atomic levels, as a result of the charge transfer the levels derived from the hydrogen atomic $1s$ states move upwards in energy and the lanthanum-derived levels move downwards. Due to overlap of the valence wave functions on neighboring atoms there is covalent interaction and broadening of the atomic levels into bands. Charge transfer to hydrogen also delocalizes the atomic orbitals and increases the band width. These effects have to be taken into account by a self-consistency procedure. However, because the LDA calculation for atomic H^0 places the $1s$ eigenvalue much too high in energy the energy difference between the La and H on-site energies is severely underestimated to begin with. As a result the band centers of the valence and conduction bands are too close and the bands overlap in the LDA calculation.

References

- [1] J.N. Huiberts, R. Griessen, J.H. Rector, R.J. Wijngaarden, J.P. Dekker, D.G. de Groot, and N.J. Koeman, *Nature (London)* **380**, 231 (1996).
- [2] P.H.L. Notten, M. Kremers, and R. Griessen, *J. Electrochem. Soc.* **143**, 3348 (1996).
- [3] P. van der Sluis, *Appl. Phys. Lett.* **73**, 1826 (1998).
- [4] P. van der Sluis, M. Ouwerkerk, and P.A. Duine, *Appl. Phys. Lett.* **70**, 3356 (1997).
- [5] D.G. Nagengast, A.T.M. van Gogh, E.S. Kooij, B. Dam, and R. Griessen, *Appl. Phys. Lett.* **75**, 2050 (1999).
- [6] J.W.J. Kerssemakers, S.J. van der Molen, N.J. Koeman, R. Gunther, and R. Griessen, *Nature* **396**, 489 (2000).
- [7] A.T.M. van Gogh, S.J. van der Molen, J.W.J. Kerssemakers, N.J. Koeman, and R. Griessen, *Appl. Phys. Lett.* **77**, 815 (2000).
- [8] J.P. Dekker, J. van Ek, A. Lodder, and J.N. Huiberts, *J. Phys. Condens. Matter* **5**, 4805 (1993).
- [9] Y. Wang and M.Y. Chou, *Phys. Rev. Lett.* **71**, 1226 (1993); *Phys. Rev. B* **51**, 7500 (1995).

- [10] T.J. Udovic, Q. Huang, and J.J. Rush, *J. Phys. Chem. Solids* **57**, 423 (1996)
- [11] P.J. Kelly, J.P. Dekker, and R. Stumpf, *Phys. Rev. Lett.* **78**, 1315 (1997)
- [12] T.J. Udovic, J.J. Rush, Q. Huang, and I.S. Anderson, *Phys. Rev. Lett.* **79**, 2920 (1997)
- [13] A. Remhof, G. Song, Ch. Sutter, A. Schreyer, R. Siebrecht, H. Zabel, F. Gütthoff, and J. Windgasse, *Phys. Rev. B* **59**, 6689 (1999)
- [14] P.J. Kelly, J.P. Dekker, and R. Stumpf, *Phys. Rev. Lett.* **79**, 2921 (1997)
- [15] T.J. Udovic, J.J. Rush, Q. Huang, and I.S. Anderson, *J. Alloys and Compounds* **253-254**, 241 (1997).
- [16] T.J. Udovic, Q. Huang, and J.J. Rush, *Mat. Res. Soc. Symp. Proc.* **513**, 197 (1998)
- [17] P. van Gelderen, P.J. Kelly, and G. Brocks, *Phys. Rev. B* **63**, R100301 (2001)
- [18] F. Aryasetiawan and O. Gunnarsson, *Phys. Rev. Lett.* **74**, 3221 (1995).
- [19] K.K. Ng, F.C. Zhang, V.I. Anisimov, and T.M. Rice, *Phys. Rev. Lett.* **78**, 1311 (1997); *Phys. Rev. B* **59**, 5398 (1999)
- [20] R. Eder, H.F. Pen, and G.A. Sawatzky, *Phys. Rev. B* **56**, 10115 (1997)
- [21] L.J. Sham and M. Schlüter, *Phys. Rev. Lett.* **51**, 1888 (1983); *Phys. Rev. B* **32**, 3883 (1985).
- [22] J.P. Perdew and M. Levy, *Phys. Rev. Lett.* **51**, 1884 (1983).
- [23] L. Hedin, *Phys. Rev.* **139**, A796 (1965); L. Hedin, and S. Lundqvist in *Solid State Physics*, edited by F. Seitz, D. Turnbull, and H. Ehrenreich (Academic, New York, 1969), Vol. 23, p. 1.
- [24] For recent reviews of the GW method and its applications see F. Aryasetiawan and O. Gunnarsson, *Rep. Prog. Phys.* **61**, 237 (1998) or L. Hedin, *J. Phys. Condens. Matter* **11** R489 (1999)
- [25] M.S. Hybertsen, and S.G. Louie, *Phys. Rev. Lett.* **55**, 1418 (1985); *Phys. Rev. B* **34**, 5390 (1988)
- [26] R.W. Godby, M. Schlüter, and L.J. Sham, *Phys. Rev. Lett.* **56**, 2415 (1986); *Phys. Rev. B* **37**, 10159 (1988)
- [27] F. Aryasetiawan and O. Gunnarsson, *Phys. Rev. Lett.* **74**, 3221 (1995)

- [28] S. Massidda, A. Continenza, M. Posternak, and A. Baldereschi, Phys. Rev. Lett. **74**, 2323 (1995)
- [29] P. van Gelderen, P.A. Bobbert, P.J. Kelly, and G. Brocks, Phys. Rev. Lett. **85**, 2989 (2000)
- [30] H.N. Rojas, R.W. Godby, and R.J. Needs, Phys. Rev. Lett. **74**, 1827 (1995)
- [31] Martin M. Rieger, L. Steinbeck, I.D. White, H.N. Rojas and R.W. Godby, Computer Physics Communications **117** 211-228 (1999)
- [32] R. Stumpf and M. Scheffler, Comput. Phys. Commun. **79**, 447 (1994)
- [33] N. Troullier, and J.L. Martins, Phys. Rev. B **43**, 1993 (1991).
- [34] J.-J. Didisheim K. Yvon, P. Fischer, W. Hälg, and L. Schlappbach, Phys. Lett. **78A**, 111 (1980).
- [35] P. van Gelderen, P.J. Kelly, and G. Brocks, to be published
- [36] D.J. Peterman, J.H. Weaver, and D.T. Peterson, Phys. Rev. B **23**, 3903 (1981)
- [37] P.K. de Boer, private communication
- [38] A.T.M. van Gogh, *Probing the Metal-Insulator Transition in Rare-Earth Based Switchable Mirrors*, Ph.D. Thesis, Vrije Universiteit, Amsterdam (2001) and to be published.
- [39] O. Gunnarsson, B.I. Lundqvist, and J.W. Wilkins, Phys. Rev. B **10**, 1319 (1974).

Chapter 7

Quasi-particles in CaB_6

ABSTRACT

Ferromagnetism was recently observed at unexpectedly high temperatures in La-doped CaB_6 . The starting point of all theoretical proposals to explain this observation is a semimetallic electronic structure calculated for CaB_6 within the local density approximation. Here we report the results of parameter-free quasiparticle calculations of the single-particle excitation spectrum which show that CaB_6 is not a semimetal but a semiconductor with a band gap of 0.8 ± 0.1 eV. Magnetism in $\text{La}_x\text{Ca}_{1-x}\text{B}_6$ occurs just on the metallic side of a Mott transition in the La-induced impurity band.

This chapter is based on: *CaB₆: a new semiconducting material for spin electronics*, H.J. Tromp, P. van Gelderen, P.J. Kelly, G. Brocks, and P.A. Bobbert, Phys. Rev. Lett. **87**, 016401 (2001).

The recent observation of ferromagnetism in La doped alkaline-earth hexaboride compounds at high temperatures [1] presents three puzzles. Firstly, ferromagnetism is usually associated with elements with a partly filled $3d$, $4f$ or $5f$ shell. Secondly, ferromagnetic ordering is only observed for a narrow dopant concentration range and for a surprisingly low dopant concentration. The maximum observed moment in $\text{Ca}_{1-x}\text{La}_x\text{B}_6$ is 0.07 Bohr magnetons per La atom for $x = 0.005$. Thirdly, and most surprising of all is the observation of very large Curie temperatures; for $\text{La}_{0.01}\text{Ca}_{0.99}\text{B}_6$ a value close to 900 K has recently been reported [2]. Such a large value virtually excludes the possibility of the observed magnetism being related to magnetic impurities.

In an initial comment on the experimental observations, Ceperley suggested [3] that it might be an example of the long-predicted but never observed ferromagnetic phase of a dilute electron gas; improved calculations increase the estimated density at which this might occur [4]. An alternative explanation proposed by Zhitomirsky was that the ferromagnetic hexaborides might be doped excitonic insulators [5]. This explanation requires that the exciton binding energy should be comparable in size to the single-particle band gap. Jarlborg suggested [6] that the magnetism may be conventional itinerant magnetism. Although magnetism in materials which do not have partly filled $3d$, $4f$ or $5f$ shells is rare, it is not unprecedented. A handful of materials does exist, of which ZrZn_2 is the best known example, in which the Fermi energy falls at or close to an exceptionally narrow peak in the electronic density of states so that the Stoner criterion for the occurrence of itinerant magnetism is fulfilled. The problem posed by the hexaborides is not so much the occurrence of magnetic ordering but rather the strength of the magnetic coupling as reflected by the very high Curie temperature, and this was not estimated in reference [6].

All three suggestions are based on electronic structure calculations which indicate that stoichiometric CaB_6 is a semimetal with a very small overlap between the conduction and valence bands [7-9] or might have a very small gap [7]. Since the theoretical predictions rely on details of this electronic structure, it is important to examine their validity. Massidda's and Rodriguez' calculations of the electronic structure were performed with the full-potential linearized augmented plane wave (FLAPW) method which is probably the most accurate available. They were carried out within the framework of density functional theory (DFT) using the local density approximation (LDA). Such calculations are known to be capable of yielding total energies with a very useful accuracy. However, it is also well known

that the eigenvalue spectrum which results from solving the Kohn-Sham equations of DFT cannot be interpreted unreservedly as an excitation spectrum [10,11] and sometimes the results are spectacularly wrong. In particular, the band gaps of semiconductors are typically underestimated by 50% and in extreme cases such as Ge the conduction and valence bands are found to overlap resulting in metallic or semimetal character.

In order to study single-particle excitations, one should solve Dyson's equation for the single-particle Green's function expressed in terms of the self-energy operator Σ . Σ can be expanded as a perturbation series in the Green's function G and the dynamically screened Coulomb interaction W . The so-called GW approximation introduced by Hedin [12] includes only the first term in this series. In addition, one usually assumes a quasi-particle (QP) expression for the Green's function G . For a large number of semiconductors and insulators such calculations produce band gaps which are in very close quantitative agreement with experimental single-particle band gaps [13]. The main purpose of the present paper is to apply these parameter-free calculations with their proven predictive capability to CaB_6 . From our results we shall conclude that, contrary to what is currently being assumed, the parent material is actually a semiconductor with quite a large band gap. This finding has far-reaching consequences for understanding the basic properties of the doped, ferromagnetic phase and opens up the prospect of a range of novel applications.

The starting point for our GW study is an LDA calculation for CaB_6 performed with a plane-wave basis and using norm-conserving pseudopotentials to describe the interaction between the valence electrons and the ionic cores [14]. Using the experimentally determined structure, we reproduce essentially perfectly the energy bands calculated by Massidda [8] using an all-electron method. The results are shown in Fig. 7.1(a). There are ten valence bands (bonding orbitals derived from the boron 2s and 2p levels) well-separated from the conduction bands (antibonding states) with the exception of an overlap of about 0.3 eV in a small region around the X point of the highest occupied and lowest unoccupied bands. The occurrence of such small band overlap (or the presence of a comparably small band gap) is an important criterion for the stability of an excitonic insulator phase [5]. The effective masses in units of the free electron mass for the bands near X, $m_e^\perp = 0.215 \pm 0.004$ and $m_e^\parallel = 0.50 \pm 0.02$ for the electrons and $m_h^\perp = 0.196 \pm 0.003$ and $m_h^\parallel = 1.8 \pm 0.2$ for the holes, are close to values reported earlier [7-9]. We use the LDA electronic wave functions and eigenvalues as input for the GW calculations for which we adopt the space-time

approach suggested by Rojas [15] in which all operators are represented on grids in real and reciprocal space, in the time and energy domains; details of our implementation have been given by van der Horst [16]. By varying the size of these grids we estimate that the calculated QP energies are converged within 0.1 eV. The densest grids we used were a $(12 \times 12 \times 12)$ real-space grid and a $(6 \times 6 \times 6)$ \mathbf{k} -grid. The Green's function is constructed including the LDA wave functions and energies of the lowest 300 bands.

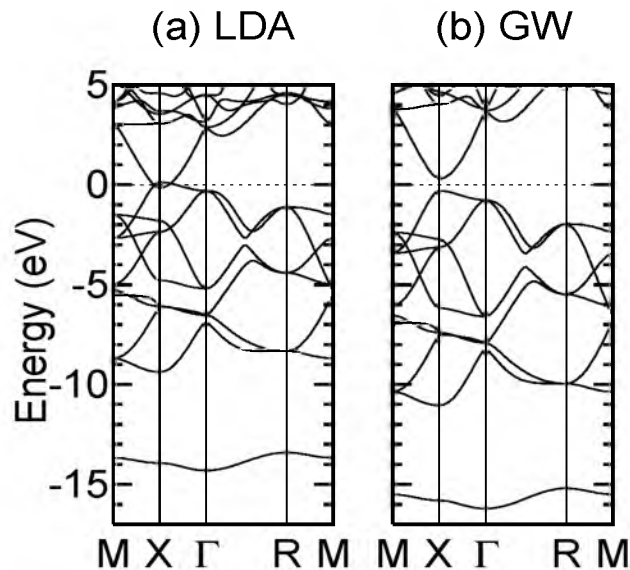


Figure 7.1: Energy bands for CaB_6 in (a) the LDA approximation, (b) the GW approximation. The Fermi energy is indicated by the dotted line at 0 eV.

The results of the GW calculations are plotted in Fig. 7.1(b). Throughout the Brillouin zone, the QP corrections to particular LDA bands are rather uniform so that the dispersion of the GW bands is very similar to the LDA band dispersion and the effective masses differ only slightly from the values obtained from the LDA calculation. They are reduced on average by less than 10%, to $m_e^\perp = 0.196 \pm 0.003$ and $m_e^\parallel = 0.48 \pm 0.02$ for the electrons and $m_h^\perp = 0.174 \pm 0.003$ and $m_h^\parallel = 1.7 \pm 0.2$ for the holes. The sign and size of the corrections to the energy bands depend on their wavefunction character and vary considerably from band to band. Of particular importance are the

relative shifts of the bands at X near the Fermi level. The hole band and electron bands are moved, respectively, downwards and upwards in energy resulting in the opening of a sizeable band gap of about 0.8 ± 0.1 eV. The downward and upward shifts can be understood from the bonding and antibonding character of the wave functions in the valence and conduction bands, respectively. This is quite analogous to the situation in silicon [17]. The largest shift in the occupied bands is calculated for the lowest valence band which is lowered in energy by about 1.5 eV. Given the similarity between the LDA band structures of CaB_6 and SrB_6 [8], we expect a *GW* calculation to yield similar results for these two materials.

Our finding that bulk CaB_6 is a semiconductor is consistent with the large value of the low-temperature resistivity and with its increase with decreasing temperature recently reported by Ott [2] and by Vonlanthen [18]. The temperature dependence of the resistivity of the ‘stoichiometric’ sample (labelled $\text{Ca}_{1+\delta}\text{B}_6$ in Ref. [18]) can be interpreted as that of a doped semiconductor. In the saturation range, around room temperature, all the impurities are ionized, the number of charge carriers in the bands is temperature independent and the resistivity has a weak temperature dependence. Below $T = 230$ K the impurity charge carriers gradually freeze out and their number decreases exponentially. One might tentatively associate the 84 meV activation energy found for this process by Vonlanthen with an impurity binding energy [19,20]. At temperatures below ~ 50 K most of the charge carriers are frozen out and the resistivity is determined by hopping between impurity sites. Assuming nearest neighbor hopping, the latter process can be described by an activation energy that is easily an order of magnitude smaller than the impurity binding energy [21,22]. The La-doped samples correspond to a high doping regime, where the impurity concentration is on the metallic side of a Mott transition in an impurity band (see below). For these samples, therefore, a metallic-like resistivity is observed over the whole temperature range. We do not attempt to explain the decrease in resistivity observed below $T = 0.4$ K [2,18].

Our result that CaB_6 is a semiconductor is also consistent with recent angle-resolved photoemission experiments by Denlinger on SrB_6 [23], in which a gap of a size similar to what we calculate was found. Using the fact that photoemission experiments are sensitive to the surface electronic structure and assuming that the bulk is a semimetal, the authors interpreted their results in terms of an electron rich surface region (of thickness 6 nm) in which the structure differs from that of the bulk leading to the formation of a large band gap. This surface region has to be large enough to give the

bands a bulk-like dispersion. While we cannot exclude the importance of surface states, our results indicate that the photoemission spectrum can be interpreted without invoking such a special surface region. The optical data of Ref. [18] cannot be explained in a simple way, neither on the basis of the (semimetal) LDA nor of the (semiconductor) GW band structures. The imaginary part of the calculated dielectric function shows a steep rise only at around 2 and 3 eV, respectively, since transitions between the highest valence and lowest conduction bands are only weakly allowed whereas the experimental dielectric function shows such a rise below 1 eV.

The result for the stoichiometric phase has important implications for the models proposed to explain the ferromagnetism observed in the doped phase. A low density electron gas is expected to show a ferromagnetic phase; Ceperley [3,4] report critical values for the electron gas parameter of this phase of $r_s = 80$ and $r_s = 20$, respectively. In a solid this electron gas parameter has to be rescaled because the background dielectric constant and the effective masses rescale the potential and kinetic energies of the electron gas and thus change the density at which one expects the ferromagnetic phase to occur [5,9]. Within GW one calculates the dielectric response function at the random phase approximation level [12,15,17]. Similar to Ref. [9], using our calculated values for the effective masses and static dielectric constant of 5, we obtain a scaled density parameter r_s of 1.5. This is at least an order of magnitude smaller than the values reported by Ceperley [3] and Ortiz [4] which makes the low density electron gas an unlikely candidate for the observed ferromagnetism. Within the effective mass approximation we estimate an exciton binding energy of about 0.07 eV. The excitonic binding energy is an order of magnitude smaller than the calculated QP band gap. The excitonic insulator model requires them to be comparable in size [5], so it is unlikely that this model can be applied to CaB_6 .

Instead we note that the ferromagnetism occurs for an impurity concentration which is just on the metallic side of a Mott transition in the impurity band: $n^{1/3}a_H = 0.4$, where n is the dopant concentration 7×10^{19} electrons cm^{-3} and $a_H = 10 \text{ \AA}$ is the Bohr radius of an isolated effective mass impurity. Some support for the possible role of an impurity band may be found in the very recent experimental studies on doped hexaborides reported by Terashima [24]. He found that some of his La-doped samples were paramagnetic, exhibiting the Curie-Weiss behaviour which is to be expected if the dopant concentration were below Mott's critical value. In other samples no indication of saturation of the magnetic moment even in the highest magnetic field reported (10 kOe) was found. Such behaviour might be expected

for a Stoner model of weak ferromagnetism with partly filled narrow bands on the metallic side of a Mott transition. This model might also be capable of explaining the different values reported for the magnetic moment per dopant atom [1,2,24] if there were a significant deviation from the nominal stoichiometry. Since the effective valence of an impurity atom in a semiconductor is very sensitive to the local environment, it is important to know where the La goes and if all of it actually occupies Ca sites as assumed. In the same context, one should determine the abundance of vacancies on the boron sublattice and whether they have donor or acceptor character. This is particularly relevant in view of the observation of ferromagnetic ordering in an undoped CaB_6 sample with an apparent Ca deficiency [18]. Experimental difficulties in making the samples are apparent from the attribution of de Haas-van Alphen signals to Al inclusions [24].

Starting from the assumption that the magnetism occurs mainly in the impurity band, we are currently attempting to determine the effective exchange interaction between impurities from total energy calculations, in order to estimate the Curie temperature, and to determine the impurity-state related parameters which govern the physical behaviour of the doped system such as the hopping matrix elements between impurity states, the charge and spin fluctuation parameters (Hubbard U and Stoner I , respectively), as well as the impurity binding energy, going beyond the effective mass approximation. The position of the impurity state with respect to the bottom of the conduction band is particularly difficult to estimate reliably because it requires taking into account simultaneously the central cell potential and the long-range Coulomb interaction. One way to assess the importance of dopant atoms experimentally would be to use a field-effect device to inject charge into undoped CaB_6 [25].

Irrespective of the origin of the high Curie temperature in the doped material, the existence of a large gap for the undoped material means a new class of magnetic semiconductors [26] is available. Magnetic semiconductors have attracted a lot of attention recently in the context of spin electronics. The size of the magnetization in doped hexaborides is not high but it is not obviously inferior to the materials used in Refs. [27,28]. The doped hexaborides possess the unique characteristic of having a Curie temperature sufficiently high to allow room-temperature operation of semiconducting spin devices, something which has only very recently been achieved at low temperatures [27,28]. With the hexaborides it should be possible to inject a spin-polarized current from the doped into the undoped material in the ballistic regime and study the spin dynamics as a function of temperature,

and of current density without the complication of having to apply an external magnetic field [27,28] or without the problems encountered when attempting to inject spins from a low resistivity ferromagnetic metal into a conventional semiconductor in the diffusive regime [29]. It should also be possible to make a field-effect device to modulate a spin-polarized current in the doped hexaboride material and achieve gain. If a p -type hexaboride with some of the Ca replaced by a monovalent ion were also found to be ferromagnetic, it should even be possible to make the spin-analogues of bipolar devices.

Both Ca and B are light elements so that the spin-orbit coupling is small. Since the lowest conduction band and highest valence band are both singly degenerate, the intrinsic spin-flip scattering should be weak with spin-flip scattering lengths comparable to what has recently been observed in carbon nanotubes [30]. This should also hold for the impurity states if the latter can be described within an effective mass model. Because of the small size of the spin-orbit coupling, because the magnetic moment is so tiny, and because the hexaborides are cubic, the material should be magnetically extremely soft with a very small intrinsic magnetocrystalline anisotropy. This could be important for sensor applications.

Note added: After submission of the manuscript, evidence for the existence of a band of partly localized, partly itinerant defect states and thus implicitly for the existence of a band gap has emerged from NMR spin-lattice relaxation measurements [31] and from thermopower measurements [32].

References

- [1] D.P. Young, D. Hall, M.E. Torelli, Z. Fisk, J.L. Sarrao, J.D. Thompson, H.-R. Ott, S.B. Oseroff, R.G. Goodrich, and R. Zysler, *Nature* **397**, 412 (1999)
- [2] H.R. Ott, J.L. Gavilano, B. Ambrosini, P. Vonlanthen, E. Felder, L. Degiorgi, D.P. Young, Z. Fisk, and R. Zysler, *Physica B* **281-282**, 423 (2000).
- [3] D. Ceperley, *Nature* **397**, 386 (1999).
- [4] G. Ortiz, M. Harris, and P. Ballone, *Phys. Rev. Lett.* **82**, 5317 (1999).
- [5] M.E. Zhitomirsky, T.M. Rice, and V.I. Anisimov, *Nature* **402**, 251 (1999); M.E. Zhitomirsky and T.M. Rice, *Phys. Rev. B* **62**, 1492 (2000).
- [6] T. Jarlborg, *Phys. Rev. Lett.* **85**, 186 (1999).

-
- [7] A. Hasegawa, and A. Yanase, J. Phys. C **12**, 5431 (1979).
- [8] S. Massidda, A. Continenza, T.M. de Pascale, and R. Monnier, Z. Phys. B **102**, 83 (1997).
- [9] C.O. Rodriguez, R. Weht, and W.E. Pickett, Phys. Rev. Lett. **84**, 3903 (2000).
- [10] J.P. Perdew, and M. Levy, Phys. Rev. Lett. **51**, 1884 (1983).
- [11] L.J. Sham, and M. Schlüter, Phys. Rev. Lett. **51**, 1888 (1983); Phys. Rev. B **32**, 3883 (1985)
- [12] L. Hedin, Phys. Rev. **139**, A796 (1965).
- [13] F. Aryasetiawan, and O. Gunnarsson, Rep. Prog. Phys. **61**, 237 (1998); L. Hedin, J. Phys. Condens. Matter **11**, R489 (1999).
- [14] N. Troullier, and J.L. Martins, Phys. Rev. B **43**, 1993 (1991).
- [15] H.N. Rojas, R.W. Godby, and R.J. Needs, Phys. Rev. Lett. **74**, 1827 (1998).
- [16] J.-W. van der Horst, P.A. Bobbert, P.H.L. de Jong, M.A.J. Michels, G. Brocks, and P.J. Kelly, Phys. Rev. B **61**, 15817 (2000).
- [17] R.W. Godby, M. Schlüter, and L.J. Sham, Phys. Rev. B **37**, 10159 (1988).
- [18] P. Vonlanthen, E. Felder, L. Degiorgi, H. R. Ott, D. P. Young, A. D. Bianchi, and Z. Fisk, Phys. Rev. B **62**, 10076 (2000).
- [19] J. S. Blakemore, *Semiconductor Statistics*, (Pergamon, Oxford, 1962).
- [20] This behavior is consistent with an impurity concentration of (at least) $\sim 10^{17}\text{cm}^{-3}$. With a band gap of 0.8 eV, the intrinsic regime, where the number of charge carriers that are thermally excited across the band gap exceeds the number of impurity charge carriers, then starts at a very high temperature of ~ 1500 K.
- [21] B. I. Shklovskii and A. L. Efros, *Electronic Properties of Doped Semiconductors*, (Springer, Berlin, 1984).
- [22] Alternatively, Mott's variable range hopping might play a role in this regime. The details of the hopping process depend upon the nature and distribution of the impurities, the amount of compensation, etc. See e.g. [21].
- [23] J.D. Denlinger *et al.* Bandgap recovery and electron doping on cleaved [100] surfaces of divalent semi-metal hexaborides. cond-mat/0009022.

- [24] T. Terashima, C. Terakura, Y. Umeda, N. Kimura, H. Aoki, and S. Kunii, *J. Physical Society of Japan* **69**, 2423 (2000).
- [25] J. H. Schön, Ch. Kloc, and B. Batlogg, *Nature* **406**, 702 (2000).
- [26] H. Ohno, *Science* **281**, 951 (1998).
- [27] R. Fiederling, M. Keim, G. Reuscher, W. Ossau, G. Schmidt, A. Waag, and L.W. Molenkamp, *Nature* **402**, 787 (1999).
- [28] Y. Ohno, D.K. Young, B. Beschoten, F. Matsukura, H. Ohno, and D.D. Awschalom, *Nature* **402**, 790 (1999).
- [29] G. Schmidt, D. Ferrand, L.W. Molenkamp, A.T. Filip, and B.J. van Wees, *Phys. Rev. B* **62**, 4790 (2000).
- [30] K. Tsukagoshi, B.W. Alphenaar, and H. Ago, *Nature* **401**, 572 (1999).
- [31] J.L. Gavilano, Sh. Mushkolaj, D. Rau, H.R. Ott, A. Bianchi, D.P. Young, and Z. Fisk, *Phys. Rev. B* **63**, 140410 (2001).
- [32] K. Giannò, A.V. Sologubenko, H.R. Ott, A.D. Bianchi, and Z. Fisk. Doping dependence of the electrical and thermal transport properties of CaB_6 . cond-mat/0104511.

Samenvatting

De band gap in schakelbare spiegel metaalhydriden

Dit proefschrift is gewijd aan parameter-vrije berekeningen op het gebied van de vaste stoffysica. Door de quantummechanische vergelijkingen voor de elektronen op te lossen kan begrip worden verkregen van de karakteristieken van specifieke materialen. Omdat het hier zeer ingewikkelde vergelijkingen en grote aantallen elektronen betreft kunnen deze vergelijkingen slechts met de hulp van supercomputers worden opgelost.

Het grootste deel van dit proefschrift beschrijft berekeningen van de elektronenstructuur van metaalhydriden die gebruikt kunnen worden als schakelbare spiegels. De ontdekking van deze spiegels vond enkele jaren geleden plaats aan de Vrije Universiteit in Amsterdam. Schakelbare spiegels zijn dunne lagen van yttrium-, lanthaan- of zeldzame aard-hydriden waarvan de waterstof-belading kan worden gevarieerd. Als functie van de hoeveelheid waterstof veranderen de elektrische en optische eigenschappen van deze films. Een dunne yttrium- of lanthaanhydride laag is metallisch en reflecterend bij een lage waterstofbelading, maar bij een waterstof-metaal verhouding van ongeveer 2.8 wordt de dunne laag transparant voor zichtbaar licht. Doordat de hoeveelheid waterstof in de film vervolgens weer kan worden verminderd, kan de dunne laag terug worden *geschakeld* naar de metallische toestand. Het doel van de berekeningen aan YH_3 en LaH_3 in dit proefschrift is een verklaring te geven voor de karakteristieken van de fase van deze schakelbare spiegels, waarin zichtbaar licht wordt doorgelaten.

Aangezien het proces van schakelen reversibel is, in relatief korte tijd kan plaatsvinden, en bij kamertemperatuur kan worden gerealiseerd, kunnen schakelbare spiegels mogelijk geschikt worden gemaakt voor een aantal spectaculaire toepassingen. Vanuit een meer fundamenteel oogpunt zijn de schakelbare spiegels intrigerend omdat ten tijde van hun ontdekking een goed begrip ontbrak van het mechanisme dat verantwoordelijk is voor de

metaal-isolator overgang. Hoewel de eigenschappen van YH_2 en LaH_2 met succes konden worden geïnterpreteerd op basis van berekeningen van de elektronenstructuur gebaseerd op dichtheidsfunctionaaltheorie in de zogenaamde lokale dichtheidsbenadering, konden berekeningen van hetzelfde type het lichtdoorlatende karakter van YH_3 en LaH_3 niet verklaren. Uit optische experimenten voor $\text{YH}_{3-\delta}$ met $\delta \sim 0.1$ is een *optische* band gap bepaald van 2.6 elektronvolt. De sterke toename van de elektrische weerstand wanneer de trihydride fase wordt gevormd, de negatieve temperatuurafhankelijkheid van de weerstand in deze fase en de omgekeerd evenredige afhankelijkheid van deze weerstand van δ , suggereren dat YH_3 een halfgeleider is. De grootte van de *fundamentele* band gap is tot op heden echter niet experimenteel bepaald. Voor LaH_3 is de experimenteel gevonden optische band gap 1.9 elektronvolt.

Uit neutronendiffractie experimenten is geconcludeerd dat YH_3 dezelfde, gecompliceerde roosterstructuur heeft als HoD_3 . Berekeningen van de elektronenstructuur in de lokale dichtheidsbenadering voorspellen dat YH_3 in deze roosterstructuur een metaal zou moeten zijn met bandoverlap van meer dan een elektronvolt. Hoewel bekend is dat in de lokale dichtheidsbenadering band gaps in het algemeen worden onderschat, is de voor YH_3 gevonden discrepantie van zo'n 4 elektronvolt tussen deze theoretische waarde en de experimentele band gap bijzonder groot. Dergelijke discrepanties zijn bekend voor overgangsmetaaloxiden zoals NiO en MnO , waarin sterke lokale correlaties tussen *d*-elektronen een belangrijke rol spelen maar slecht beschreven worden in de lokale dichtheidsbenadering. Naar analogie van deze systemen is gesuggereerd dat in YH_3 eveneens sterke lokale correlaties bestaan tussen de elektronen. Voor geparameteriseerde model Hamiltonianen waarin men zulke sterke lokale correlaties aanneemt, heeft men laten zien dat deze inderdaad een grote band gap in het spectrum van YH_3 en LaH_3 zouden kunnen verklaren.

In een andere studie werd uitgegaan van zwakkere elektroncorrelaties in YH_3 en LaH_3 . Hierin werd gesuggereerd dat de verklaring voor het band gap probleem gezocht moest worden in een betere behandeling van elektronische excitaties gebaseerd op standaard elektrongas-theorie. Voor vele materialen is bekend dat een nauwkeurige beschrijving van het één-deeltjes excitatiespectrum (inclusief de band gap) kan worden verkregen door de zogenaamde quasi-deeltje vergelijking op te lossen met een niet-lokale, energieafhankelijke zelfenergie-operator. In berekeningen die gebruik maken van de zogenaamde *GW*-benadering worden voor een groot aantal materialen band gaps voorspeld die zeer dicht bij de experimenteel gevonden waar-

den liggen. Aangezien voor LaH_3 de discrepantie tussen de experimentele waarde voor de gap en de berekende waarde in de lokale dichtheidsbenadering niet veel groter is dan voor vele andere materialen, mag worden verwacht dat een GW -berekening voor dit materiaal een band gap oplevert die in overeenstemming is met de experimenteel bepaalde gap. Voor YH_3 is de discrepantie echter zo groot dat dit niet voor de hand ligt.

Voor het voorspellen van de totale energie van een systeem zijn dichtheidsfunctionaalberekeningen zeer nauwkeurig. Met behulp hiervan kan de ionenconfiguratie worden gezocht die correspondeert met de laagste totale energie en kan derhalve de roosterstructuur van een materiaal worden voorspeld. Voor YH_3 is op basis van dergelijke berekeningen gevonden dat niet de HoD_3 -structuur aanleiding geeft tot de laagste totale energie, maar dat er een op subtiele wijze afwijkende structuur bestaat die correspondeert met een lagere totale energie. Omdat deze structuur ook een lagere symmetrie heeft dan de HoD_3 structuur wordt soms de naam gebroken symmetrie structuur gebruikt. De symmetrie-breking gaat in de lokale dichtheidsbenadering gepaard met het openen van een band gap van ongeveer 0.8 elektronvolt. Als een correctie wordt gemaakt voor het feit dat dergelijke berekeningen band gaps in het algemeen onderschatten, zou men op basis van deze symmetriebreking de grote band gap kunnen begrijpen, die experimenteel voor YH_3 is gevonden. Echter, in diffractiemetingen heeft men de voorspelde symmetrie-breking vooralsnog niet kunnen bevestigen.

Hoofdstuk 2, 3 en 6 van dit proefschrift behandelen GW -berekeningen voor YH_3 en LaH_3 . De enorme hoeveelheid databewerking die met deze berekeningen gepaard gaat vereist langdurig rekenen door supercomputers en grote hoeveelheden diskruimte. Om deze berekeningen uit te kunnen voeren is allereerst een efficiënt computerprogramma geschreven. Uit de resultaten van de GW -berekeningen volgt dat YH_3 en LaH_3 niet wezenlijk verschillen van zwak gecorreleerde materialen zoals silicium, en dat de onderschatting van de band gap door berekeningen in de lokale dichtheidsbenadering van vergelijkbare aard is. De GW -berekeningen voor YH_3 resulteren in een fundamentele band gap van 1 elektronvolt. Doordat matrix elementen voor optische overgangen tussen de hoogste valentieband en de laagste geleidingsband verdwijnen is de optische gap groter. De berekende waarde van 2.6 elektronvolt stemt goed overeen met de experimenteel bepaalde waarde. Voor LaH_3 volgt een band gap die eveneens in goede overeenstemming is met de experimentele waarde.

Door het resultaat van deze GW berekeningen is het bestaan van een gebroken symmetrie structuur voor YH_3 is niet langer cruciaal voor het verklaren

van de band gap in het spectrum van dit materiaal. Echter, op grond van de *GW*-berekeningen kan niet geconcludeerd worden dat deze symmetriebreking niet bestaat. Omdat de symmetrie-brekende waterstofverplaatsingen erg klein zijn, bestaat de mogelijkheid dat ze van dezelfde orde grootte zijn als de quantummechanische onzekerheid in de posities van de atomen; de zogenaamde nulpuntsbeweging. Deze nulpuntsbeweging kan berekend worden vanuit het roostervibratiespectrum. In hoofdstuk 4 en 5 worden deze berekeningen beschreven. De berekende nulpuntstrillingen zijn groot en het energieverval tussen de HoD_3 structuur en de gebroken symmetrie structuur is klein. Daardoor ligt het voor de hand dat het systeem zich bevindt in een quantumsuperpositie van 4 verschillende, maar equivalente gebroken symmetriestructuren. Deze superpositie heeft de symmetrie van de HoD_3 structuur, waardoor de structuur van YH_3 die wordt gezien in diffractie experimenten geïnterpreteerd zou kunnen worden als de HoD_3 structuur. Wanneer de toestandsdichtheid corresponderend met het berekende vibratiespectrum van YH_3 wordt vergeleken met de resultaten van inelastische neutronenverstrooiing blijkt dat de experimenteel gevonden rangschikking en opsplitsing van de pieken in het spectrum beter correspondeert met de berekeningen waarin een symmetrie gebroken structuur wordt aangenomen dan met berekeningen waarin de HoD_3 structuur wordt verondersteld. Ook andere, recente resultaten van nucleaire magnetische resonantie experimenten en van Raman metingen wijzen in de richting van een gebroken symmetrie structuur.

Het laatste hoofdstuk van dit proefschrift beschrijft berekeningen aan de elektronenstructuur van CaB_6 . Dit is een materiaal waarvan onlangs bijzondere magnetische eigenschappen zijn gevonden wanneer het zeer licht wordt gedoopt. Er bestaan verschillende mechanismen ter verklaring van deze eigenschappen, waarin men er vanuit gaat dat het ongedoopte materiaal een halfmetaal is. Deze veronderstelling wordt bevestigd door berekeningen van de elektronenstructuur in de lokale dichtheidsbenadering die een kleine overlap laten zien van de valentieband en de geleidingsband. Echter, *GW*-berekeningen die in het algemeen een stuk nauwkeuriger zijn in het voorspellen van het excitatiespectrum, leveren een aanzienlijke band gap van 0.8 elektronvolt op voor CaB_6 . Recente foto-emissie experimenten zijn in goede overeenstemming met het berekende spectrum. Hiermee lijken de in de literatuur gesuggereerde verklaringen voor de bijzondere magnetische eigenschappen van de hexaborides niet op te kunnen gaan.

Peter van Gelderen

Curriculum vitae

Peter van Gelderen
geboren op 14 maart 1971 te Nijmegen

- | | |
|-------------|---|
| 1983 - 1989 | Gymnasium β aan het Dominicus College te Nijmegen |
| 1989 - 1995 | Studie experimentele en theoretische natuurkunde aan de Katholieke Universiteit Nijmegen |
| 1995 - 2000 | Onderzoeker in Opleiding in dienst van de Stichting voor Fundamenteel Onderzoek der Materie (FOM), aan het Philips Natuurkundig Laboratorium, de Katholieke Universiteit Nijmegen en de Universiteit Twente |
| 2000 - | Adviseur |

Publicaties

1. P. van Gelderen, S. Crampin, and J.E. Inglesfield
Quantum well states in Cu/Co overlayers and interlayers
Phys. Rev. B **53**, 9115 (1996).
2. P. van Gelderen, S. Crampin, Th. Rasing, and J.E. Inglesfield
Effect of interface magnetic moments and quantum-well states on magnetization-induced second-harmonic generation
Phys. Rev. B **54**, 2343 (R) (1996).
3. P. van Gelderen, P.A. Bobbert, P.J. Kelly, and G. Brocks
Parameter-free quasiparticle calculations for YH_3

- Phys. Rev. Lett. **85**, 2989-2992 (2000).
4. P. van Gelderen, P.J. Kelly, and G. Brocks
Phonon spectrum of YH_3 : Evidence for a broken symmetry structure
Phys. Rev. B **63**, 100301 (R) (2001).
 5. H.J. Tromp, P. van Gelderen, P.J. Kelly, G. Brocks, and P.A. Bobbert
 CaB_6 : a new semiconducting material for spin electronics
Phys. Rev. Lett. **87**, 016401 (2001)
 6. P. van Gelderen, P.A. Bobbert, P.J. Kelly, G. Brocks, and R. Tolboom
Parameter-free calculation of single-particle electronic excitations in YH_3
Submitted to Phys. Rev. B.
 7. P. van Gelderen, P.J. Kelly, and G. Brocks
Structural and dynamical properties of YH_3
Submitted to Phys. Rev. B.
 8. P. van Gelderen, P.J. Kelly, G. Brocks, and P.A. Bobbert
Quasiparticle calculations for LaH_3
To be submitted.